International
WOCE
Newsletter

Number 28 October 1997

IN THIS ISSUE

Published by the WOCE International Project Office at Southampton Oceanography Centre, UK

Summer in Geneva

W. John Gould, Director, WOCE IPO

John Church, Breck Owens and I have just returned from the World Climate Research Programme Conference held in Geneva at the end of August. We were there to represent WOCE as one of the component WCRP projects. The conference was attended by over 300 delegates from over 100 countries and was an excellent showcase for science related to the earth's climate system and the contributions that WCRP projects are making. In our area of interest there were presentations by Carl Wunsch who explored the two paradigms of a passive steady-state ocean circulation and of a turbulent ocean active in the climate system. This was followed by a paper by Bob Dickson showing some specific examples of how the ocean acts to produce climate impacts that directly effect aspects of the global economy.

John Church made a brief presentation on the achievements of WOCE up to the present and the challenges that remain – specifically the need for an investment of money and personnel into WOCE synthesis (particularly modelling and data assimilation) and the need to maintain a comprehensive ocean observing system beyond the end of WOCE. A conference statement will be widely publicised that will stress these requirements.

Naturally enough, as many of you will have learnt from media reports, the 1997–98 El Niño was a topic of great interest that give the conference greater global coverage than would normally have been the case.

The WOCE IPO prepared a brochure summarising WOCE objectives, achievements and challenges and a copy is being circulated with this newsletter. Further copies are available from the IPO.

Workshops

Workshops on the South Atlantic and Southern Ocean were held in Brest and Hobart respectively in June/July. They were well arranged (thanks to the organising committees and their chairs), well attended and did much to stimulate the exchange of data and ideas between WOCE researchers. A number of large synthesis projects involving new groupings of international collaborators were initiated at the Southern Ocean meeting.

This Newsletter contains a number of articles on the South Atlantic based on science presented in Brest. Newsletter No. 29 at the end of the year will contain Southern Ocean papers. Special sections in JGR (Oceans) are being planned. Papers from the first WOCE regional workshop (held last summer on the Pacific) are presently undergoing review and revision and are expected to appear in JGR in Spring 1998.

The Indian Ocean workshop has now been scheduled for New Orleans in September 1998. A full announcement is on page 39 of this Newsletter.

As well as the regional workshops there is an initiative to hold a workshop on ocean modelling sponsored jointly by WOCE and CLIVAR. It is planned to have a limited attendance (basically by invitation) and is being organised by a committee headed by Claus Böning. The specific theme is "Ocean modelling for climate studies" and will address topics such as "The representation of ocean dynamics in climate models", "The accuracy and limitations of ocean models" and "Oceanic fields for use in model testing".

WOCE Conference

With this Newsletter we are also mailing the main announcement for the WOCE Conference. By the end of August, we had already received over 300 expressions of interest from scientists in 45 countries (a far wider group than those active in WOCE research). What is encouraging is that many of these requests are from people who were not previously on our IPO mail list so this seems to promise a large attendance. Lectures are from invited speakers but we hope that there will be a large number of poster presentations.

Measuring the output of WOCE

As many of you will know, the WOCE IPO, through the UK National Oceanographic Library, extracts a WOCE bibliography that is maintained on-line and in a searchable format at the WOCE DIU. Up to now we have been indiscriminate in including both publications and reports stemming from WOCE research and publications that are of relevance to WOCE but not necessarily resulting from modelling or observations that were part of the project. We are aware that some effort will have to be made to quantify the output of WOCE research and therefore in future we will try to index the publications that stemmed from WOCE in an identifiable manner. It is impossible to be precise over what should be included but we hope that this exercise of flagging "real" WOCE publications will be brought up to date by the end of the year.

P.S. A "New venue for the IPO?"

There was an evening reception during the WCRP Conference hosted by Prof. Obasi, the Secretary-General of WMO. I was amused that the venue was "The WIPO". To most of us this would mean the WOCE IPO but to those in Geneva it is the World Intellectual Property Organisation. We thought our new premises in Southampton were quite grand but the "real" WIPO is in a quite different league with fountains and chandeliers!

The Heat and Mass Transport in the South Atlantic

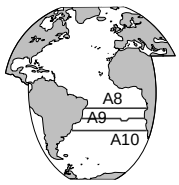

Jürgen Holfort and Gerold Siedler, Institut für Meereskunde Kiel, Germany.
jholfort@ifm.uni-kiel.de

The South Atlantic provides the passage for the oceanic heat transport between the convection regions in the North Atlantic and the other oceans. In contrast to the South Pacific and the southern Indian Ocean, the mean meridional heat transport is northward in South Atlantic.

Here we present an estimate of the meridional heat and freshwater transports in the South Atlantic between 11°S and 30°S. The description of the method and the uncertainties will focus on the heat transport, but the method is also applicable with only minor changes to the freshwater transport.

The oceanic heat transport W is defined as (Bryan, 1962):

$$W = \int_0^H \int_{\lambda_1}^{\lambda_2} \theta \rho c_p v \delta z \delta x$$

where H is the water depth, θ the potential temperature, ρ the density, c_p the specific heat, v the velocity and λ_1, λ_2 are the start and end positions of a section. Whereas θ, ρ, and c_p are known at discrete intervals from CTD measurements the velocity has to be determined. We assume that the ocean is in geostrophic balance with an additional wind-driven velocity part near the surface. This Ekman part is calculated using the wind stress data from Hellermann and Rosenstein (1983) and assuming that this part is evenly distributed over the top 50 m of the water column. The baroclinic part of the geostrophic velocity is known from the density field obtained by CTD measurements, whereas the barotropic field is first estimated using a level of no motion approach, and this first guess is then refined using an inverse technique (Wunsch, 1978).

The hydrographic data used for the calculation of the meridional transports result from 6 zonal CTD sections between 11°S and 30°S (see Table 1 and Fig. 1). The meridional sections also shown in Fig. 1 are used in the inverse approach to further constrain the flow, but will not be discussed in any detail. The WOCE A10 section was considered the main section in the South Atlantic to calculate the heat transport, and direct current measurements from several moorings between the coast of Brazil and the Rio Grande Rise along A10 are available (Tarbell et al., 1994). Transport estimates from these moorings for the Brazil Current and the flow through the Vema Channel (Holfort, 1994) are used as constraints in the inverse method.

A broad range of assumptions on a level of no motion (LNM) to obtain the barotropic velocity component leads to results which in many cases are incompatible with earlier results and also with respect to neighbouring section results. In the inverse approach we take initial guesses (from a LNM) of the barotropic velocities at each station and adjust the velocities in order to meet the constraints approximately. The main constraints in the present inversion are:

- The total salt transport across the zonal section is $26.7 * 10^6$ kg s^{-1}. This number is based on the Bering Strait salt transport and the assumption of a steady state salt balance within the Atlantic.
- Salt is conserved in boxes bounded by different sections and/or the continents in the horizontal plane, and by selected density surfaces in the vertical plane.
- The flow within layers deeper then 3000 dbar in the eastern basins of the South Atlantic is taken to be zero due to the blocking of such flows by the Walvis and Mid-Atlantic Ridges.
- The transport of the Brazil Current at 30°S (0-600 dbar) is 10 Sv to the south.
- The flow of Antarctic Bottom water through the Vema Channel is 5 Sv and the total transport is 7 Sv.
- The net meridional phosphate transport is constant for all zonal sections.

These constraints lead to a linear system of equations which is solved using singular value decomposition. Because the constraints only provide a first-order representation of the real flow in the ocean, the linear system is not solved exactly but only within certain error margins. Also the

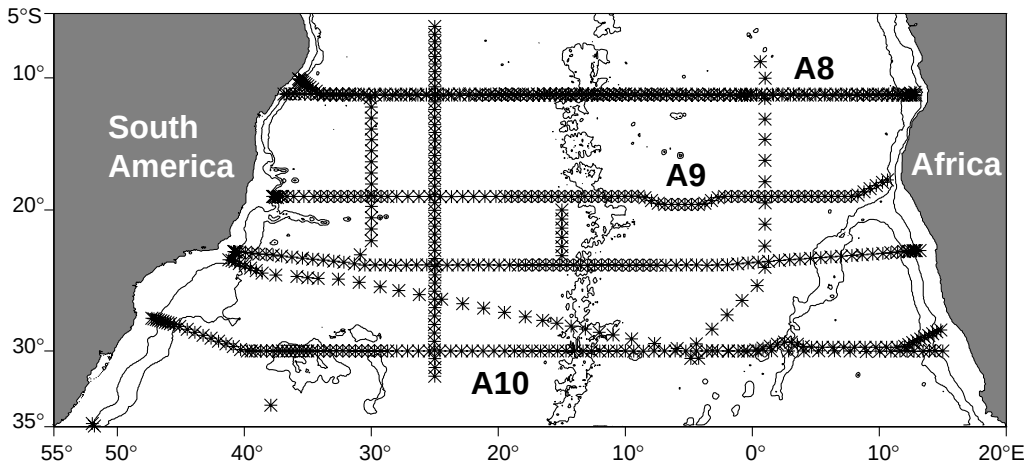

Figure 1. Position of the hydrographic sections used in the inverse analysis.

Table 1. Zonal sections used in the calculation			
Cruise	Date	Approx. latitude	Institution
Oceanus 133	Mar 1983	11°S	WHOI
WHP-A8	Feb 1994	11°S	IfM-Kiel
WHP-A9	Feb 1991	19°S	IfM-Kiel
Oceanus 133	Feb 1983	23°S	WHOI
SAVE-3/4	Feb 1988	27°S	SIO
WHP-A10	Jan 1993	30°S	IfM-Kiel

constraints are allowed to vary within certain error margins.

Ideally the solution does not depend on the initial guess of a level of no motion and also not on the specific constraints. In reality, however, we find different solutions depending on the weighting and scaling of the linear system and on the matrix rank used in constructing the solution. The weighting and scaling determines the importance of constraints and also the error of the barotropic velocity for stations. Finally the rank defines the importance of the initial guess compared to the constraints. At low matrix rank the deviations from the initial state are small but the difference between the solution and the constraints (the residual) is high. Higher ranks show a greater deviation from the initial state and lower residuals, but also increase the noise level of the system. The values for the heat and mass transport reported here are therefore the mean values of different inverse models for an intermediate rank. The solutions depend only slightly on the initial level of no motion, and the constraints are solved within reasonable error margins. The solutions are not dominated by noise.

The mass and salt transports are presented in Table 2, together with the CO_2 transport estimates from Holfort *et al.* (1997) using the same inverse analysis and an estimate for the WOCE A11 section from a first attempt to incorporate this section in the inverse analysis. There is a difference between the various transports here. Whereas salt and mass transport is clearly defined the heat transport is only independent of a temperature reference point if mass is conserved. The values of the heat transport which we present are therefore referenced to the mean temperature of the respective section, which is equivalent to balancing the mass transport with a barotropic velocity which is uniform over the whole section.

The standard deviations of the mean transports are about 0.02 Tg/s for mass, 0.05 PW for heat and 200 kmol/s for CO_2. We can take these values (or more cautiously twice these values) as an estimate of the error due to the barotropic velocity part. These errors are small compared to other errors. Speer et al. (1996) showed that the variation in the heat transport at 11°S that results from the use of different wind stress data is ±0.2 PW. A similar error can be expected due to annual and/or longer term temporal variations in the flow and temperature fields. The error due to the discrete spatial resolution is difficult to assess. It can be assumed that the new high resolution sections resolve the important scales of motion, and a coarse estimate gives an error smaller then 0.04 PW. By subsampling the high-resolution sections to a horizontal and vertical spacing commensurate with historical data (Meteor 1925/27, IGY) the difference between full-resolution and subsampled heat transport (about 0.2 PW) shows that very coarse resolution historical data lead to a substantial error due to the unsatisfactory resolution.

The heat transport values are found to be in the broad range of previously calculated transports. Our value for the Oceanus section at 11°S differs from a previous estimate of Speer et al. (1996) using the same data with a level of no motion approach by 0.1 PW which is within the error margin. More intriguing is the difference of 0.2 PW between the Oceanus and Meteor sections at 11°S. The reason most probably is temporal (annual/interannual) variability. We find considerable differences in the temperature and velocity fields of the two sections. The inverse analysis with the set of sections can be used to minimise the differences in the velocity field by adjusting the barotropic flow. We can also take as a constraint for the inverse model the condition that the two sections have the same heat transport. This gave a heat transport of about 0.6 PW and also influenced the heat transport numbers of the other sections. However it is not clear to us if there is a reasonable assumption. Clearly the temporal variability has to be studied in more detail. An earlier heat flux determination at 30°S (Holfort, 1994) gave an estimate of 0.4 PW while the present calculation results in the lower value of about 0.3 PW. This is due to the inclusion of more sections and an additional phosphate conservation constraint. We have also done some first runs with the inverse approach including the section A11 at 45°S (Saunders and King, 1995), but the results are not sufficiently well established yet to include them in the present report.

Table 2. Northward meridional fluxes from the inverse calculation, including the CO_2 flux from Holfort et al. (1997)				
Cruise	Approx. latitude	Heat PW	Mass Tg/s	CO_2 kmol/s
Oceanus 133	11°S	0.71	-1.00	2420
WHP-A8	11°S	0.50	-0.92	2080
WHP-A9	19°S	0.69	-0.87	2470
Oceanus 133	23°S	0.35	-0.65	1920
SAVE-3/4	27°S	0.40	-0.61	2100
WHP-A10	30°S	0.26	-0.53	1920

The mass transport shows a consistent pattern with decreasing values of southward transports and a convergence between 11°S and 30°S is consistent with the freshwater surface flux of 0.43 Sv from Baumgartner and Reichel (1975). The integration of the freshwater fluxes north of 11°S (Wijffels et al., 1992) gives a lower net southward flux of only 0.72 Sv at 11°S, however with an error at the equator of 0.42 Sv. Our values are thus within this error limit.

A next step in the determination of the South Atlantic heat transport will have to be incorporating all WOCE sections in an inverse model. Although this will probably lead to better estimates of mean fluxes, the question of

long-term temporal variability will remain open. We will need other data (XBT, altimeter, etc.) to investigate how representative the sections are for the mean transports. These additional data must also include a better estimate of the wind stress to decrease the uncertainties in the Ekman part.

References

Baumgartner, A., and E. Reichel, 1975: Die Weltwasserbilanz. Oldenburg Verlag, München, 179p.

Bryan, K., 1962: Measurements of meridional heat transport by ocean currents. J. Geophys. Res., 67, 3403–3414.

Hellermann, S., and M. Rosenstein, 1983: Normal monthly wind stress over the world ocean with error estimates. J. Phys. Oceanogr., 13, 1093–1104.

Holfort, J., 1994: Großräumige Zirkulation und meridionale Transporte im Südatlantik. Berichte aus dem Institut für Meereskunde, Kiel University, Nr. 260.

Holfort, J., K. M. Johnson, B. Schneider, G. Siedler, and D. W. R. Wallace, 1997: The meridional transport of dissolved inorganic carbon in the South Atlantic Ocean. J. Geophys. Res., submitted.

Saunders, P. M., and B. A. King, 1995: Oceanic fluxes on the WOCE A11 section. J. Phys. Oceanogr., 25, 1942–1958.

Speer, K. G., J. Holfort, T. Reynaud, and G. Siedler, 1996: South Atlantic heat transport at 11°S. In: Wefer, G., W. H. Berger, G. Siedler, and D.J. Webb (eds.), The South Atlantic: Present and past circulation, Springer-Verlag, Berlin, Heidelberg, New York, 105–120.

Tarbell, S., R. Meyer, N. Hogg, and W. Zenk, 1994: A moored array along the southern boundary of the Brazil Basin for the Deep Basin Experiment – report of a joint experiment 1991-1992. Berichte aus dem Institut für Meereskunde, Kiel University, Nr. 243.

Wijffels, S. E., R. W. Schmidt, H. L. Bryden, and A. Stigebrandt, 1992: Transport of freshwater by the Ocean. J. Phys. Oceanogr., 22, 155–162.

Wunsch, C., 1978: The North Atlantic general circulation west of 50°W determined by inverse methods. Reviews of Geophysics and Space Physics, 16, 583–620.

Comparisons of the LANL POP Model and Observations in the South Atlantic

Julie McClean, Naval Postgraduate School, Monterey, USA; Mathew Maltrud, Los Alamos National Laboratory, Los Alamos, USA; and Albert Semtner, Naval Postgraduate School. mcclean@nps.navy.mil

The heat transport associated with the Atlantic meridional overturning cell is equatorward in the mid-latitudes of the South Atlantic. The export of North Atlantic Deep Water (NADW) in the overturning cell is balanced by thermocline, intermediate and bottom waters. Two pathways, one from the Drake Passage (Rintoul, 1991) and the other from the Indian Ocean thermocline and Agulhas eddy-shedding (Gordon et al., 1992), supply the upper limb of the overturning. The relative contributions to these "warm" and "cold" paths is still a matter of debate as is the temporal variability of this ratio on many time scales.

Here we provide a preliminary examination of the Los Alamos National Laboratory (LANL) Parallel Ocean Program (POP) global $\frac{1}{6}°$ model in the light of this issue. The model is first compared with data, providing an assessment of its ability to reproduce the observed mean flow, variability, hydrographic structure, and meridional heat transports in the South Atlantic. Model weaknesses identified by these comparisons will be used to make improvements in the model formulation. Output is then used to examine the mean meridional water mass transports and the pathways supplying the upper limb of the overturning cell.

Model description

The $\frac{1}{6}°$ POP model is an eddy-resolving, 20-level, primitive equation model that was run on the Connection Machine 5 at LANL (Smith et al., 1992; Maltrud et al., 1997). It is forced with high-frequency ECMWF wind stresses and monthly climatological surface heat fluxes obtained from ECMWF analyses (Barnier et al., 1995). It employs a Mercator grid to better track eddy length scales between 77°S and 77°N. It is initialised using a 35-year spin-up from a lower resolution Semtner and Chervin (1992) run (started from Levitus (1982) climatology), followed by more than 30 years at the present resolution.

Results

A snapshot of sea surface height (cm) from POP is seen in Fig. 1 (page 19). It demonstrates the broad range of variability (mesoscale through large-scale) reproduced by the model and is qualitatively similar to altimetric fields. Mesoscale eddies shed from the Agulhas Current move into the South Atlantic along paths largely consistent with those observed. Quantitative comparisons between TOPEX/POSEIDON (T/P) and POP statistics (eddy energy levels, length scales) have been documented by Fu and Smith, 1996, McClean et al. (1997), and Maltrud et al. (1997). A movie of the POP SSH fields can be found at

http://web.nps.navy.mil/~mcclean/woce.html.

The mean surface circulation is represented in Fig. 2 by the depth-integrated flow $\left(\mathrm{m}^2\,\mathrm{s}^{-1}\right)$ over the top 135 m of the POP model calculated from 10-year mean velocity fields. The well-known details of the observed surface flow are seen. Note that the Antarctic Circumpolar Current (ACC) displays several filaments across the southern basin. Flow in the thermocline (135–1000 m), deep (1000–3300 m), and abyssal (3300–5000 m) layers can be found at the Web site mentioned above.

The characteristic water masses of the overturning

cell of the Atlantic basin are seen in the salinity section from WOCE hydrography line A16 (Fig. 3a). The co-located 10-year mean POP salinity field is shown in Fig. 3b. Data/output were collected or extracted between 54°S, 36°W and 0, 25°W, and were projected onto a constant longitude line. Tsuchiya et al. (1994) described the observed water properties in detail; hence, we only discuss notable model/data differences. The salinity minimum associated with Antarctic Intermediate Water (AAIW) dominates the upper 1500 m of the water column. The observed 34.4 isohaline extends poleward to about 25°S, while in the model it only reaches 44°S. At 30°S, the minimum salinity value is 34.4 in the data and 34.6 in the model. Antarctic Bottom Water (AABW) is found roughly below the 34.7 isohaline in the lower 2000 m of the water column at the southern end of the transect. In the model, this water does not penetrate as far equatorward as observed. Flow fields in the lower levels of the model (not shown) reveal that inadequate representation of the topography is partly responsible, particularly in the Vema Channel. Other factors such as lack of ice and associated processes also contribute to this behaviour.

Meridional heat transports across several of the zonal South Atlantic WOCE hydrographic lines in the tropics and mid-latitudes have been calculated by Holfort and Siedler using an inverse model (see this issue). At 30°S (A10), 20°S (A9), and 5°S (A7) they obtain 0.3, 0.5, and 1.2 PW, respectively. From the 10-year mean POP field, the total meridional transports are 0.3, 0.5, and 0.5 PW, respectively. From the monthly-averaged POP fields corresponding to the time of the cruises the values are 0.5, 0.5, and 0.9 PW, respectively. Some of these differences are likely to be due to the effects of seasonal wind forcing on the subtropical gyre, as suggested by Barnier et al. (1996) from examining the seasonal variability of heat fluxes at this latitude in a sigma-coordinate model.

Mean meridional water mass transports across 30°S were calculated using the classification of Rintoul (1991). NADW (11 Sv) is mainly balanced by the thermocline water (9.5 Sv) with AAIW and AABW contributing 1.5 Sv and 0.2 Sv, respectively. Similar balances are seen in the 1995 monthly fields (not shown), with the largest quantities of thermocline water occurring in the austral winter. From the model/data hydrographic data comparison above, it is clear that the model is not producing sufficient AAIW, hence the overturning circulation is largely balanced by thermocline water. This, in turn, will most likely impact the contributions to the overturning from the "cold" and "warm" paths.

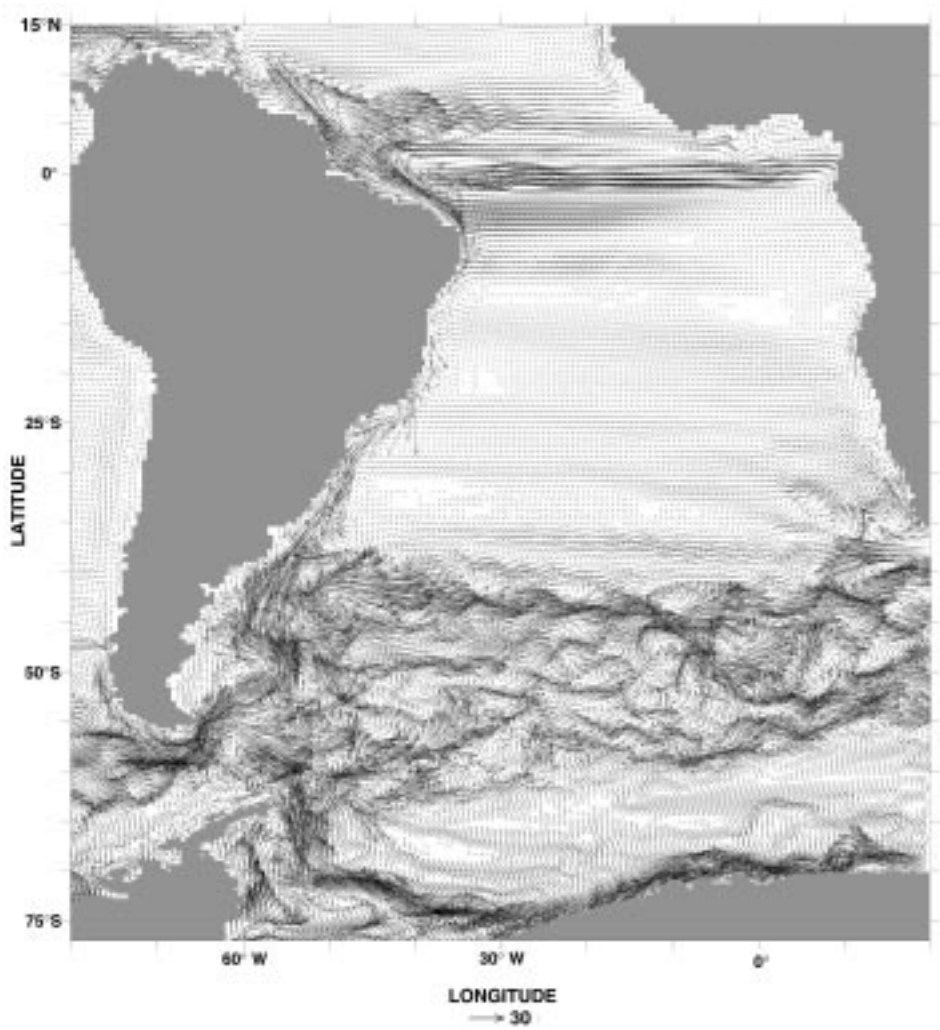

Figure 2. Depth-integrated POP velocities $\left(m^2\,s^{-1}\right)$ over the top 135 m of the water column using 10-year mean fields.

The depth of the salinity minimum over the model South Atlantic subtropical gyre is on average 1100 m. To appreciate the general pathways taken by this minimum salinity water to reach these depths along the WOCE A16 line, trajectories were integrated backwards in time using the mean POP velocity fields from 25°W (the nominal longitude of A16) and 1100 m (Fig. 4, page 20). Note that this in effect generates mean streamlines (here coloured by the value of the salinity); the specific picture would be somewhat different if the trajectories were calculated forward in time (concurrent with the model itself) due to the presence of eddies and diffusion. The salinities range from 34.5 (blue) to 34.7 (red). The minimum salinity water (blue) originates from the Drake Passage and Indian Ocean. In

the latter case, it appears that water parcels cross the Atlantic with higher salinities at shallower depths (seen in trajectory depth figure not shown here) and mix within the Malvinas–Brazil Current Confluence producing lower salinity water that sinks in the process.

Conclusions

Comparisons with data have revealed that the POP model is reproducing many facets of the South Atlantic circulation and variability. It is insufficiently replenishing AAIW, due to inadequate model physics, resulting in more thermocline water balancing the southward flow of NADW. Both "cold" and "warm" water pathways are supplying the recirculation cell, however it is likely that more water is coming from the "warm" water route as a result of the under-production of AAIW.

Acknowledgements

This work was supported by the US National Science Foundation and the Department of Energy's CHAMMP program. The authors wish to thank the WOCE Hydrographic Program Office, Lynne Talley and William Smethie for the WOCE A16 data. Peter Braccio assisted with the graphics and created the SSH simulation.

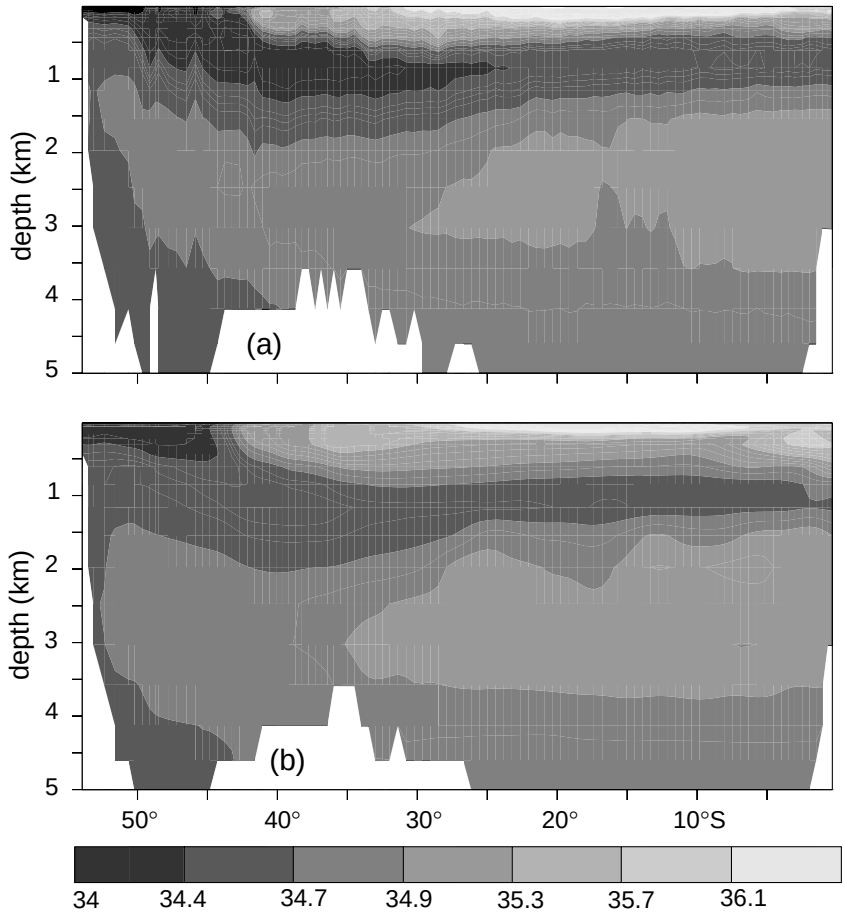

Figure 3. (a) Salinity along WOCE hydrographic line A16. Data is projected onto a constant longitude line. (b) POP 10-year mean salinity field co-located with WOCE A16 line.

References

Barnier, B., L. Siefridt, and P. Marchesiello, 1995: Thermal forcing for a global ocean circulation model using a three-year climatology of ECMWF analyses. J. Marine Sys., 6, 363–380.

Barnier, B., P. Marchesiello, and A. Pimenta de Miranda, 1996: The impact of seasonal forcing on the variability of the meridional heat flux at 30°S using a sigma-coordinate primitive equation model. International WOCE Newsletter, 24, 16–17.

Fu, L.-L., and R. D. Smith, 1996: Global Ocean circulation from satellite altimetry and high-resolution computer simulation, Bull. Amer. Met. Soc., 77, 2625–2636.

Gordon, A. L., R. F. Weiss, W. M. Smethie, and M. J. Warner, 1992: Thermocline and intermediate water communication between the South Atlantic and Indian Oceans. J. Geophys. Res., 97, 7223–7240.

Levitus, S., 1982: Climatological atlas of the world ocean. NOAA Prof. Paper N013, US Government Printing Office, Washington, DC, 173pp.

Maltrud, M. E., R. D. Smith, A. J. Semtner, and R. C. Malone, 1997: Global eddy-resolving simulations driven by 1985–94 atmospheric winds. J. Geophys. Res., submitted.

McClean, J. L., A. J. Semtner, and V. Zlotnicki, 1997: Comparisons of mesoscale variability in the Semtner-Chervin quarter-degree model, the Los Alamos POP sixth-degree model, and TOPEX/POSEIDON data. J. Geophys. Res., in press.

Rintoul, S. R., 1991: South Atlantic interbasin exchange. J. Geophys. Res., 96, 2675–2692.

Semtner, A. J., and R. M. Chervin, 1992: Ocean general circulation from a global eddy-resolving model. J. Geophys. Res., 97, 5493–5550.

Smith, R. D., J. K. Dukowicz, and R. C. Malone, 1992: Parallel ocean general circulation modeling. Physica D, 60, 38–61.

Tsuchiya, M., L. D. Talley, and M. S. McCartney, 1994: Water-mass distributions in the western South Atlantic; A section from South Georgia Island (54°S) northward across the equator. J. Mar. Res., 52, 55–81.

Pathways of Weddell Sea Deep Water in the Argentine Basin Examined Using a Primitive Equation Model

J. A. Murphy, D. P. Stevens, and G. R. Bigg, University of East Anglia, Norwich, UK.
j.murphy@uea.ac.uk

The Drake Passage (see Fig. 1) prescribes the densest water that can enter the South Atlantic. The Antarctic Circumpolar Current (ACC) at Drake Passage can only supply temperatures greater than 0.2°C; so within the Argentine Basin the source of waters colder than 0.2°C must be from the Weddell Sea. Water with potential temperature -0.7°C<θ<-0.2°C will be defined as Weddell Sea Deep Water (WSDW). New WSDW can enter the Argentine Basin through the Georgia Basin, or through the passage

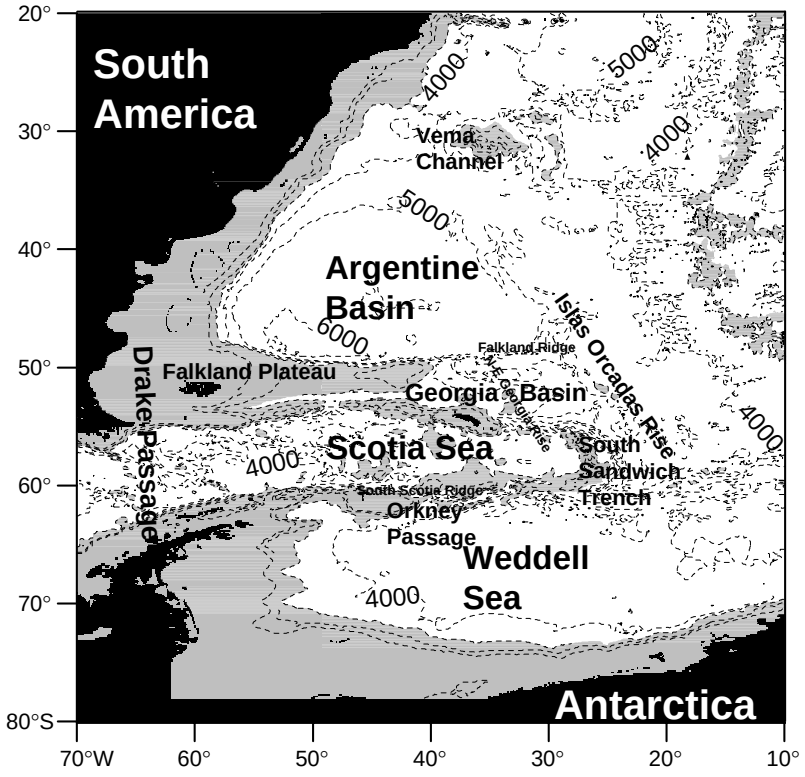

Figure 1. Bathymetry of the South Atlantic. Depths less than 3000 m are shaded.

situated between the Islas Orcadas Rise and the Mid-Atlantic Ridge. According to Stommel and Arons' (1960) theory it should flow in a deep boundary current towards the coast of South America and then north along the western boundary of the Argentine Basin. Since water colder than -0.2°C does not escape the Basin, the coldest water in the boundary current should return to the south-east as part of an interior flow regime.

Traditional tracer measurements cannot distinguish new WSDW from water that has been circulating for some time. CFC data however should be able to provide some insight into the relative ages of the deep and bottom waters of the Argentine Basin. CFCs have been introduced to the atmosphere only recently so we expect the highest signal to be in the deep boundary current predicted by Stommel and Arons (1960), and for there to be substantially lower concentrations in the rest of the basin, which comprises the slower-moving interior recirculation. However, interior waters with low-CFC concentrations are not found in the south-east Argentine Basin. Warner et al. (1990) and Weiss et al. (1990) show CFC distributions from the SAVE leg-E cruise (nominally at 45°S). Some higher concentrations were found on the western boundary, and lower concentrations were found in the interior of the south-west region of the Argentine Basin. But, there was a sharp increase in CFCs just north of the Georgia Basin that persisted eastwards to the Mid-Atlantic Ridge.

Pathways of Antarctic Bottom Water in the South Atlantic

We use a numerical model to look at the arrival of WSDW in the Argentine Basin and to examine its route north once there. The area to be modelled is shown in Fig. 1. The model domain is limited to 70°W–20°E, 20°S–75°S. Exchanges with other oceans are accounted for by having active open boundaries at the Drake Passage, at 20°S, and between Africa and Antarctica at 20°E. In the vertical we have 32 model levels and a horizontal resolution of approximately 55 km. Monthly Levitus temperature and salinity data and Hellerman-Rosenstein winds were used to force the model. The use of idealised tracers in the numerical model may help us to shed some light on the problem. Following England (1995) we use a transient dye tracer. The concentration of dye (D) is governed by the standard tracer conservation equation:

$$\frac{dD}{dt} + (u \cdot \nabla)D + w\frac{\delta D}{\delta z} = F^D + S^D,$$

where D obeys the following boundary condition:

$$D(x, y, z) = 1 \,\text{unit}\, m^{-3}$$

over the considered source water volume V_s, and initial condition:

$$D(x, y, z) = 0 \,\text{unit}\, m^{-3} \text{ for all } (x, y, z) \notin V_s.$$

u is the horizontal velocity, w the vertical velocity, F^D represents the diffusion and S^D the source. As such, water

in direct contact with the source, has a concentration of $1\,\text{unit}\,\text{m}^{-3}$ throughout the integration, whereas interior grid boxes are gradually filled with the dye. The dye tracer provides useful information on the pathways taken by the water masses.

The source volume chosen initially was within WSDW south of 60°S and above the level of the Orkney Passage (near 40°W) at 3500 metres; this was denoted WSDW1. The other source volume chosen was WSDW below 3500 m and south of 60°S and this was denoted WSDW2.

Routes north out of the Weddell Sea

The ocean bathymetry constrains WSDW to enter the Argentine Basin from either the Georgia Basin or east of the Islas Orcadas Rise. WSDW may reach these locations through:

1. The South Sandwich Trench Route (Georgi, 1981). We will refer to the water following this route as T-WSDW.
2. The Scotia Sea Route (Locarnini et al., 1993). This route was first established by Locarnini et al. (1993), henceforth L93, as an alternative to the traditional South Sandwich Trench route, although it was previously identified by Hollister and Elder (1969). The water following this route will be called S-WSDW herein.

In the model the T-WSDW can reach the Georgia Basin at least as fast as the S-WSDW, but it is the S-WSDW that fills the south-east Scotia Sea and enters the Georgia Basin. L93 and Weiss et al. (1990) show high CFCs throughout the south-east Scotia Sea and in the deep waters the high CFC signal can be traced northeast through the Scotia Sea as far as the Georgia Basin.

Entry of WSDW to the Georgia Basin

After flowing into the Georgia Basin the S-WSDW meets with the T-WSDW above the northern end of the South Sandwich Trench. The WSDW tracer distributions suggest that only the S-WSDW flows significantly to the south of the North-East Georgia Rise into the western part of the Georgia Basin. Water as cold as -0.5°C can enter the northern part of the basin from the east, north of the North-East Georgia Rise, in accordance with maps of bottom temperature shown by Whitworth et al. (1991), henceforth W91, and L93. This water is T-WSDW. In the model the lowest temperature involved in the S-WSDW route is θ~-0.2°C. Fig. 2 shows that it is the WSDW2 (the cooler part of the T-WSDW) which dominates the Georgia Basin at this level.

WSDW between the Islas Orcadas Rise and the Mid-Atlantic Ridge

Model results showing the deep velocity vectors (Fig. 3 shows those from 4336 metres) indicate a path northwards from the Weddell Sea flowing to the east of the Islas Orcadas Rise. Arhan et al. (1997), using data from the eastern leg of SAVE-5, calculates a transport of 0.68 Sv for WSDW (-0.2°C<θ<0.2°C) on the northern side of the Falkland Ridge which must have passed around the Islas Orcadas Rise. This is consistent with the model results showing water from east of the Islas Orcadas joining the

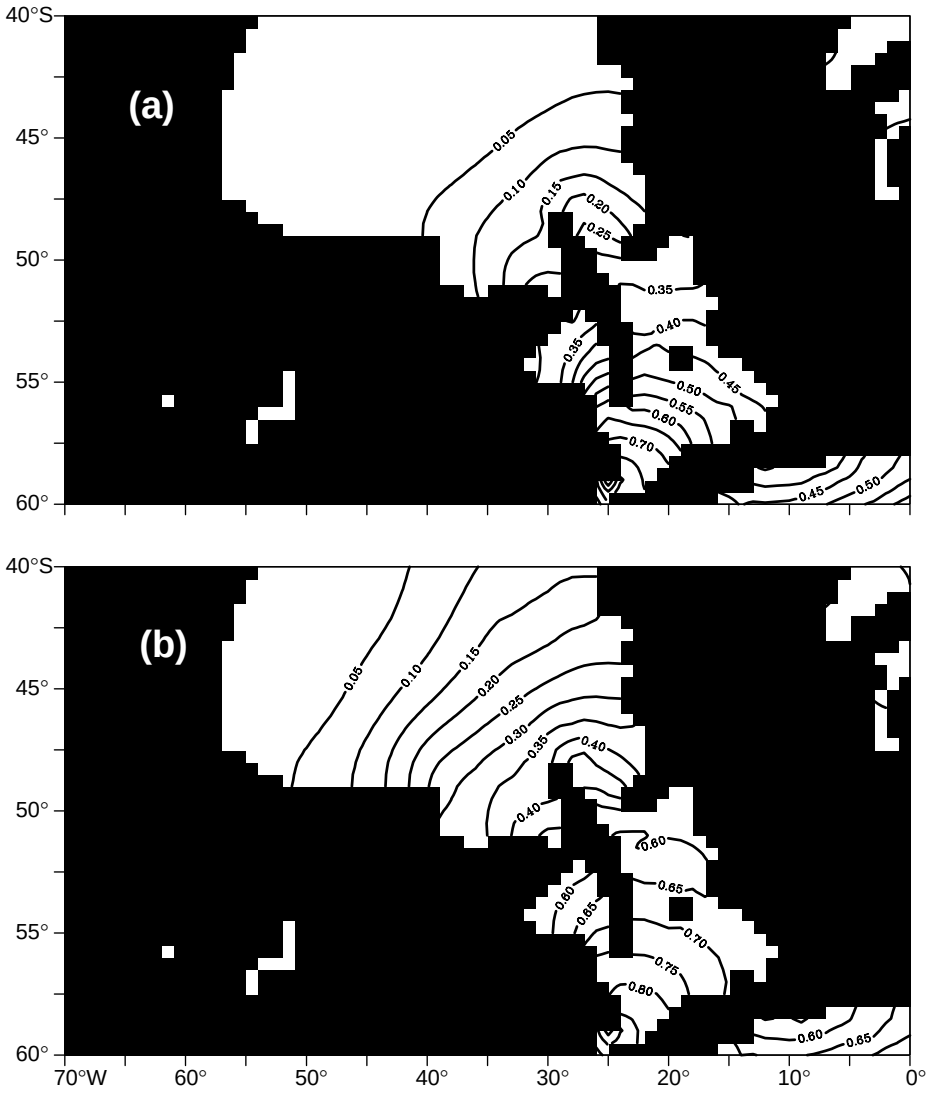

Figure 2. Deep WSDW model tracer distributions at 4336 m, (a) after 10 years of integration, (b) after 20 years of integration.

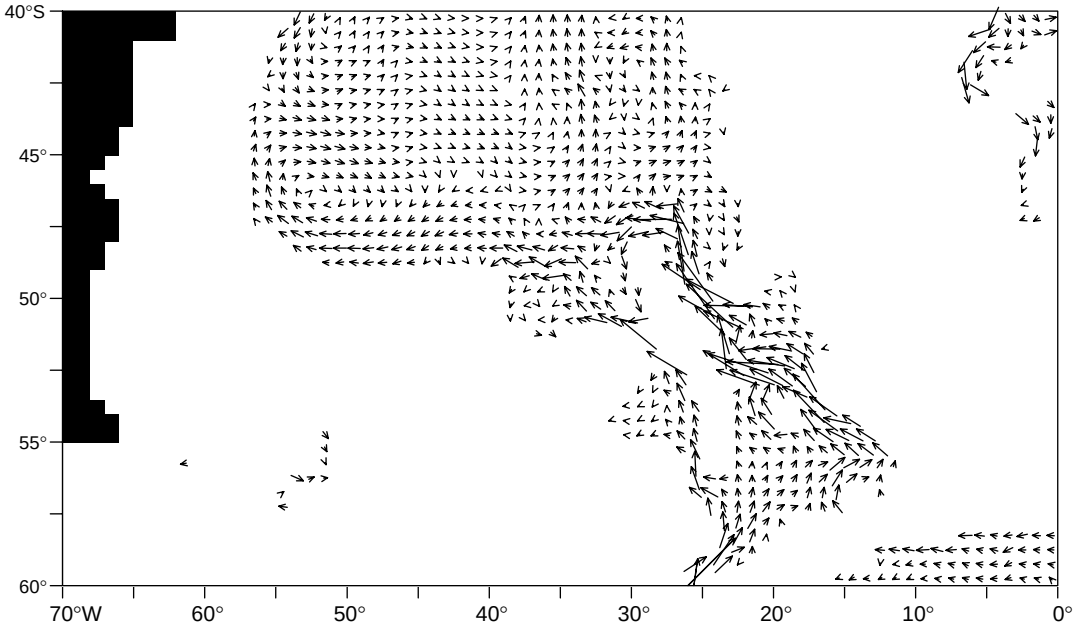

Figure 3. Model velocity vectors from 4336 m depth after 20 years of model integration.

deep boundary current north of the Falkland Ridge and travelling westwards.

The model transports at 43°W, north of the Falkland Plateau, compare favourably with W91. The model prescribes 3.04 Sv of WSDW net westward transport (1.9 Sv in W91) of which 1.84 Sv is "new" WSDW according to W91 terminology (1.2 Sv in W91). The model proportions of water in different temperature ranges is similar.

Flow of WSDW in the Argentine Basin

CFC data does not appear to agree with a simple Stommel and Arons circulation scheme with high-CFC values being found at the eastern side of the Argentine Basin. Warner et al. (1990) suggest that these high CFCs are consistent with a separate cyclonic gyre in the abyssal circulation. W91 pose an alternative involving entrainment and eastward advection of water from the Georgia Basin within the ACC. They showed evidence that the entry of deep waters from the Georgia Basin to the Argentine Basin is related to the meandering of the Subantarctic and Polar fronts. They suggest that water thus entrained by the ACC is carried eastwards with the propagating meander at a rate that exceeds its northward diffusion into the open Argentine Basin to the north. This process would limit the influence of high CFC concentrations to regions downstream (east) of the source region and one meander amplitude north of the source region. We do not believe this story is sufficient.

Results from the idealised tracers

The lighter WSDW spills over the South Scotia Ridge, especially at the Orkney Passage, and fills the south-east Scotia Sea by turning eastwards under the influence of the ACC. WSDW has also travelled north via the South Sandwich Trench route (east of the South Sandwich Arc). The deeper WSDW (WSDW2) shown in Fig. 2a has left the Weddell Sea via the South Sandwich Trench and then entered the eastern side of the deep Georgia Basin as well as travelling to the east of the Islas Orcadas. Some of the lighter WSDW dye has also reached this level but the signature of the deeper WSDW is much stronger.

From Fig. 2b we see that WSDW2 does enter the deep boundary current, as is evident from Fig. 3, but it also appears to spread primarily from the south-east part of the Argentine Basin, northward from the Georgia Basin and from between the Islas Orcadas Rise and the Mid-Atlantic Ridge. The high WSDW2 signal does not penetrate rapidly into the deep boundary current of the Argentine Basin as can be seen from Fig. 2. This behaviour is reminiscent of the CFC signal in the data of W91. We suggest that the deep boundary current is strongly affected by the deep-reaching ACC and that this is causing the rapid recirculation which limits the very high-CFC value waters to the area east and north of the Islas Orcadas Rise region. It may be that part of the boundary current is becoming entrained in the ACC, and it is being advected eastwards to the north of the main boundary current. A zonal picture of the deeper WSDW tracer WSDW2 from 45°S (Fig. 4, page 22) shows a remarkably similar distribution to the SAVE CFC data (Weiss et al., 1990) and to that of A11 (Smythe-Wright and Boswell, 1995) with very high concentrations along the western flank of the Mid-Atlantic Ridge, low-CFC interior waters in the south-western basin and an increase in the westernmost part of the basin in the deep boundary current.

This picture is different to that offered by W91, which suggests that meanders of the ACC capture blobs of WSDW and advect them to the east faster than they can diffuse north. It is unlikely that this scenario can produce the high-CFC signal as far north as 42°S (A11 data) and data with the same high volume (the high-CFC area is quite large). We suggest that a more continuous entrainment by the ACC results in the eastward advection of high-CFC water and that when this water arrives at the Mid-Atlantic Ridge it turns north. This schematic produces an approach for the Vema Channel from the south-east consistent with Flood and Shor (1988) and Hogg et al. (1982).

Acknowledgements

The financial support of NERC through a WOCE-funded PhD studentship for Judith Murphy is gratefully acknowledged. We are also grateful to K. Heywood, M. Meredith and M. Wadley for useful discussions.

References

Arhan, M., K. Heywood, and B. King, 1997: Scientific Programme and Abstracts of the WOCE South Atlantic Workshop 1997. Poster 29.

England, M. H., 1995: The Age and Ventilation Timescales in a Global Ocean Model. J. Phys. Oceanogr., 25, 2756–2777.

Flood, R. D., and A. N. Shor, 1988: Mud Waves in the Argentine Basin and their Relationship to Regional Bottom Circulation Patterns. Deep-Sea Res., 35, 6, 943–971.

Georgi, D. T., 1981: Circulation of the Deep and Bottom Waters in the South-western Atlantic. Deep-Sea Res., 28A, 9, 959–979.

Hogg, N., P. Biscaye, W. Gardner, and W. J. Schmitz, 1982: On the Transport and Modification of Antarctic Bottom Water in the Vema Channel. J. Mar. Res., 40, suppl., 231–263.

Hollister, C. D., and R. B. Elder, 1969: Contour Currents in the Weddell Sea. Deep-Sea Res., 16, 99–101.

Locarnini, R. A., T. Whitworth, and W. D. Nowlin, 1993: The Importance of the Scotia Sea on the Outflow of Weddell Sea Deep Water. J. Mar. Res., 51, 135–153.

Smythe-Wright, D., and S. Boswell, 1995.: Is the Deep Water Circulation in the Argentine Basin Going Round the Wrong Way? WOCE International Newsletter, 21, 33–34.

Stommel, H., and A. B. Arons, 1960: On the Abyssal Circulation of the World Ocean; An Idealised Model of the Circulation Pattern and Amplitude in Oceanic Basins. Deep-Sea Res., 6, 217–233.

Warner, M. J., R. F. Weiss, and W. F. Smethie, 1990: Chlorofluorocarbon Distributions in the Deep Argentine Basin (abstract), EOS Trans. AGU, 71, 168.

Weiss, R. F., J. L. Bullister, M. J. Warner, F. A. Van Woy, and P. K. Salameh, 1990: Ajax Expedition Chlorofluorocarbon Measurements, Ref. 90-6, 190 pp., Scripps Inst. of Oceanogr., La Jolla, CA, USA.

Whitworth, T., W. D. Nowlin, R. D. Pillsbury, M. I. Moore, and R. F. Weiss, 1991: Observations of the Antarctic Circumpolar Current and Deep Boundary Current in the Southwest Atlantic. J. Geophys. Res., 96, C8, 15105–15118.

Deep Circulation in the Western Tropical Atlantic Inferred from CFCs and L-ADCP Measurements During ETAMBOT Cruises

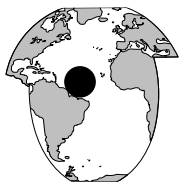

C. Andrié, LODYC, ORSTOM/CNRS/Université Pierre et Marie Curie, Paris, France; Y. Gouriou, B. Bourlès and C. Oudot, ORSTOM Brest, France; J. F. Ternon, ORSTOM Cayenne, French Guiana. andrie@lodyc.jussieu.fr

Direct velocity measurements have pointed out the complexity of the deep circulation in the western tropical Atlantic (Johns et al., 1993; Schott et al., 1993; Colin et al., 1994; Hall et al., 1994; Rhein et al., 1995; Fischer and Schott, 1997). The estimation of the net southward transport of the Deep Western Boundary Current (DWBC), which flows along the continental margin of the American continent, is complicated by the recirculations and their associated variability. The fate of the DWBC at the equator is of fundamental importance for the south Atlantic budget. SOFAR floats have shown that zonal flow, with strong variability, exists at depth along the equator (Richardson and Schmitz, 1993; Richardson, 1994). To address those questions, transient tracers, such as CFCs, are particularly useful in identifying the water masses. They have been measured during recent equatorial cruises: along repeated sections at 44°W and 35°W during Meteor cruises from 1990 to 1994 (Rhein et al., 1995; Rhein et al., 1996), and during the WOCE CITHER 1 cruise (along 7°30'N and 4°30'S, and at 35°W and 4°W in between) (Andrié et al., 1996).

In this context, one of the main objectives of the ETAMBOT programme was to study the western equatorial circulation between the American continent and the Mid Atlantic Ridge (MAR). The two cruises which have been carried out during the ETAMBOT programme took place during opposite seasons: ETAMBOT 1 in September–October 1995 and ETAMBOT 2 in April–May 1996. Both cruises followed the same tracks. The cruise tracklines (Fig. 1) consist of three sections, along 7°30'N between the coast and 35°W, along 35°W from 7°30'N to 5°S, and a slanted section crossing the Ceara rise, off Brazil. During those cruises, direct measurements of current were made from the surface to the bottom with a L-ADCP, Acoustic Doppler Current Profiler, attached to the rosette. During the ETAMBOT 1 cruise, profiles of current could only be made for the first 33 stations, between the coast and 37°W, at 7°30'N. During the ETAMBOT 2 cruise, profiles of current were made at every station. The data have been processed following the method described in details by Fischer and Visbeck (1993).

Here, we focus principally on the circulation features inferred from CFC-11 and L-ADCP measurements performed during the ETAMBOT 1 and 2 cruises.

ETAMBOT 1 - 7°30'N section

Figs. 2a and 2b display the CFC-11 and L-ADCP measurements obtained during the ETAMBOT 1 cruise (in September 1995) along 7°30'N, from the coast to 35°W. At the coast, the two maxima of CFC-11, which characterise the North Atlantic Deep Water (NADW), are clearly visible around 1700 m and 3900 m. The upper core (1500 m–1800 m) originates from the Labrador Sea. The vertical extension of that core is limited, presumably because of the weakness of the convection processes in the Labrador Sea

before the late 80s. The lower core (3800 m–3900 m) originates from the Nordic Seas through the Denmark Strait. Those layers of maximum of freons are respectively called Shallow Upper NADW (SUNADW) and Overflow Lower NADW (OLNADW) after Rhein et al. (1995). Both freon cores are clearly conveyed southward by the DWBC between 1000 m and the bottom (Fig. 2b). The upper core of the DWBC, between 1000 m and 3000 m, has its maximum of velocity around 1500 m (>40 cm/s). The lower core is found farther offshore, centred around 3500 m, with velocities lower than 20 cm/s. At the level of the upper core (1500 m–1800 m), CFC-11 enriched waters extend to the MAR (Fig. 2a) and secondary maxima are observed around 150 km, 300 km, 500 km, and 800 km from the coast. The three former cores can be related to a southward drift (Fig. 2b), but the last core, centred on 800 km, is at the eastern border of a strong northward recirculation which extends from the surface to the bottom, between 600 km and 800 km.

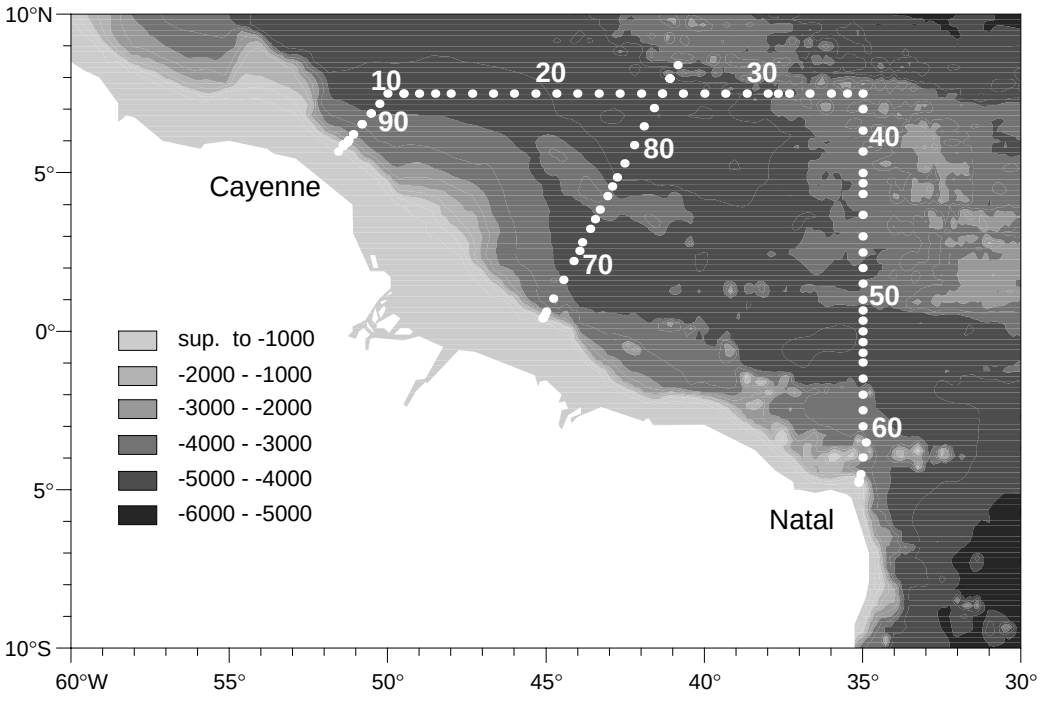

Figure 1. ETAMBOT stations (white dots) superimposed on the principal features of the bathymetry: the Mid Atlantic Ridge in the east, the Ceara Rise centred around 4°N–43°W and the equatorial channel, east of 35°W, centred around 1°S with depth greater than 4500 m.

The deeper CFC-11 core has a smaller eastward extension than the upper core (Fig. 2a): the topography plays an important role in blocking the eastward and southward progression of the lower DWBC. During the ETAMBOT 1 cruise, there is no real evidence of a northward deep recirculation west of the MAR as suggested by Plähn and Rhein (1997). The slanted section, which crosses the Ceara rise, leads to the same conclusion (figure not shown). Similar observations are inferred from CFC-11 and L-ADCP measurements during the ETAMBOT 2 cruise, in April–May 1996. Results on that cruise are displayed on two isopycnal levels corresponding to the UNADW $\sigma_2 = 36.88$; Fig. 3a, page 21) and the LNADW ($\sigma_3 = 41.50$; Fig. 3b, page 21).

UNADW circulation

During the ETAMBOT 2 cruise, CFC-11 and L-ADCP velocity maxima are trapped against the Continental Rise at 7°30'N, on the slanted section, and at 35°W (Fig. 3a). The maximum of CFC-11 concentration has increased, at 7°30'N and on the slanted section, compared to the ETAMBOT 1 cruise. Centred on 46°W at 7°30'N, the northward recirculating flow with high CFC-11 concentration, already observed during the ETAMBOT 1 cruise, is clearly visible.

On the slanted section there is a sharp front in the CFC-11 concentration south of the Ceara Rise, at 4°N. North of the Ceara Rise, one isolated CFC-11 core is observed near 5°N, associated with a southeastward flow. For both ETAMBOT cruises there is no evidence for a recirculated flow between the Ceara Rise and the MAR. This observation differs from the mean circulation scheme proposed at that depth by Friedrichs et al. (1994). On the other hand, there is a strong northwestward flow, centred on 2°N, during ETAMBOT 2 between the coastal DWBC and the Ceara Rise (Fig. 3a).

The most important difference between the ETAMBOT 1 and ETAMBOT 2 cruises appeared along the 35°W section. During the ETAMBOT 1 cruise, the CFC-11 pattern presents a north-south asymmetry with CFC-11 enriched cells preferentially concentrated south of the equator (not shown). This situation was already observed during the CITHER 1 cruise, in January–February 1993, when a CFC-11 core was observed around 3°S (Andrié, 1996). A very different situation is noticeable during the ETAMBOT 2 cruise as the most important CFC-11 core is observed in the 5°N–7°N latitude range. This maximum of concentration of CFC-11 corresponds to a moderate southward flow. It is difficult to link that core to the measurements along 7°30'N and along the slanted section.

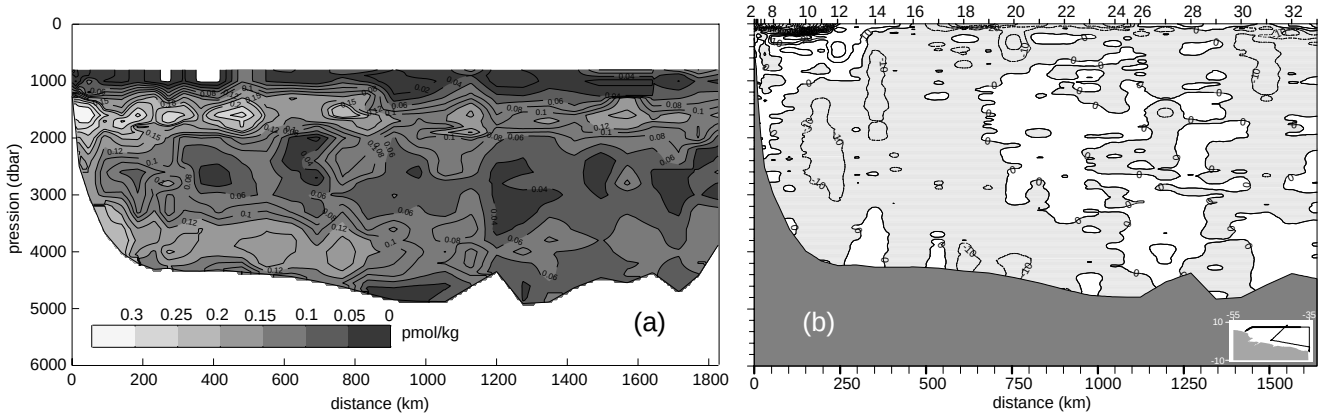

Figure 2. Vertical sections along 7°30'N during ETAMBOT 1 of (a) CFC-11 concentrations in pmol/kg, (b) the north-south component of L-ADCP measurements (negative values for southward flows, in grey) .

LNADW circulation

Rhein et al. (1995) and Andrié et al. (1997) have shown that the LNADW circulation within the DWBC is strongly constrained by the topography, mainly the Ceara rise, between 3°N and 6°N, and the flanks of the equatorial channel centred around 1°S (Fig. 1). Offshore, along the 7°30'N section, the ETAMBOT cruises exhibit high CFC-11 concentrations linked to re-circulated northward flows (between 44°W and 48°W during ETAMBOT 2, Fig. 3b).

Along the slanted section, the LNADW is revealed, on both side of the Ceara rise, by strong concentrations of CFC-11 and southeastward flows, at 2°N and 4°N (Fig. 3b). As it was also observed at the upper level core, L-ADCP measurements do not show evidence of northward recirculation west of the MAR. This is in contradiction with the assumption of Plähn and Rhein (1997). In the equatorial channel, at 35°W, a strong eastward flow is associated with high concentration of CFC-11. This flow seems to be a permanent feature of the deep circulation as it was observed in the repeated sections of the METEOR (Rhein et al., 1995, 1996) and during CITHER 1 (Andrié, 1996).

Acknowledgements

This investigation was supported by ORSTOM in the framework of the Programme National d'Etude de la Dynamique du Climat (PNEDC) and its WOCE/France subprogramme.

References

Andrié, C., 1996: Chlorofluoromethanes in the deep Equatorial Atlantic Revisited. In The South Atlantic: Present and Past Circulations. Wefer, G., Berger, W. H., Siedler, G., and Webb, D. J. (eds), Springer Verlag, 273-288.

Andrié, C., J. F. Ternon, M. J. Messias, L. Mémery and B. Bourlès, 1997: Chlorofluoromethanes distributions in the deep equatorial Atlantic during January–March 1993. Accepted in Deep Sea-Res.

Colin, C., B. Bourlès, R. Chuchla and F. Dangu, 1994: Western boundary current variability off French Guiana as observed from moored current measurements. Oceanol. Acta, 17, 4, 345–354.

Fischer, J., and M. Visbeck, 1993: Deep velocity profiling with self-contained ADCPs. J. Atmos. Oceanic Technol., 10(5), 764–773.

Fischer, J., and F. Schott, 1997: Seasonal transport variability of the Deep Western Boundary Current in the equatorial Atlantic. Accepted in J. Geophys. Res.

Friedrichs, M. A., M. S. McCartney, and M. M. Hall, 1994: Hemispheric asymmetry of deep water transport modes in the Western Atlantic. J. Geophys. Res., 99, C12, 25165–25179.

Hall, M. M., J. A. Whitehead and M. M. McCartney, 1994: Moored measurements of Antarctic Bottom Water at the equator. International WOCE Newsletter, No. 117, Nov. 1994, 5–9.

Johns, W. E., D. M. Fratantoni, and R. Zantopp, 1993: Deep western boundary current variability off north-eastern Brazil. Deep Sea-Res., 40, 2, 293–310.

Plähn, O., and M. Rhein, 1997: Measured and modeled CFC distribution of lower NADW in the Guiana Basin. Submitted to J. Geophys. Res.

Rhein, M., L. Stramma and U. Send, 1995: The Atlantic Deep Western Boundary Current: Water masses and transports near the equator. J. Geophys. Res., 100, 2441–2457.

Rhein, M., F. Schott, L. Stramma, J. Fischer, O. Plähn and U. Send, 1996: The Deep Western Boundary Current in the Tropical Atlantic: Deep Water distribution and circulation off Brazil. International WOCE Newsletter, No. 123, July 96, 11–14.

Richardson, P., 1994: Cross-equatorial flow of the Atlantic deep western boundary current. International WOCE Newsletter, No. 116, July 1994, 3–5.

Richardson, P. L., and W. J. Schmitz, Jr., 1993: Deep cross-equatorial flow in the Atlantic measured with SOFAR floats. J. Geophys. Res., 98, 8371–8387.

Schott, F., J. Fischer, J. Reppin, and U. Send, 1993: On mean and seasonal currents and transports at the western boundary of the equatorial Atlantic. J. Geophys. Res., 98, C8, 14353–14368.

Critical Control at Deep Ocean Passages

J. A. Whitehead, Department of Physical Oceanography, Woods Hole Oceanographic Institution, Woods Hole, USA. jwhitehead@whoi.edu

Flux of oceanic water masses is a fundamental quantity in physical oceanography, important to understanding aspects of the ocean's role in climate, flux of dissolved and particulate chemicals, and movement of biological species, (especially small organisms) in the ocean. Records of past circulation of deep and bottom water from isotope or skeletal analysis are valuable indicators of past climate variations. Flows found at the deepest saddle points between benthic ocean basins (Whitehead, 1989; Whitehead et al., 1974), yield some of the best measurements of volume flux, and produce deep ocean mixing estimates. They are frequently unidirectional as dictated by the source of bottom water from convection far upstream. If the interface between bottom and above-bottom water controls flux, flows should be in a state of critical (maximised) control (Whitehead et al., 1974) so speeds are equal to internal wave speeds (Gill, 1977). This dynamics (called "rotating hydraulics", Whitehead et al., 1974; Pratt and Lundberg, 1991) produces simple and inexpensive predictions of flux for these important benthic water masses. Unfortunately, verification has lagged as it requires extensive and expensive measurements. Moreover, earlier tests used differing approximations and methods (Bethoux, 1979; Borenäs and Lundberg, 1986) so accuracy determination was difficult. Here, flux predictions, admittedly overestimates, (Killworth, 1992; Killworth and McDonald, 1993; Killworth, 1994) are made for the eight most highly measured sill flows in the world oceans using one method (Whitehead, 1989) requiring only data from two CTD hydrocasts and bathymetric data. Comparison with estimates using current meters and geostrophic calculations gives ratios of prediction to measurement from 1.0 to 2.7.

Maps of the Atlantic, Pacific, and Indian Oceans (Fig. 1) with the 4000 m and 5000 m contours separating three shades of grey show that water below 5000 metres lies in distinct isolated basins. Typically, bottom water must rise to depths between 4000 and 5000 metres to flow into the next basin through the deepest connecting passageway, some are labelled in Fig. 1. Flows near the saddle point of those passages are found to be relatively unidirectional and steady. Table 1 contains some estimates of volume flux (from current meter and/or geostrophic calculations) through sill-shaped gaps.

For close to two decades, theory of abyssal ocean circulation pictured a continuous "western boundary current" in conjunction with recirculation gyres in the oceanic interior (Warren, 1981). Many predictions about the western-intensified current are in beautiful accordance with ocean observations. The theory works best for a deep homogeneous layer over a flat bottom in large ocean basins on a rotating, spherical earth. Below this layer, interbasin bottom water flow over saddle points must have dynamics

Table 1.Estimates of volume flux (Q_e), values of density difference ($\Delta\rho/\rho$), height (h), width (W), calculated Rossby Radius (R), and predicted volume flux (Q_p) for deep sills in the world's oceans which have measurements with current meters over a reasonable length of time, and/or geostrophic calculations supplemented with current meters. In three cases the width W is less than R and in the other five it is greater than R. Below these are some other estimates of volume flux over sills based on smaller amounts of geostrophic data.

Sill	Q_e (Sv)	$\Delta\rho/\rho$ $\times 10^4$	h (m)	W (km)	R (km)	Q_p (Sv)
Denmark Straits (Dickson et al., 1990)	2.9	3.0	580	350	14	3.8
Ceara Abyssal Plain (Hall et al., 1997)	2	0.5	430	700	65	4.6
Vema Channel (Speer and Zenk, 1993)	6	1.0	1540	446	25	16.3
Discovery Gap (Saunders, 1987)	0.21	0.1	600	80	4	0.21
Samoa Passage (Johnson et al., 1994)	6	0.3	1050	240	34	7
Vema Gap (Fischer et al., 1996)	2.1	0.5	1000	9	35	3.3
Faeroe Bank Channel (Saunders, 1990)	1.9	5.0	400	20	15	3
Romanche Fracture Zone (Polzin et al., 1996)	1	0.47	380	20	369	2.2
Bornholm Strait (Petrin and Walin, 1976)	0.02					
Iceland-Faeroe Passage (Steele et al., 1962)	~1					
Chain Fracture Zone (Polzin et al., 1996)	0.1					
Hunter Channel (Speer and Zenk, 1993)	0.7					
Charlie-Gibbs Fracture Zone (Saunders, 1994)	2.4					
Strait of Sicily (Grancini and Michelato, 1987)	0.6–0.8					
(Morel, 1971)	0.65					
(Molcard, 1972)	1.23					
(Garzoli and Maillard, 1975)	1.21					
Anagada-Jungfern Passage (Stalcup et al., 1975)	0.056					

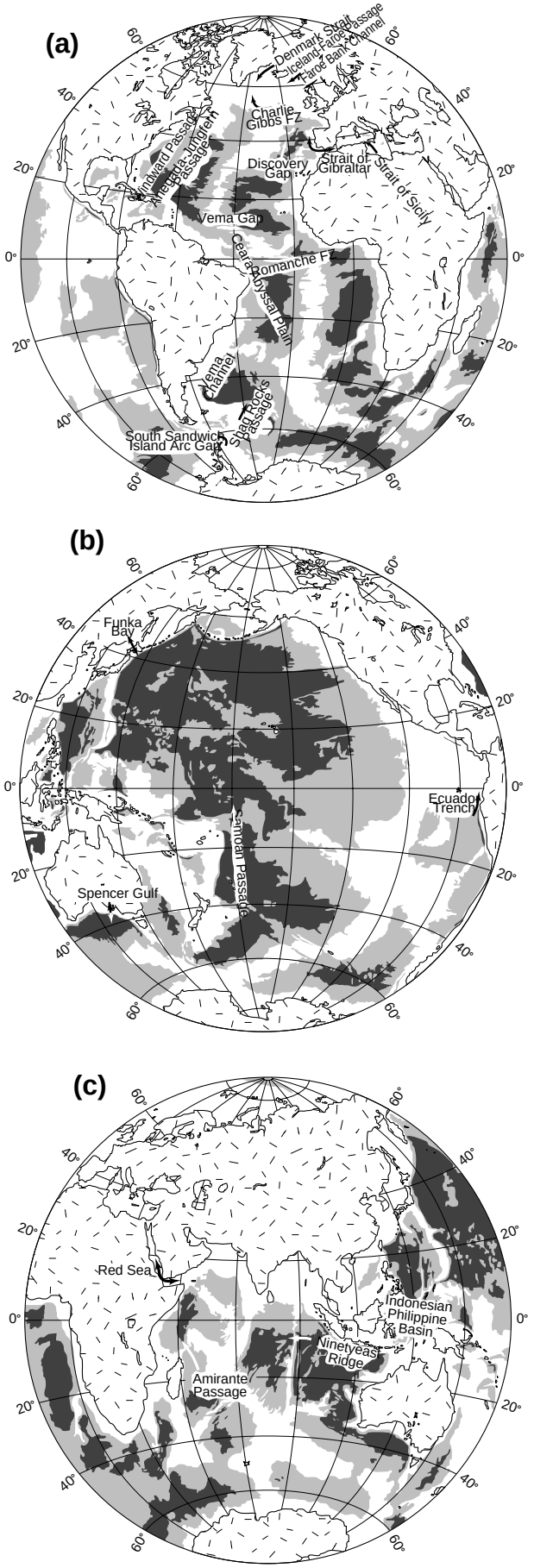

Figure 1. The oceans with depth below 5000 m in black, and above 4000 m in light grey. A number of known saddle points between deep basins (usually, but not always, in black) are labelled. (a) Atlantic Ocean. (b) Pacific Ocean. (c) Indian Ocean.

that differ from abyssal circulation theory for many reasons. First, the region is localised rather than global so f-plane approximations are more relevant than beta plane ones, especially since bathymetry has large local changes. Second, bottom shoaling also means that the flow must accelerate locally. Third, the vertical variation of density with depth must come into play since the fluid remains stably stratified in such regions. By retaining these three aspects, local rotation rate, acceleration, and stratification, one can find three dynamic relations (Whitehead et al., 1974; Gill, 1997): (1) a geostrophic relation, (2) the conservation of potential vorticity and (3) Bernoulli's law. By combining these, assorted solutions have been found. All involve considerable simplifications, for example continuous variation of density with depth is invariably abandoned and incorporating a simplifying assumption for upstream potential vorticity is virtually required to get uncomplicated solutions (Pratt and Lundberg, 1991). Even so, volume flux is usually predicted by complicated relations (Whitehead et al., 1974; Gill, 1977; Pratt and Lundberg, 1991), so we use the simplest one (zero potential vorticity (infinite depth upstream) and one layer in a rectangular channel, Whitehead et al., 1974) here:

$$Q_p = \frac{g\Delta\rho h^2}{4\rho Q \sin\theta'} \quad W > R\left(=\left(\frac{g\Delta\rho h}{2\rho(Q\sin\theta)^2}\right)^{1/2}\right)$$

otherwise

$$Q_p = \left(\frac{2}{3}\right)^{3/2} W\sqrt{g\Delta\rho}\left[h - \frac{\rho Q^2 \sin\theta^2 L^2}{2g\Delta\rho}\right]^{3/2}$$

where g is gravity, $Q\sin\theta$ is the local vertical angular earth rotation vector, h is height of the interface of the fluid above the floor of the channel, W is width of the channel, $\rho + \Delta\rho$ is density of a layer of fluid that is infinitely deep upstream, and a motionless fluid of density ρ lies above the flowing fluid layer. Such flux differs by less than 22% from that with upstream depth constant (Whitehead, 1989).

Do these formulae reliably predict oceanic measurements like those listed in Table 1? A consistent method (Whitehead, 1989) was used in 1988, to generate values of $\Delta\rho$,h, and L (values of *g* and θ are obvious) using features of the bifurcation diagram in Fig. 2. Predictions were 1.6 to 4.2 times greater than observations for the only four sills with sufficient current meter measurements and geostrophic calculations to estimate volume flux. Here, we review three predictions at old locations which have new measurements. The fourth old location (Whitehead, 1995) is deleted as the current source region was not obvious. Five new current meter-based estimates augmented with geostrophic

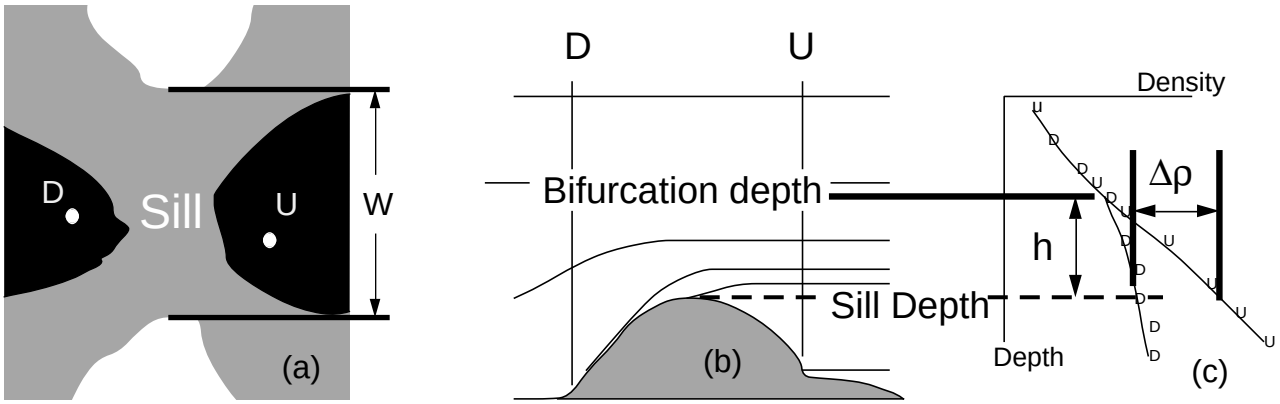

Figure 2. A sketch of the major features of critical control at a sill and outline of the method to produce values to use in the equations. (a) Plan view of bathymetry near a saddle point (sill) (b) Elevation view of a saddle point with isopleths of constant density sketched in the asymmetry of the isopleths denote flow from right (upstream U) to left (downstream Δ). (c) Two stations of density versus depth, one in the upstream basin and one downstream. Stations must be in basin interiors as sketched in (a) so that interior density is sampled. At some height h above the sill depth, upstream and downstream curves of density versus depth bifurcate. Width W is bathymetric width at bifurcation depth (a) and Δ_ρ is upstream and downstream density difference at sill depth (b). Using g=9.8 m/s and local latitude, values were used in the above equations to predict volume flux Q_p in Table 1.

calculations come from major ocean programmes. Most estimates required a large effort, with numerous moorings set for long intervals using two or more oceanographic cruises.

Here we compare the eight sets of oceanic measurements against predictions repeating the simple method outlined above. Bifurcation diagrams and bathymetric information of seven have been presented (Whitehead, 1995) elsewhere. The eighth is in press (Whitehead, 1997). Predicted volume fluxes are displayed along with estimates in Table 1 and Fig. 3. Ratios of prediction to estimates have decreased to the range from 1.0 to 2.7, the decrease from 4.2 being from better ocean data. Essentially the simple predictions are within the range of volume flux estimates over a broad range of parameters.

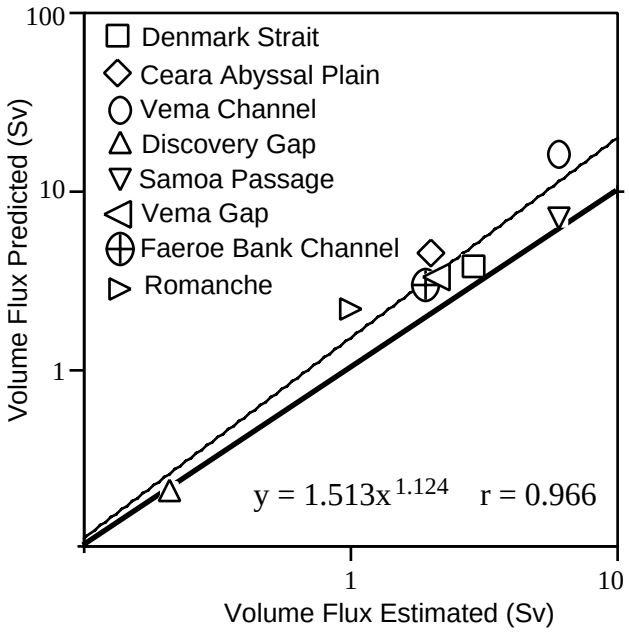

Figure 3. Comparison of Q_p with Q_e for the eight cases with best measurements listed in Table 1. The light line is a least squares power law fit to the data. The equation is the best fit equation, and r is the least squares regression value. The heavy line locates perfect fit between prediction and measurement. The predictions and estimates form a linear trend over a wide range of parameters. Predictions consistently form an overestimate as expected.

Of course, disagreement is still sizeable and there are many sources of difference. The admittedly simplified theory is both an overestimate (Whitehead, 1989; Whitehead et al., 1974; Gill, 1977; Pratt and Lundberg, 1991; Killworth, 1992; Killworth and McDonald, 1993; Killworth, 1994) and ignores continuous stratification, friction, complex bathymetry and turbulence. None have been incorporated in theories of rotating hydraulic control of unidirectional flow over a sill. In addition, measurements, never completely resolve a current, either in space or time. Errors of both theoretical shortcomings and measurement resolution each probably exceed 30%.

In summary, this simple and cheap method can apparently produce a crude prediction of flux over a range of parameters using only archived data in many regions. Additional data would clarify many questions concerning critical control, friction, and the many simplifications needed to analyse rotating hydraulics. With improvement this may produce an accurate, cheap estimate of flow through numerous oceanic sills.

References

Bethoux, J. P., 1979: Budgets of the Mediterranean Sea. Their dependence on the local climate and the characteristics of the Atlantic waters. Oceanol. Acta., 2, 157–163.

Borenäs, K., and P. Lundberg, 1986: On the Deep-Water Flow Through the Faeroe Bank Channel. J. Fluid Mech., 167, 309–326.
Dickson, R. R., E. M. Gmitrowicz, and A. J. Watson, 1990: Deep Water Renewal in the Northern Atlantic. Nature, 344, 848–850.
Fischer, J., M. Rhein, F. Schott, and L. Stramma, 1996: Deep Water Masses and Transports in the Vema Fracture Zone. Deep-Sea Res., 43, 1067–1074 (1996).
Garzoli, S., and Maillard, 1976: Hydrologie et circulation hivarnales dans les canaux de Sicile et de Sardaigne. C. Rapp. Int. Lab. Oceanogr. Paris. Museum National d'Histoire Naturelle, Paris, 21 pp.
Gill, A. E., 1977: The hydraulics of rotating channel flow. J. Fluid Mech., 80, 641–671.
Grancini, G. F., and Michelato, 1987: Current Structure and variability in the Strait of Sicily and adjacent area. A. Annales Geophysicae, 5B, (1) 75–88.
Hall, M. M., M. E. McCartney, and J. A. Whitehead, 1997: Antarctic Bottom Water Flux in the Equatorial Western Atlantic. J. Phys. Oceanogr. In press.
Killworth, P. D., 1992: Flow properties in rotating, stratified hydraulics. J. Phys. Oceanogr., 22, 997–1017.
Killworth, P., 1994: On reduced-gravity flow through sills. Geophys. Astrophys. Fluid Dyn., 75, 91–106.
Killworth, P. D., and N. R. McDonald, 1993: Maximal reduced-gravity flux in rotating hydraulics. Geophys. Astrophys. Fluid Dyn., 70, 31–40.
Morel, A., 1971: Caracteres hydrologiques des eaux echanges entre le bassin oriental et le bassin occidental de la Mediterranée. Cah. Oceanogr., 22, 4, 329–42.
Molcard, R., 1972: Preliminary results of current measurements in the Strait of Sicily in May 1970. Proc. Saclant Conf., 7, 82–95.
Petrin, O., and G. Walin, 1976: Some observations of the deep flow in the Bornholm Strait during the period June 73–December 74. Tellus, 28, 74–87.
Polzin, K. L., K. G. Speer, J. M. Toole, and R. W. Schmitt, 1996: Intense Mixing of Antarctic Bottom Water in the equatorial Atlantic Ocean. Nature, 380, 54–57.
Pratt, L. J., and P.A. Lundberg, 1991: Hydraulics of rotating strait and sill flow. Ann. Rev. Fluid Mech. 23, 81–106.
Rudnick, D. L., 1997: Direct Velocity Measurements in the Samoan Passage. J. Geophys. Res., 102, 3293–3302.
Saunders, P. M., 1987: Flow through Discovery Gap. J. Phys. Oceanogr., 17, 631–643.
Saunders, P. M., 1990: Cold Outflow from the Faeroe Bank Channel. J. Phys. Oceanogr., 20, 29–43.
Saunders, P. M., 1994: The flux of overflow water through the Charlie-Gibbs Fracture Zone. J. Geophys. Res., 99, 12343–12355.
Speer, K. G., and W. Zenk, 1993: The flow of Antarctic Bottom Water into the Brazil Basin. J. Phys. Oceanogr., 23, 2667–2682.
Stalcup, M. C., W. G. Metcalf, and R. G. Johnson, 1975: Deep Caribbean inflow through the Anegada-Jungfern Passage. Marine Res. (Suppl.), 33, 15–35.
Steele, J. H., J. R. Barrett, and L. V. Worthington, 1962: Deep currents south of Iceland. Deep-Sea Res., 9, 465–474.
Warren, B. A., 1981: Deep Circulation of the World Ocean. In Evolution in Physical Oceanography, pp. 6-41, Warren, B. A. and Wunsch, C., Eds., MIT Press.
Whitehead, J. A., 1989: Internal hydraulic control in rotating fluids – applications to oceans. Geophys. Astrophys. Fluid Dyn., 48, 169–192.
Whitehead, J. A., 1995: Critical control by Topography - Deep Passages, Straits and Shelf Fronts. In Topographic Effects in the Ocean, pp. 141–156, Müller, P., and Henderson, D. eds., SOEST Special Publication.
Whitehead, J. A., 1997: Critical Control by Ocean Passages. Rev. Geophys. In press.
Whitehead, J. A., A. Leetmaa, and R. A. Knox, 1974: Rotating hydraulics of strait and sill flows. Geophys. Fluid Dyn., 6, 101–125.

Topography and Barotropic Transport Control by Bottom Friction

William K. Dewar, Department of Oceanography, Florida State University, Tallahassee, USA. bill@ocean.ocean.fsu.edu

Introduction

Saunders and King (1995), in an analysis of WOCE cruise A11 South Atlantic observations, have inferred the existence of a major anticyclonic flow. This flow appears to be centred on the so-called Zapiola Drift, a bottom topographic feature consisting of a local high. The transport associated with the anticyclone was estimated to be roughly 100 Sv, and bottom flows on the order of 10 cm/s were found. Evidence from other sources (Flood and Shor, 1988; Weatherly, 1993) argue the Zapiola anticyclone is a mean feature of the circulation in the area. Here we present some simple theoretical ideas which potentially apply to the Zapiola anticyclone. A fuller accounting can be found in Dewar (1997).

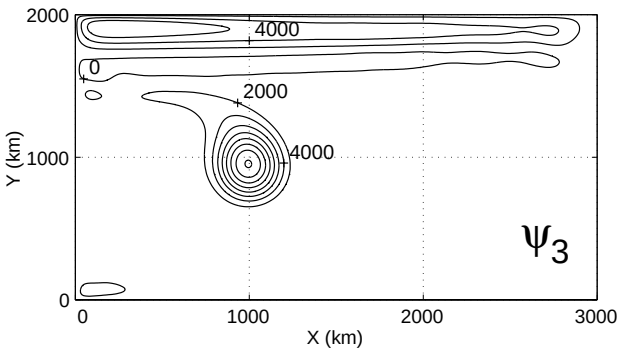

Figure 1. Third layer streamfunction from a quasi-geostrophic model. A strong anticyclonic circulation occurs over a Gaussian bump. CI = 2000 m^2/s.

Theoretical development

The equations of motion for a quasigeostrophic two layer ocean are:

$$J(\psi_i, q_i) = \frac{f_0 w_e}{H_1}\delta_{i,1} + R\nabla^2 q_i - D\nabla^2\Psi_2\delta_{i,2}$$

$$q_i = \beta y + \frac{f_0{}^2(\Psi_2 - \Psi_1)(-1^{i+1})}{g'H_i} + \frac{f_0 h_b \delta_{i,2}}{g'H_2} \qquad (1)$$

where we restrict our attention to spatial scales well in excess of the deformation radius, and therefore the explicit appearance of relative vorticity has been eliminated. Notation is standard, $\delta_{i,j}$ is the Kronecker delta function, the bottom topography appears via the 'h_b' in q_2 and bottom friction is represented by the bottom drag coefficient D. The eddies are parameterised by means of down-gradient potential vorticity diffusion at a rate governed by R. Note that this implies some mixing of the topographic contribution to q_2 in the lower layer.

If it is assumed in general that the eddies and bottom friction are 'weak', the approximate solution of (1,i=2) is that layer 2 potential vorticity and streamfunction are functionally related. A feature as tall as the Zapiola Drift easily generates regions of isolated lower layer potential vorticity, about which the eddy stresses parameterised by R can accelerate a deep flow. Such dynamics determine the functional $q_2 - \Psi_2$ relationship to be linear. Substitution of this into (1,i=1) and some straightforward, if tedious, algebra, demonstrates that, roughly speaking, if the 'barotropic geostrophic contours', $f/(H-h_b)$, are closed, the upper layer also generates isolated regions where eddy accelerations can operate. An area integration of (1,i=1) over such a zone then yields a generalisation of Welander's (1968) result for a barotropic fluid. In simple cases, the analytical solution is available and one obtains the result in the limit of weak bottom friction that the depth integrated transport is inversely proportional to D. Thus weak bottom frictions generate large transports.

Numerical experiments

The basic ideas outlined above were tested using a three layer, eddy-resolving numerical model (Holland, 1978). As an example, in Fig. 1 the transport streamfunction in the deepest layer, from an experiment forced at the surface with a typical sinusoidal anticyclonic Ekman pumping profile, is shown. This streamfunction represents the average of the last 10 years of a 40 year run. An anticyclonic circulation appears there, at the location of a 800 m Gaussian bump. The amplitude of the third layer transport is roughly 70 Sv. Comparable results have been found for varying topographic amplitudes, bottom frictions and cyclonic wind stresses.

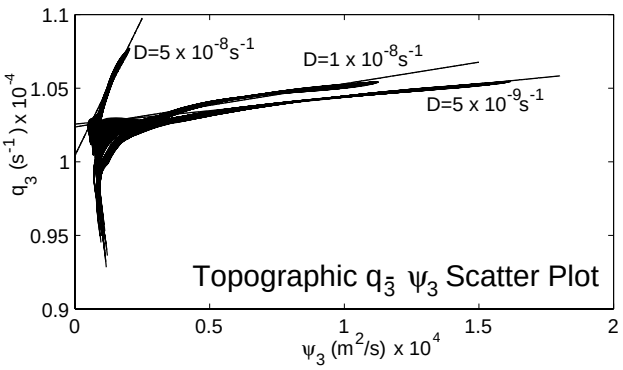

Figure 2. Numerically generated $q_3 - \Psi_3$ relationships from an eddy-resolving qg numerical model. Three experiments employing differing values for D are shown.

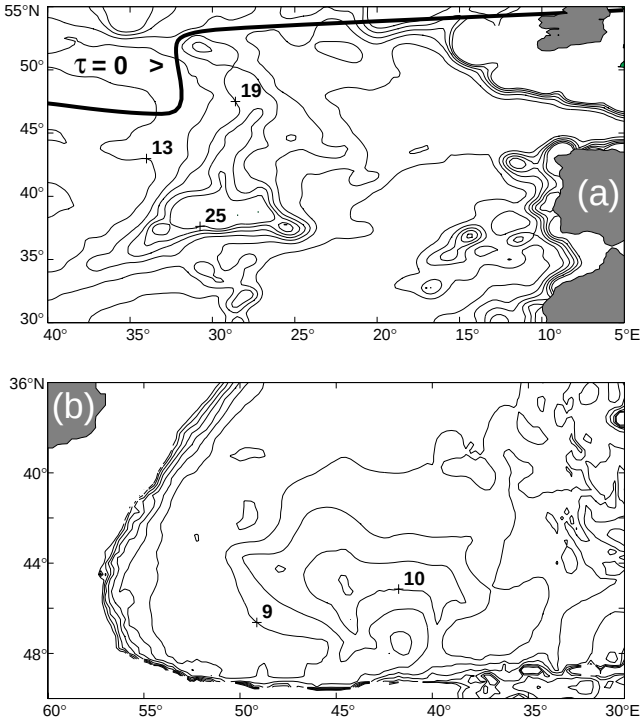

Figure 3. Contours of $f/(H-h_b)(\times 10^9)$ for (a) the Azores Plateau, and (b) the Zapiola Drift, are shown. Closed contours exist for both.

In Fig. 2, we show the numerically generated $q_3 - \Psi_3$ relationship from the area of the bottom topography for the experiment shown in Fig. 1. Three different experimental results are plotted, where the experiments are differentiated only by their value of bottom drag D. Note the essentially linear $q_3 - \Psi_3$ relationship, and the change in slope as a function of D consistent with the above theoretical predictions.

Applications

The above theory suggests that regions of closed barotropic $f/(H-h_b)$ contours are candidate areas for application of the present ideas. To this end, Fig. 3 shows $f/(H-h_b)$ for two areas in the Atlantic; namely, the Azores Plateau in the North Atlantic, and the Zapiola Drift. Note both are areas of closed $f/(H-h_b)$. Observations appearing elsewhere argue the Azores Plateau potentially hosts an anticyclonic circulation (see, e.g. Pollard et al., 1996), whose amplitude is probably no more than 15 Sv. We emphasise here, however, that the Azores Plateau is centred on the Mid-Atlantic Ridge and, within the confines of the present theory, would be characterised by a much greater value for D. In contrast, the Zapiola Drift, being considerably less rough, would be characterised by a much smaller D, and thus larger transports. This, plus regional differences in the amplitude of the eddy field (the Zapiola Drift neighbours the region of the Brazil-Malvinas current extension), are suggested as the main reasons for differences between the Azores Plateau and the Zapiola Drift, and for the existence of the 100 Sv Zapiola anticyclone.

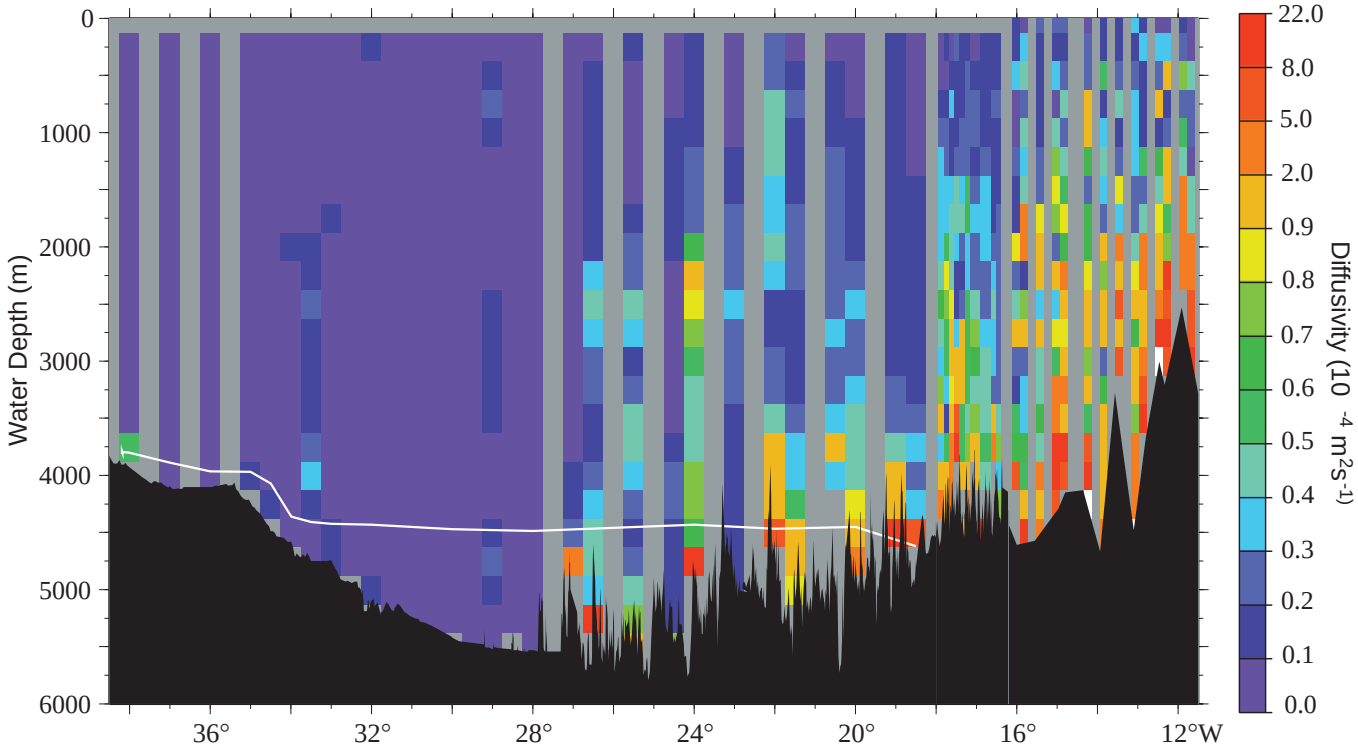

Toole et al., page 26, *Figure 2. Depth-longitude section of diapycnal diffusivity (units of* $m^2\ s^{-1}$*) inferred from velocity microstructure observations. Diffusivity estimates are displayed in 200–250 m vertical blocks for each station; no horizontal averaging or interpolation was performed. Data from the two 1996 transects have been combined with selected observations from the 1997 cruise without regard to latitude. Error bars on these estimates from statistical and measurement uncertainties are roughly a factor of two times the reported values. The high-resolution underway bathymetry is shown for the 1996 data; comparable data from 1997 have yet to be processed. The bottom shading east of 16°W is based on water depth at the selected 1997 station locations.*

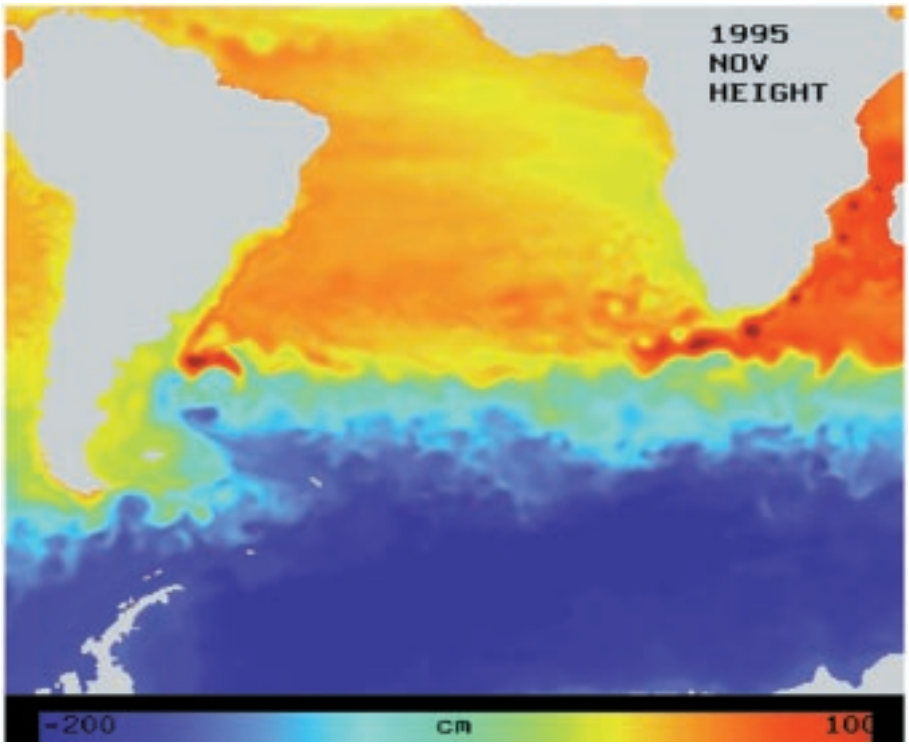

McClean et al., page 5, *Figure 1. Snapshot of sea surface height (cm) from POP.*

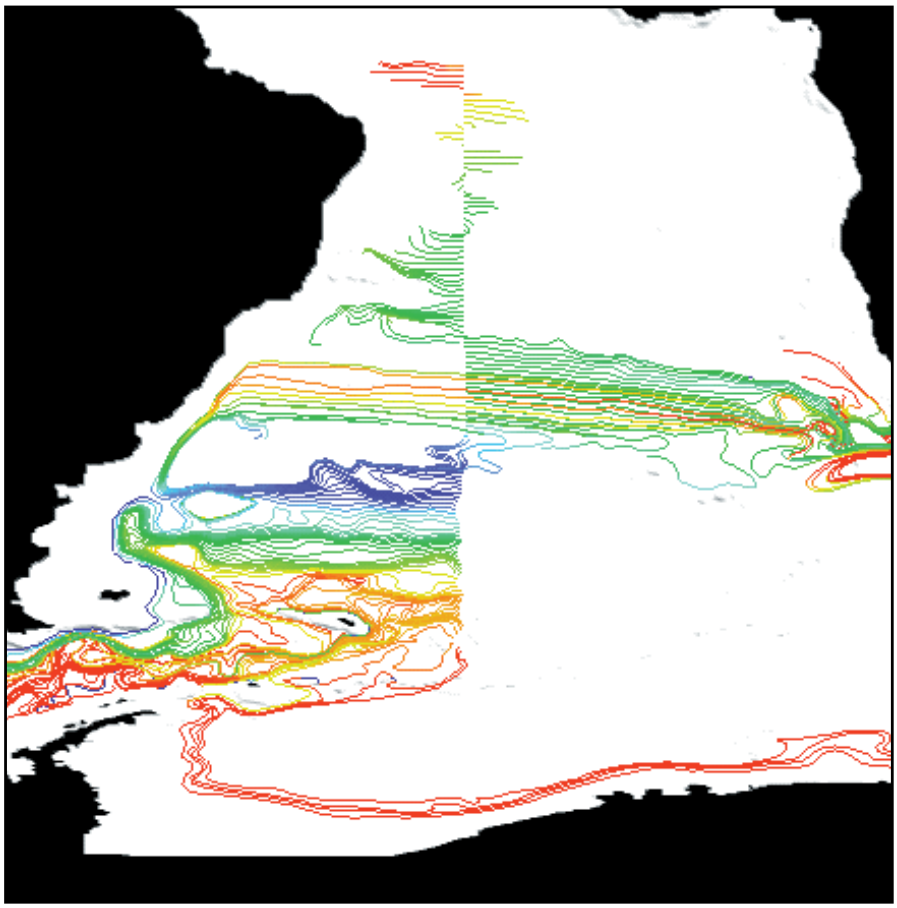

McClean et al., page 6, *Figure 4. Trajectories (coloured by salinity values) integrated backwards in time using 10-year mean POP velocities from 1100 and 25°W. Minimum and maximum salinities are blue (34.5) and red (34.7), respectively.*

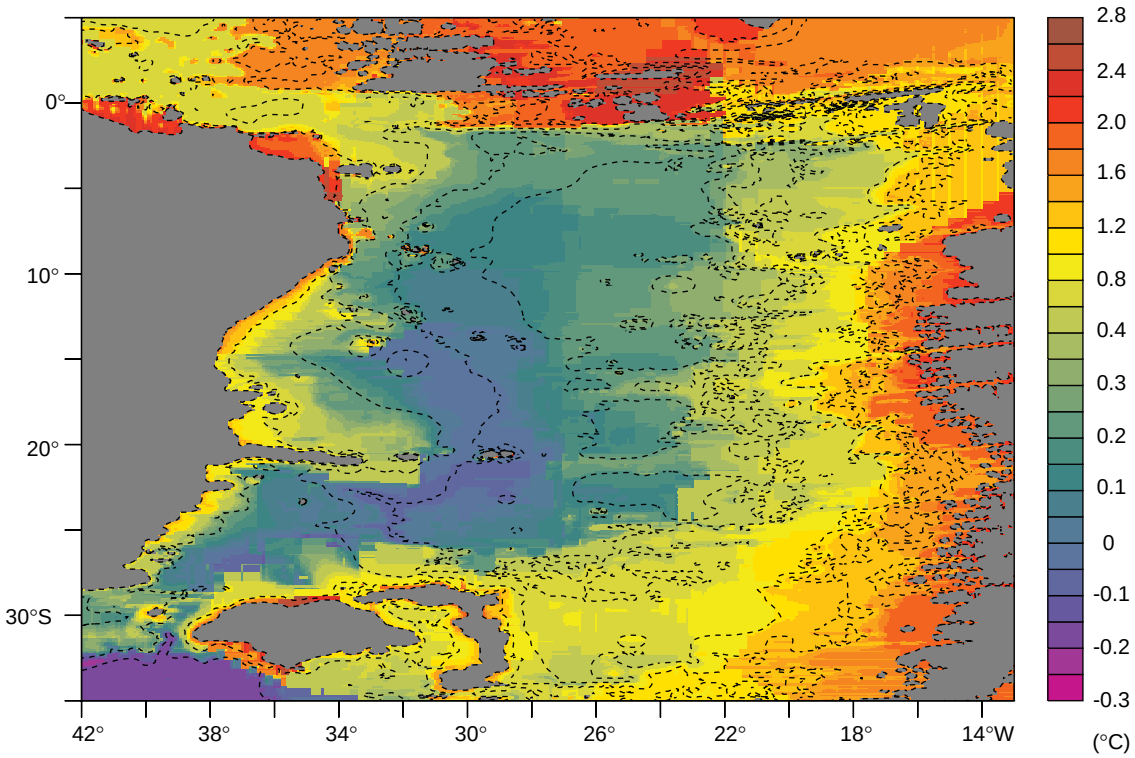

Morris et al., page 23, *Figure 2. Map of potential temperature (°C) at the sea floor made from CTD data (location shown in Fig. 1). Bathymetry is overlaid and depths shallower than 3500 m are shaded.*

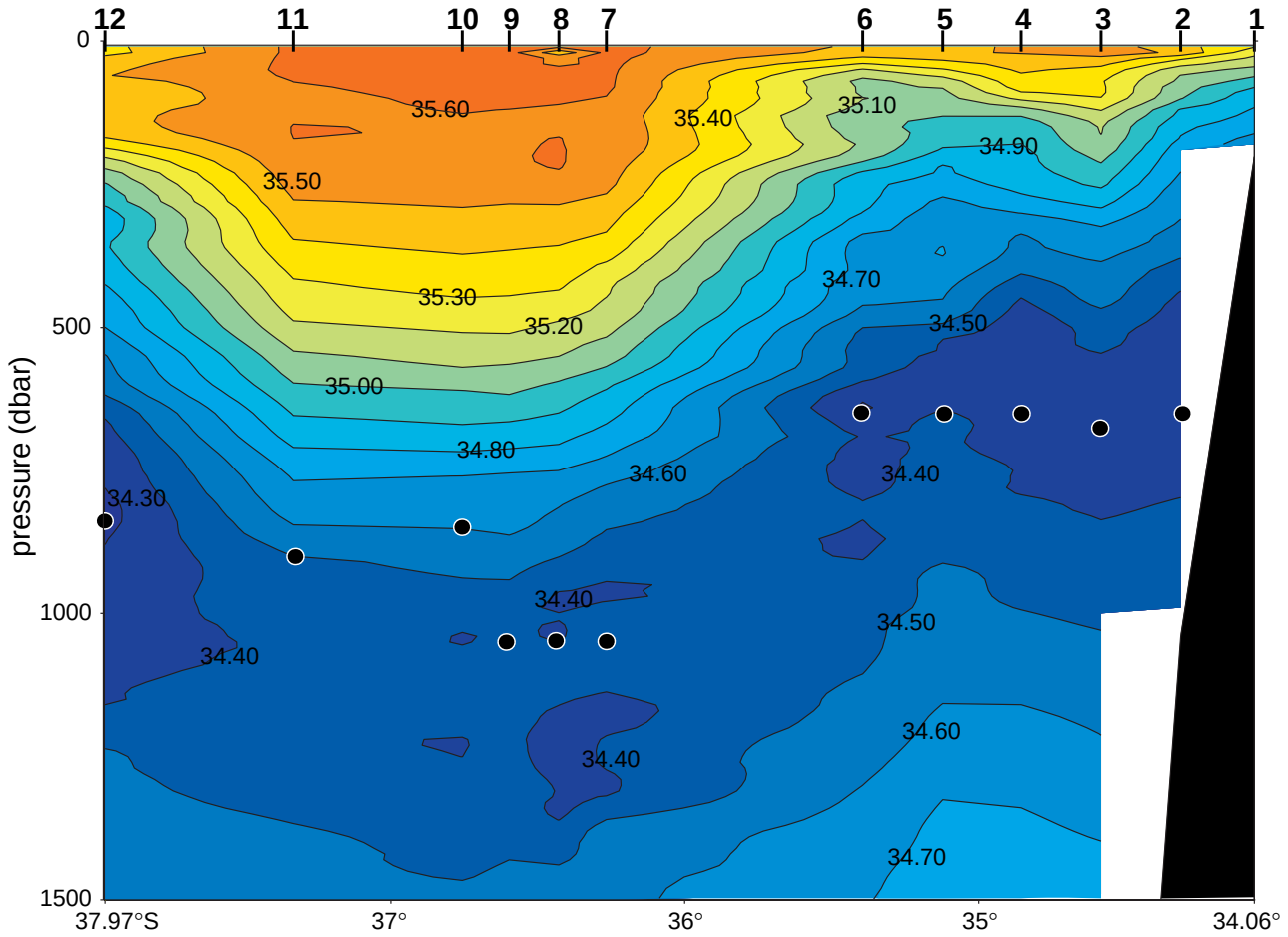

Boebel et al., page 32, *Figure 3. Section 'a' (Fig. 1): Salinity distribution as recorded during Polarstern cruise ANT XIV/4. CTD casts are indicated by numbers on the upper axis. Note the change of course at station No. 6. Solid dots indicate the launch position and estimated depth of RAFOS floats seeded during the cruise.*

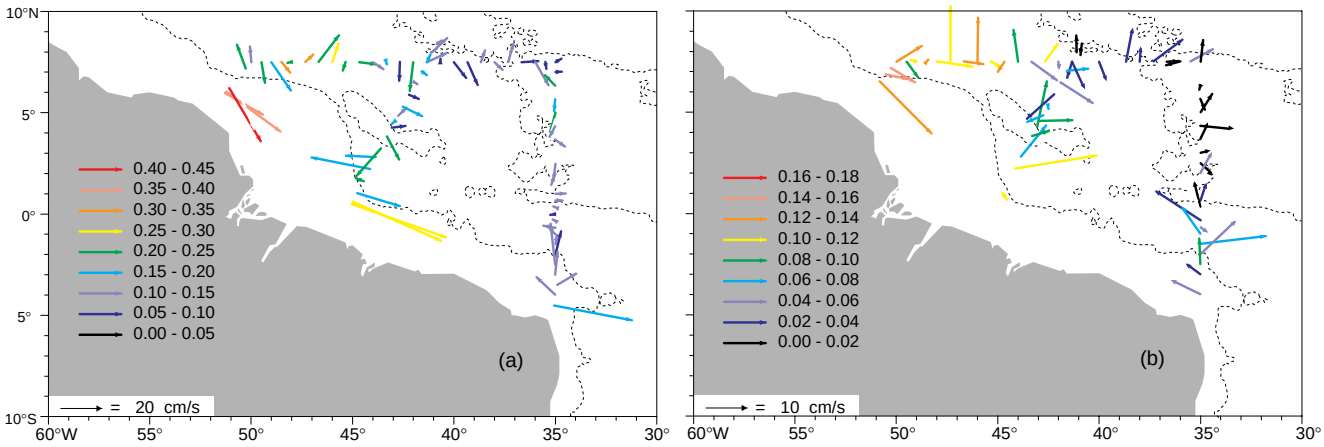

Andrié et al., page 12, *Figure 3. (a) ETAMBOT 2: Horizontal mapping of the velocity field inferred from the L-ADCP measurements on the* $\sigma_2 = 36.88$ *isopycnal (corresponding to the SUNADW, around 1600 m). Colours of the velocity arrows correspond to the sampled CFC-11 concentrations, using the colour scale shown on the right. The 4000 m isobath is shown. (b) same caption but for the* $\sigma_3 = 41.50$ *isopycnal (corresponding to the LNADW, around 3800 m). Note that the velocity scale is twice the scale used for the upper level.*

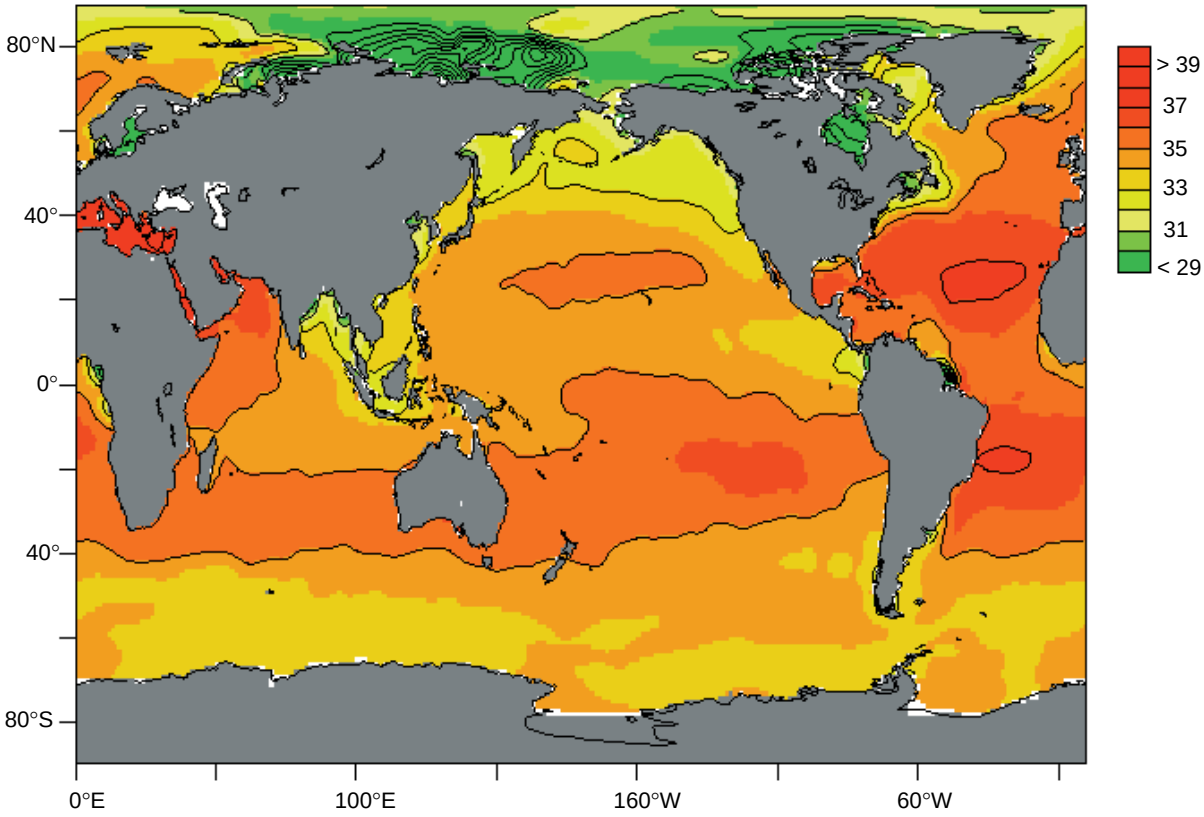

Gordon, page 37, *Figure 1. Annual mean salinity (psu) at the sea surface (from Levitus et al., 1994 (http://ferret.wrc.noaa.gov/fbin/climate.server). The Atlantic Ocean surface water north of 30°S is more saline than that of the Pacific and Indian Oceans. The contrast is most striking in the northern hemisphere, where the Atlantic and Pacific salinity difference in the subtropical region is approximately 2.0 psu and even larger differences occur within the eastern half of the temperate and subpolar regions. This difference is closely linked to the formation of North Atlantic Deep Water and is an integral part of the global-scale thermohaline circulation.*

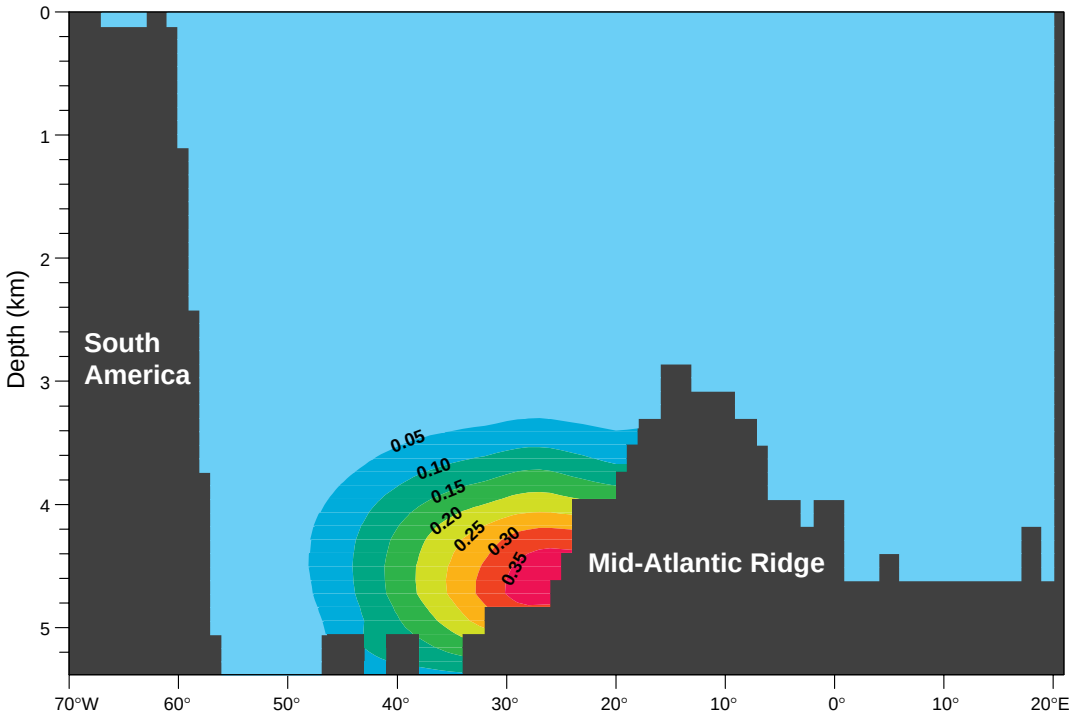

Murphy et al., page 10, *Figure 4. Zonal distribution of the model's deep WSDW tracer at 45°S.*

References

Dewar, W. K., 1997: Topography and barotropic transport control by bottom friction. J. Mar. Res., submitted.

Flood, R., and A. Shor, 1988: Project Mudwaves: a coordinated study of abyssal bedforms and sedimentation in the Argentine Basin. Trans. Amer. Geophys. Union, 69, 1258.

Holland, W., 1978: The role of mesoscale eddies in the general circulation of the ocean – numerical experiments using a wind-driven quasi-geostrophic model. J. Phys. Oceanogr., 8, 363–392.

Pollard, R., M. Griffiths, S. Cunningham, J. Read, F. Perez, and A. Rios, 1996: Vivaldi, 1991: A study of the formation, circulation and ventilation of Eastern North Atlantic Central Water. Prog. Oceanogr., 37, 167–192.

Saunders, P., and B. King, 1995: Bottom currents derived from a shipborne ADCP on WOCE cruise A11 in the South Atlantic. J. Phys. Oceanogr., 25, 329–347.

Weatherly, G., 1993: On deep-current and hydrographic observations from a mudwave region and elsewhere in the Argentine Basin. Deep-Sea Res., 40, 939–961.

Welander, P., 1968: Wind-driven circulation in one- and two-layer oceans of variable depth. Tellus, 20, 1–15.

Diapycnal Mixing Estimated from Advective Budgets in the Deep Brazil Basin

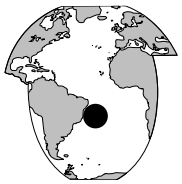

Michele Morris, Nelson Hogg and W. Brechner Owens, Woods Hole Oceanographic Institution, Woods Hole, USA. mym@bucky.whoi.edu

Introduction

The time scale for communication between the deep ocean and the surface via vertical processes, is a poorly understood issue related to climate variability. Determining accurate values for vertical mixing rates is of utmost importance to the development of climate models that attempt to simulate low frequency fluctuations in the ocean-atmosphere system. One of the objectives of the Deep Basin Experiment is to quantify deep diapycnal mixing rates and to provide insight into the relative intensity of boundary and interior mixing (Hogg et al., 1996). The small area and simple geometry of the Brazil Basin are well suited for this purpose. There are a limited number of deep passages connecting the basin to others and it is practical to subdivide the basin into smaller enclosed regions using hydrographic sections. Fig. 1 shows the extensive hydrographic dataset available to us at the present time.

Antarctic Bottom Water (AABW) follows a generally northward path through the Brazil Basin, entering and exiting through deep passages. The densest water flowing into the basin through the Vema and Hunter channels has no deep outlet and the isotherms defining the upper extent of this water type intersect the seafloor within the basin. This gradual northward warming of water flowing close to the bottom is illustrated in the bottom potential temperature map shown in Fig. 2 (page 20). Downward diffusion of heat is required to maintain a steady-state balance. Previous basin-averaged vertical diffusivities deduced from large scale mass and heat budgets give $\kappa = O(10^{-4}) \mathrm{m}^2\,\mathrm{s}^{-1}$ (Hogg et al., 1982), an order of magnitude larger than those calculated from direct ocean microstructure measurements (Polzin et al., 1997).

Mixing of heat along isopycnals may be misinterpreted as a cross-isopycnal heat flux if advective budgets are calculated over a volume bounded by an isotherm and isothermal and isopycnal surfaces do not coincide. In part to investigate the importance of this term, the calculation of Hogg et al., 1982, is revisited. Additionally, more comprehensive data coverage provided by recent WOCE hydrographic sections will improve estimates of κ. In this article, advective budgets for heat and density are examined over regions bounded by isotherms and isopycnals, respectively. If along-isopycnal mixing of heat is important and other thermodynamic mixing effects are not, then one would expect smaller turbulent transports from the latter calculation.

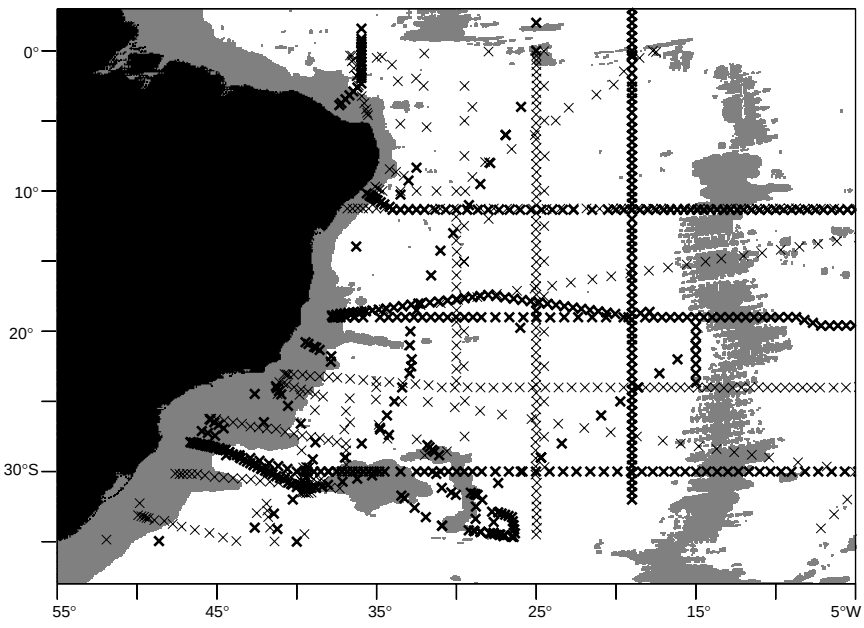

Figure 1. Locations of the historical (light x) and WOCE CTD stations (dark x) used in this study are plotted over bathymetry (depths shallower than 3500 m are shaded light grey).

Methodology

Heat budget

The diapycnal diffusivity coefficient κ is inferred using the following steady-state heat balance:

$$\int_V \nabla \cdot (\tilde{u}\theta) dV = \int_V (\kappa\theta_z)_z dV, \qquad (1)$$

where V is a volume bounded at the top and bottom by isothermal surfaces or the ocean floor. This equation can be rewritten as:

$$\int_A \tilde{u}\theta \cdot \tilde{n} dA = \left[\overline{\kappa\theta_z} A\right]_{top} - \left[\overline{\kappa\theta_z} A\right]_{bottom}. \qquad (2)$$

where A refers to the surface area of volume V and the overbar indicates an areal average. Advective fluxes appearing on the left hand side of (1) have been directly measured from current meter arrays in deep passages, and through the vertical interfaces using a vertical velocity obtained by vertical integration from the ocean floor assuming the velocity field is non-divergent. Diffusive fluxes $\overline{\kappa\theta_z}$ are further approximated as $\bar{\kappa}\overline{\theta_z}$. Interface averaged values for θ_z and interface areas are obtained from CTD data with cast locations shown in Fig. 1.

Density coordinates

An alternate estimate of $\bar{\kappa}$ is obtained from the continuity equation (Davis, 1994). The same steady-state tracer balance as in equation (1) is obtained, but with θ replaced by potential density σ or neutral density γ. In these coordinate systems, the contribution from lateral eddy fluxes is minimised as the bounding surfaces are isopycnals or neutral surfaces. Thus one would expect a reduction of turbulent transport (and $\bar{\kappa}$) if lateral mixing contributed significantly to the heat budget calculated in θ coordinates. The density budgets are complicated by density production terms due to non-linearities in the equation of state (e.g. Davis, 1994 and McDougall, 1987). These terms have been estimated and are small relative to the divergence of buoyancy fluxes.

Results

Budget results for the densest layer (θ<0°C corresponding to σ_4>46.06 in the Vema Channel) are illustrated in Fig. 3. There are 2.4 Sv of water colder than 0°C entering the Brazil Basin via the Vema channel which is the only pathway into the basin for the densest AABW. As water of this temperature does not exit the basin, there must be a volume transport of equal magnitude through the interface bounding the volume to conserve mass. The basin averaged vertical diffusivity inferred from the heat budget is $3.3 \pm 0.8\,cm^2\,s^{-1}$, which is indistinguishable from κ inferred using either potential or neutral density coordinates ($\bar{\kappa} = 2.9 \pm 0.9\,cm^2\,s^{-1}$ and $2.3 \pm 0.7\,cm^2\,s^{-1}$ respectively). There is a slight decrease in κ if density rather than θ coordinates are used, but the differences are not statistically

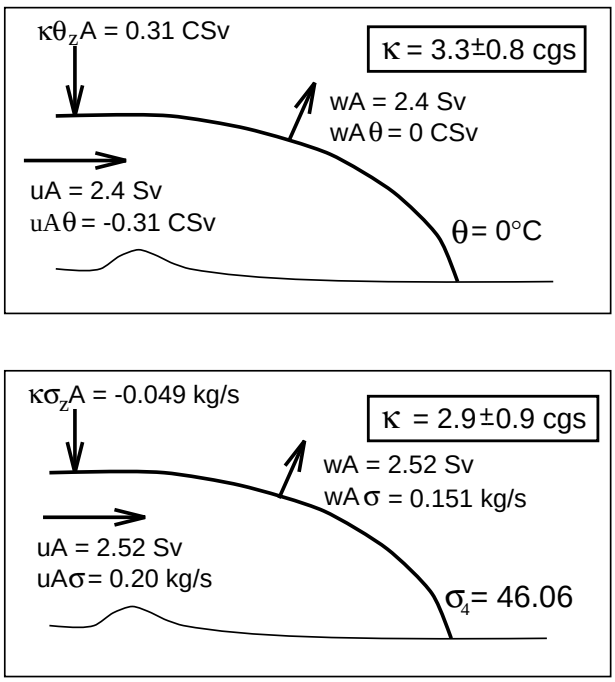

Figure 3. Results of two advective budget calculations over the densest AABW layer. Upper panel: Heat budget results over the layer bounded by θ = 0°C, Lower panel: Results from the budget calculation using density coordinates over the layer bounded by σ_4 = 46.06. The variable σ is a σ_4 anomaly $(\sigma_4 - 46)$.

significant within 95% confidence limits.

Diffusivity coefficients for three layers within the AABW are summarised in Table 1. The middle and top layer diffusivities are also insensitive to the coordinate system. Values of $\bar{\kappa}$ deduced from θ and σ_4 conservation equations agreed within uncertainty bounds.

Discussion

This calculation implies that lateral eddy fluxes of heat along isopycnals do not contribute significantly to the heat flux across the 0°C surface. This conclusion is similar to findings from a previous study by McDougall and Whitehead (1984) who also estimated the relative importance of different mixing process in modifying Antarctic Bottom

Table 1.

Layer Definition	Vertical diffusivity $\bar{\kappa}\left[cm^2 s^{-1}\right]$
θ<0°C	3.3±0.8
σ_4 >46.06	2.8±0.9
γ>28.27	2.3±0.7
0<θ<0.8°C	2.5±0.8
45.98< σ_4 <46.06	2.8±0.9
0.8<θ<1.6°C	3.0±0.7
45.90< σ_4<45.98	2.8±0.7

Water. Using a different methodology and studying transformation processes mainly in the North Atlantic, they found that diapycnal mixing dominated lateral mixing, which they also found to be insignificant.

The revised basin-averaged $\overline{\kappa}$ over the bottom layer is smaller than Hogg et al.'s 1982 estimate, but still higher than interior diffusivity coefficients obtained from direct estimates. Intense mixing at the Vema channel outflow may explain part of this discrepancy.

Mixing across the $\theta = 0.8°C$ interface is also reduced relative to the previous estimate. The middle layer extends over rough bathymetry where small-scale measurements show enhanced mixing, resulting in basin-averaged turbulent transports that are elevated above interior values, (Polzin et al., 1997). Diapycnal mixing across the $\theta = 0.8°C$ surface is a little over twice as large as the most recent basin-averaged estimate from ocean microstructure measurements (Toole et al, 1997).

Acknowledgements

We thank W. Smethie, Jr. (LDEO), G. Siedler and T. Müller (both at Institut für Meereskunde, Kiel) for the early release of their WOCE data. Directly measured advective estimates at the equatorial passage were provided by M. Hall (WHOI).

At Hunter Channel, advective estimates were abstracted from Speer and Zenk (1993) and values for the Romanche and Chain fracture zones were estimated from Mercier and Speer (1997). Neutral surfaces were computed using CSIRO software (described by Jackett and McDougall, 1997).

References

Davis, R., 1994: Diapycnal mixing in the ocean: equations for large-scale budgets, J. Phys. Oceanogr., 24, 777–800.

Hogg, N., P. Biscaye, W. Gardner, and W. Schmitz, Jr., 1982: On the transport and modification of Antarctic Bottom Water in the Vema Channel. J. Mar. Res., 40, Suppl. 231–263.

Hogg, N., W. Owens, G. Siedler, and W. Zenk, 1996: Circulation in the Deep Brazil Basin. In The South Atlantic, Present and Past Circulation, edited by G. Wefer, W. Berger, G. Siedler and D. Webb, pp. 249–260, Springer-Verlag.

McDougall, T., 1987: Thermobaricity, cabelling and water-mass conversion. J. Geophys. Res., 92, 5448–5464.

McDougall, T., and J. Whitehead, 1984: Estimates of the relative roles of diapycnal, isopycnal and double-diffusive mixing in Antarctic Bottom Water in the North Atlantic. J. Geophys. Res., 89, 10479–10483.

Polzin, K., J. Toole, J. Ledwell, and R. Schmitt, 1997: Spatial variability of turbulent mixing in the Abyssal Ocean, Science, 276, pp. 93–96.

Toole, J., K. Polzin, J. Ledwell, R. Schmitt, and L. C. Laurent, 1997: Spatial variability of turbulent mixing in the Abyssal Ocean. In WOCE South Atlantic Workshop Abstracts, Brest, France, 16–20 June 1997.

The Brazil Basin Tracer Release Experiment

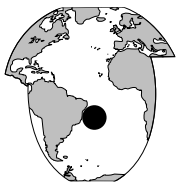

J. M. Toole, J. R. Ledwell, K. L. Polzin, R. W. Schmitt, E. T. Montgomery, L. St. Laurent and W. B. Owens, Woods Hole Oceanographic Institution, Woods Hole, USA.
jtoole@whoi.edu.

The intensity and spatial distribution of turbulent mixing in the abyssal ocean have been topics of speculation in oceanography for many decades. That mixing must occur at depth follows directly from large-scale budget considerations. Dense waters, produced by heat loss to the atmosphere at high latitudes, sink to, and spread along the bottom to fill the deep ocean. Newly formed bottom waters intrude below older waters, forcing upwelling. To maintain an approximate steady-state temperature distribution, this upward advection of cold water is believed to be compensated by a downward diffusive heat flux (Wyrtki, 1961; Munk, 1966). In recent years, heat budgets for bottom waters in semi-enclosed basins have been used to diagnose these turbulent fluxes (Whitehead and Worthington, 1982; Hogg et al., 1982; Saunders, 1987; Barton and Hill, 1989; Roemmich et al., 1996, McCarthy and Talley, 1997). Results are commonly reported in terms of an average vertical diffusivity (K), with inferred K values generally ranging between 1 and $10 \times 10^{-4}\ m^2\ s^{-1}$. Significantly, these values are 10 to 100 times greater than those deduced from ocean microstructure data from the upper 1000 m of the ocean (apart from the surface mixed layer, the ocean margins, and highly sheared flows such as the equatorial undercurrent, Gregg, 1987; Polzin et al., 1995). Small mixing rates have also been suggested in the abyssal ocean away from boundaries by a handful of deep microstructure profiles (Gregg, 1977; Moum and Osborn, 1986; Toole et al., 1994): a seeming discrepancy with results from the abyssal heat budget studies. However, those few data from the deep ocean gathered near rough bathymetric structures hint of significantly enhanced mixing in stratified boundary layers there (Toole et al., 1994, 1997).

To explore diapycnal mixing in the deep ocean in greater detail, we are conducting a tracer dispersion experiment in the Brazil Basin of the South Atlantic Ocean, augmented by profile observations of hydrodynamic variables (Polzin et al., 1997). This geographic area was chosen because heat-budget-derived estimates of K are available for the bottom waters in this region (Hogg et al., 1982), and extensive complementary data have recently been collected as part of WOCE. Our study was initiated in February–March 1996, and continued with a survey cruise in March–April 1997. A final survey will be conducted in March/April 1998. We made physical observations in 1996 and 1997 with a freely-falling instrument, the High

Resolution Profiler (HRP, Schmitt et al., 1988). Deployments were made between the South American continental slope and the crest of the Mid-Atlantic Ridge (MAR), Fig. 1. The HRP returns temperature, salinity and horizontal velocity information as a function of depth, along with dissipation rate estimates for kinetic energy and temperature variance. Turbulent diffusivity estimates are derived from the dissipation data following Osborn and Cox (1972), and Osborn (1980). The tracer dispersion component of our experiment uses the techniques developed for the North Atlantic Tracer Release Experiment (Ledwell et al., 1993). During the 1996 cruise, approximately 110 kg of sulphur hexafluoride (SF_6) were released on an isopycnal about 4000 metres deep near 21°40'S, 18°25'W, Fig. 1. This site lies over a system of ridge spurs and canyons that run zonally towards the crest of the MAR. The spurs attain depths of about 4400 metres in the vicinity of the tracer release and the canyon valleys reach about 5000 metres depth. Spurs and canyons both shoal to the east towards the MAR crest (located at 12°W at these latitudes) where individual bathymetric peaks extend to about 2000 m depth.

As recently reported by Polzin et al. (1997), the HRP observations document weak turbulent dissipation at all depths (supporting a diapycnal diffusivity of approximately $0.1\times10^{-4}\ m^2\ s^{-1}$) in the western half of the Brazil Basin where the bottom is smooth, Fig. 2 (page 19). These diffusivity values are well below the $3-4\times10^{-4}\ m^2\ s^{-1}$ deduced by Hogg et al. (1982) for the bottom waters. A particular surprise was the small amount of mixing over the South American continental slope; diffusivity values only slightly greater than background levels were observed within 100 m of the bottom. This is the region occupied by the bottom-intensified deep western boundary current: a flow hypothesised as an important mixing agent in the abyssal Brazil Basin (De Madron and Weatherly, 1994). In contrast to the mid-basin and western regions, greatly elevated mixing rates were observed to the east over the rough bathymetry of the MAR. Diffusivity values of order $1\times10^{-4}\ m^2\ s^{-1}$ were observed extending well into the water column. Using the 1996 microstructure observations, we estimated diapycnal diffusivity values of about $0.5\times10^{-4}\ m^2\ s^{-1}$ for the depth and region of the tracer injection, values comparable to that deduced from the tracer distribution surveyed within 2 weeks of its release (Polzin et al., 1997). Diapycnal diffusivity estimates increased to the east towards the crest of the MAR and towards the rough bottom to values greater than $1\times10^{-4}\ m^2\ s^{-1}$.

Work on the 1997 cruise, approximately 14 months after the release of the tracer, involved water sampling and analysis to document the three-dimensional distribution of the SF_6 patch, and additional finestructure and microstructure profiling work, Fig. 1b. Floats that were released with the tracer and surfaced prior to the cruise suggested that the tracer patch would be approximately isotropic, with a radius of about 210 km, centred within 25 km of the release point. This, together with the 1996 estimate of K for this region at the tracer injection depth, forecasted only moderate vertical dispersion of the SF_6. In

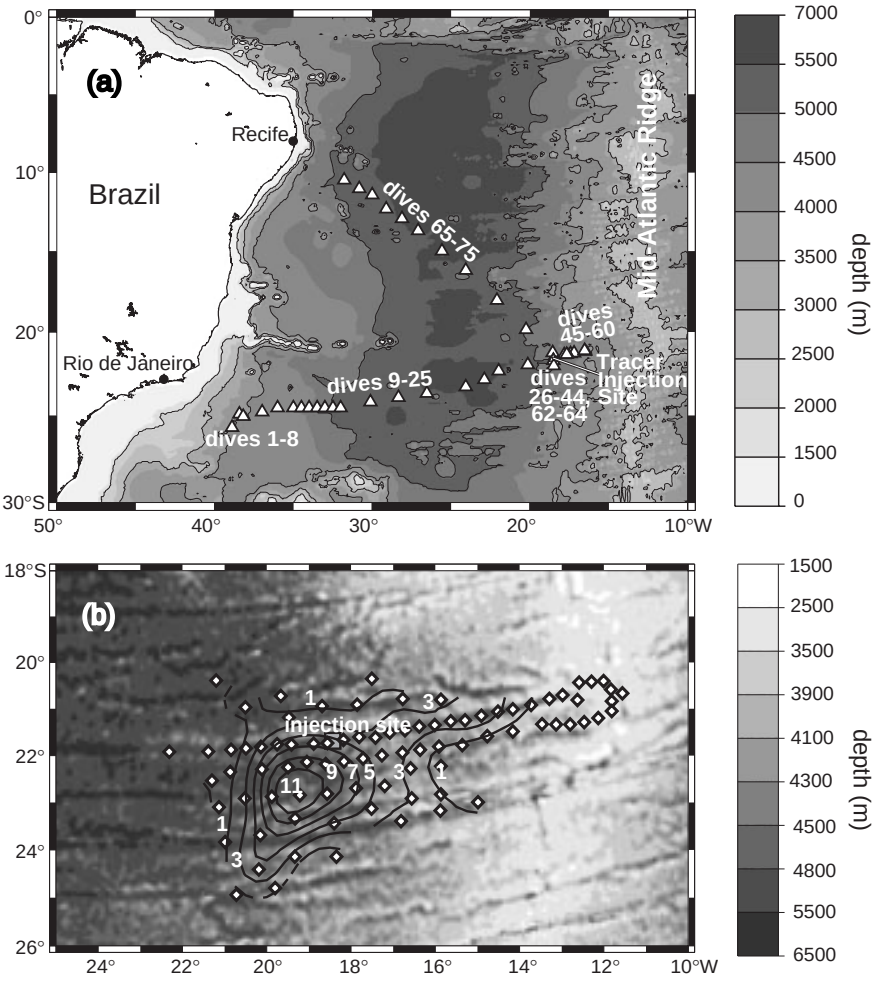

Figure 1. Station maps for sampling in the Brazil Basin Tracer Release Experiment. Panel (a) shows the distribution of High Resolution Profiler observations from February–March 1996; panel (b) is for the March–April 1997 cruise. Casts to collect water samples were made at all of the HRP stations west of 13°W. The bathymetric data in (b) come from Sandwell and Smith (1995). The area where tracer was injected in 1996 is marked in panel (b), along with the contoured distribution of vertically integrated tracer concentration from the 1997 observations. Crude estimates indicate that virtually all of the tracer deployed in 1996 was found on the 1997 cruise.

fact, the tracer dispersed a great deal more than expected. The average diffusivity over the 14 months on the injection isopycnal estimated from water samples collected near the release point appears to have been at least $1.5 \times 10^{-4}\ m^2\ s^{-1}$. Much larger diffusivities appear to have prevailed between the level of the release and the bottom. From the more extensive 1997 microstructure observations that sampled a full spring-neap tidal range (see below), we estimate an average diapycnal diffusivity for the tracer injection isopycnal that is somewhat greater than $1 \times 10^{-4}\ m^2\ s^{-1}$. Thus the two techniques seem again to be roughly consistent with one another. Larger diffusivity estimates were inferred from velocity microstructure in the canyons and about the MAR crest where averaged values were $10 \times 10^{-4}\ m^2\ s^{-1}$ or more: a similar pattern to that observed in 1996.

In addition to pronounced downward dispersion, the tracer also appears to have been carried east by flows within the MAR fracture zones. Tongues of tracer were sampled within these canyons that extended well east of the tracer patch edge at the injection depth. Tracer was found as far east as 13°W in the canyon over which it was released in 1996, Fig. 1b. Up-canyon flow is also inferred from the heat budget of the canyon waters to balance the downward turbulent heat flux estimated from our microstructure data, and by an up-canyon horizontal pressure gradient manifested by our dynamic height data. We think the up-canyon flow is at least $0.1\ cm\ s^{-1}$; it could be much greater. If this speed is representative, up-canyon flow in something like 100 such canyons would balance the mass transport of bottom water entering the Brazil Basin via the Vema Channel. Detailed bathymetric data, such as diagnosed by Sandwell and Smith (1995), suggest the MAR may indeed be rift by this many fractures. The 1997 observations thus help confirm the spatial pattern of mixing put forth by Polzin et al., (1997) and their hypothesis of bottom water upwelling in the MAR canyons.

The lateral dispersion of the tracer was consonant with the float data, with two important exceptions. The first is the movement of SF_6 up the canyons already mentioned. The second is that the centre of mass of the tracer moved about 130 km to the south-west over 14 months, while the centre of mass of the floats moved only 20 km or so to the south-west. This may indicate a vertical shear, since the mean depth of the floats was about 330 metres less than the tracer. Some of the south-west displacement of tracer may also be the result of isopycnal diffusion, biased south by a ridge spur just north of the release site that may have acted as a topographic barrier (although its height was 400 to 800 metres below the depth of the release). We will obtain more information on the persistence of this movement, the spatial distribution of mixing and the intensity of the up-canyon flows in next year's survey. Three-dimensional modelling, with accurate bathymetry, will be necessary to extract all of the information from these surveys.

Repeated finescale velocity profiles separated in time by approximately 6 hours support the suggestion in Polzin et al., (1997) that tidal motions contribute significantly to the small-scale shear field (that in turn sustains the enhanced turbulent dissipation). These motions appear to be generated as the barotropic tide flows over bathymetric features having characteristic wavelengths smaller than 10 km. The subsequent propagation and breaking of the internal tide sustains the enhancement of turbulent dissipation well away from the bottom boundary. We are attempting to model the evolution of the internal tide as a balance between vertical propagation and the tendency for internal wave/wave interactions to transfer energy to smaller vertical scales where it is ultimately dissipated. The goal of the work is to predict the vertical profile of turbulent dissipation given the amplitude of the barotropic tide and a horizontal spectrum of bottom topography. Preliminary results are encouraging.

We have found evidence of turbulent mixing in the abyss of sufficient intensity to nearly close abyssal heat budgets (Polzin et al., 1997). The implications these observations have for the deep-ocean circulation are not yet fully clear. As formalised in the papers by Munk (1966), and Stommel and Arons (1960), turbulent mixing, vertical upwelling, and the horizontal circulation of the abyssal ocean are interrelated. To simplify their presentation (and lacking contrary information), Stommel and Arons (1960) depicted the circulation that arises from spatially uniform abyssal upwelling in a flat-bottomed ocean. In contrast to their pedagogic examples, we infer a far more structured flow in the abyss when the pattern of mixing suggested by our data is applied. Interior basin regions characterised by smooth bathymetry, background-intensity internal waves and weak vertical mixing (and consequently weak vertical stretching), likely harbour flow along lines of constant potential vorticity connecting to western boundary currents. Segregation of the mixing to regions of rough bathymetry, such as the mid-ocean ridges, in turn acts to localise the diapycnal velocity. Presumably, meridional flow forced by vertical stretching is similarly localised. But the sign of the diapycnal velocity, and of dw/dz deduced from the density equation and microstructure observations (Polzin et al., 1997), vary greatly with depth and position. Moreover, the dynamics of the currents within the Ridge canyons, flows that appear to play such a prominent role in the mass budget of the abyssal waters, are likely quite complicated. Much work remains.

Acknowledgements

We thank D. Wellwood, T. Donoghue, B. Guest, T. Bolmer, S. Sutherland, J. Sisson and S. Wetzel for their excellent technical support of our field programme and subsequent data analysis efforts, and the officers and crew of the RV Seward Johnson for their expert seamanship. This research is supported by the US National Science Foundation, Division of Ocean Sciences.

References

Barton, E. D., and A. E. Hill, 1989: Abyssal flow through the Amirante Trench (Western Indian Ocean). Deep-Sea Res., 36, 1121–1126.

Durrieu De Madron, X., and G. Weatherly, 1994: Circulation, transport and bottom boundary layers of the deep currents in the Brazil Basin. J. Marine Res., 52, 583–638.
Gregg, M. C., 1977: Variations in the intensity of small-scale mixing in the main thermocline. J. Phys. Oceanogr. 7, 436–454.
Gregg, M. C., 1987: Diapycnal mixing in the thermocline: A review. J. Geophys. Res. 92, 9686–5286.
Hogg, N. G., P. Biscaye, W. Gardner, and W. J. Schmitz, 1982: On the transport and modification of Antarctic Bottom Water in the Vema Channel. J. Mar. Res., 40 suppl., 231–263.
Ledwell, J. R., A. J., Watson and C. S. Law, 1993: Evidence for slow mixing across the pycnocline from an open-ocean tracer-release experiment. Nature, 364, 701–703.
McCarthy, M. C. and L. D. Talley, 1997: Deep upwelling in the Central Indian Basin. Geophys. Res. Let., submitted.
Moum, J. N. and T. R. Osborn, 1986: Mixing in the main thermocline. J. Phys. Oceanogr., 16, 1250-1259.
Munk, W. H., 1966: Abyssal recipes, Deep-Sea Res., 13, 207–230.
Osborn, T. R., and C. S. Cox, 1972: Oceanic fine structure. Geophys. Fluid Dyn., 3, 321–345.
Osborn, T. R., 1980: Estimates of the local rate of vertical diffusion from dissipation measurements. J. Phys. Oceanogr., 10, 83–89.
Polzin, K. L., J. M. Toole and R. W. Schmitt, 1995: Finescale parameterizations of turbulent dissipation. J. Phys. Oceanogr., 25, 306–328.
Polzin, K. L., J. M. Toole, J. R. Ledwell and R. W. Schmitt, 1997: Spatial variability of turbulent mixing in the abyssal ocean. Science, 276, 93–96.
Roemmich, D., S. Hautala and D. Rudnick, 1996: Northward abyssal transport through the Samoan Passage and adjacent regions. J. Geophys. Res., in press.
Sandwell, D. T. and W. H. F. Smith, 1995: Marine Gravity from satellite Altimetry (poster), The Geological Data Center, Scripps Inst. of Oceanography, La Jolla, CA 92093, (digital file, Version 7.2) anonymous ftp to baltica.ucsd.edu.
Saunders, P. M., 1987: Flow through Discovery Gap. J. Phys. Oceanogr. 17, 631–643.
Schmitt, R. W., J. M. Toole, R. L. Koehler, E. C. Mellinger, and K. W. Doherty, 1988: The development of a fine- and microstructure profiler, J. Ocean Atmos. Techno., 5, 484–500.
Stommel, H., and A. B. Arons, 1960: On the abyssal circulation of the world ocean. I. Stationary planetary flow patterns on a sphere. Deep-Sea Res., 6, 140–154.
Toole, J. M., K. L. Polzin and R. W. Schmitt, 1994: Estimates of diapycnal mixing in the abyssal ocean, Science, 264, 1120–1123.
Toole, J. M., R. W. Schmitt, K. L. Polzin, and Eric Kunze, 1997: Evidence of near-boundary mixing above the flanks of a mid-latitude seamount. J. Geophys. Res., 102, 947–959.
Whitehead, J. A., and L. V. Worthington, 1982: The flux and mixing rates of Antarctic Bottom Water within the North Atlantic. J. Geophys. Res., 87, 7903–7924.
Wyrtki, K., 1961: The thermohaline circulation in relation to the general circulation in the oceans. Deep-Sea Res., 7, 39–64.

Two Meridional Hydrographic Sections in the Eastern South Atlantic Ocean (WHP lines A13 and A14)

Herlé Mercier and Michel Arhan, Laboratoire de Physique des Oceans, IFREMER Centre de Brest, France. herle.mercier@ifremer.fr.

Data

Two meridional hydrographic lines were carried out in the eastern South Atlantic Ocean along 9°W (WHP line A14) and 5°W (WHP line A13) of nominal longitudes on board the French RV L'Atalante during the CITHER 3 cruise from mid-January to mid-April 1995 (Fig. 1). This cruise was organised within the framework of the CITHER programme which is the French contribution to the WHP one time survey in the South Atlantic Ocean. A14 is located at the western edge of the eastern trough of the South Atlantic Ocean. After crossing the Guinea Basin, A14 approximately follows the 4000 m bathymetric contour along the Mid-Atlantic Ridge, up to 45°S. A13 is located about 10° off the African coast, and, from North to South, intersects the Guinea Basin, the Angola-Guinea Ridge, the Walvis Ridge and the Cape Basin. In this note, we present the vertical distributions of the potential temperature, salinity and dissolved oxygen fields along A14 (Fig. 2) and A13 (Fig. 3).

Results

In the surface layers, the A14 and A13 hydrographic lines intersect three major current systems: the zonal equatorial currents north of 5°S, the cyclonic circulation cell of the tropical South Atlantic Ocean (Gordon and Bosley, 1991) centred at about 13°S and marked by a surface salinity maximum and a subsurface oxygen minimum (Figs. 2 and 3), the subtropical gyre easily distinguishable on A14 by the bowl shape of the isotherms south of 20°S, and the subtropical front found at 36°S on A14 and at 38°S on A13. In addition, A14 intersects the subantarctic front at 44.5°S. In the subtropical region, A14 run across two Agulhas rings at 26°S and 31.5°S (Fig. 2). These ring features are recognisable by their subsurface thermostads. The Agulhas ring centred at station 78 is remarkably large (more than 300 km wide) and its thermostad has a temperature of 17–18°C which is the temperature of the South Indian Subtropical Mode Water found in the Agulhas current. The second Agulhas ring, centred at station 69, is remarkably different: its core temperature is between 13°C and 14°C, much cooler than that of the first ring. Oxygen values in its thermostad are also higher than that of the first ring. These are indications that this second ring spent a winter at the higher latitude of the Agulhas retroflection region where it experienced a large heat loss.

Antarctic Intermediate Water originates near the Antarctic Circumpolar Current and spreads northward in the South Atlantic Ocean around 800 m depth. This spreading can be traced by the salinity minimum which is associated with this water mass. The Antarctic Intermediate Water circulates within the Subtropical gyre and is advected

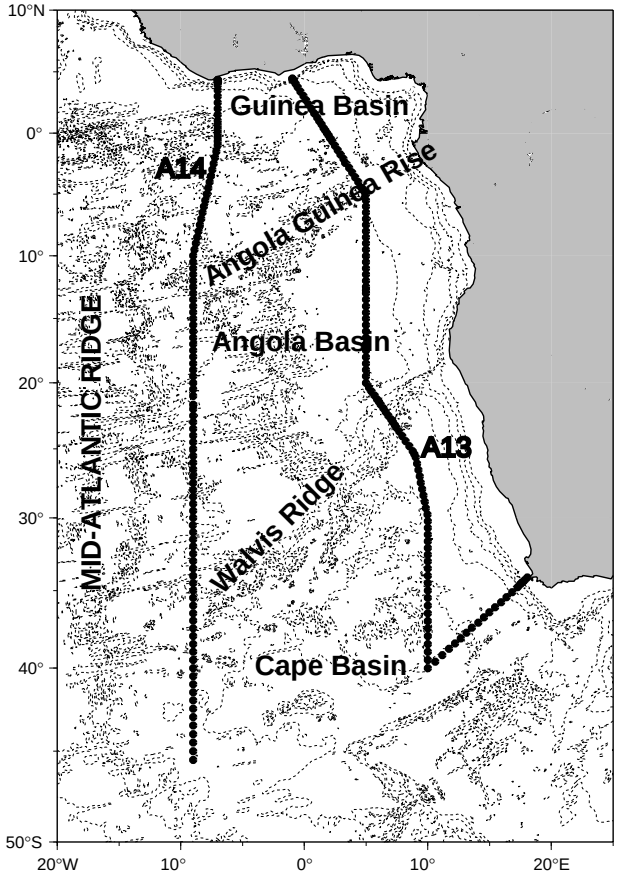

Figure 1. Locations of the hydrographic stations occupied during the CITHER 3 cruise.

north-westward by the South Equatorial Current. At the western boundary of the equatorial region, the Antarctic Intermediate Water feeds an eastward flow just south of the equator (Reid, 1989; Schott et al., 1995). The isolated oxygen maximum and salinity minimum observed on A13 in the depth range 700–800 m immediately south of the equator (Fig. 3) are indications that such an eastward flow of Antarctic Intermediate Water still exists close to the eastern boundary. The direction of the flow was confirmed by a Lowered ADCP profile at 1°45'S, 2°57'W which showed an intense eastward jet at these depths with zonal velocities as large as $20\,\mathrm{cm\,s^{-1}}$ (not shown).

The North Atlantic Deep Water enters the equatorial Atlantic as a southward flowing Deep Western Boundary Current. At the equator, the Deep Western Boundary Current interacts with zonal flows (Richardson and Schmitz, 1994) resulting in the eastward penetration of the North Atlantic Deep Water properties along the equator (Weiss et al., 1985). The mid-depth salinity and oxygen maxima observed both on A14 (Fig. 2) and A13 (Fig. 3) at the equator are evidence that the Upper and Middle North Atlantic Deep Water tracer signatures cross the Mid-Atlantic Ridge and reach the eastern equatorial basin. The bottom oxygen maximum found in the Guinea Basin on A14 is the signature of a mixture of Lower North Atlantic Deep Water and Antarctic Bottom Water formed during the eastward transit of these two water masses across the Mid-Atlantic Ridge through the Romanche Fracture Zone and the Chain Fracture Zone (Mercier and Morin, 1997). Along A13, the bottom oxygen signal in the Guinea Basin is now a minimum due to a chemical reaction at the interface with the sediments. The Lower North Atlantic Deep Water oxygen maximum flows southward through cuts in the Angola-Guinea Ridge (see A13 line, Fig. 3) and penetrates into the Angola Basin where it will upwell (Warren and Speer, 1991).

The mid-depth oxygen maxima centred around 22°S on A14 (Fig. 2) and A13 (Fig. 3) mark a second pathway for the North Atlantic Deep Water from the western trough toward the eastern South Atlantic Ocean. Warren and Speer (1991) showed that part of this mid-latitude eastward flow of North Atlantic Deep Water crosses the Walvis Ridge at the Namib Col (the Namib Col was cut at Sta. 170 on A13, Fig. 3). At station 59 (A14 line, Fig. 2), the mid-depth oxygen maximum associated with the North Atlantic Deep Water extends downward up to the sea floor, an observation probably related to the existence of the Rio de Janeiro Fracture Zone, a cut in the Mid-Atlantic Ridge east of that station, which could favour exchanges with the western basin. South of 25°S, the upper part of the North Atlantic Deep Water oxygen maximum on A14 is eroded by the oxygen-poorer Circumpolar Deep Water.

The coldest Antarctic Bottom Water is found in the Cape Basin where it circulates within a clockwise gyre

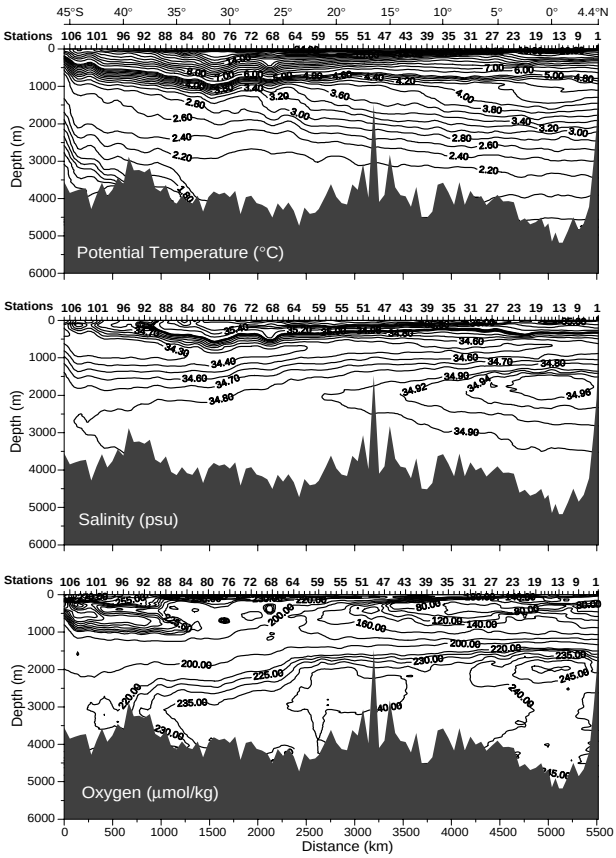

Figure 2. Vertical distribution of potential temperature, salinity and dissolved oxygen along A14.

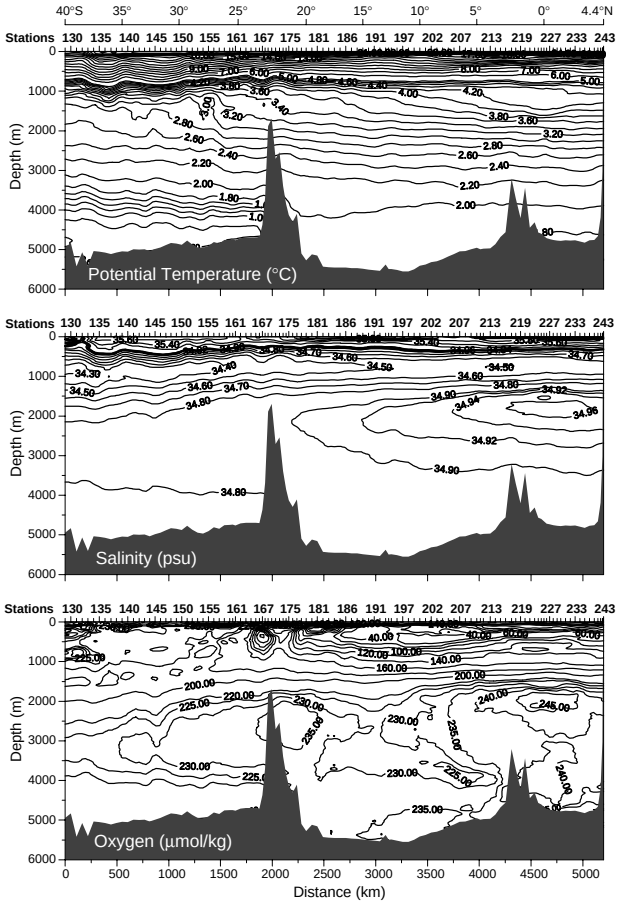

Figure 3. Vertical distribution of potential temperature, salinity and dissolved oxygen along A13.

(Reid, 1989). The northward spreading of the Cape Basin Antarctic Bottom Water is limited by the Walvis Ridge, although some leakage as cold as 1.6°C of Cape Basin Antarctic Bottom Water into the Angola Basin can been seen on A14 (Fig. 2).

Acknowledgements

This work was supported by the Institut Français pour l'Exploitation de la Mer (IFREMER), the Centre National de la Recherche Scientifique (CNRS) and the Institut National des Sciences de l'Univers (INSU).

References

Gordon, A. T., and K. T. Bosley, 1991: Cyclonic gyre in the tropical South Atlantic. Deep-Sea Res., 38, Supp. 1, 323–343.

Mercier, H., and P. Morin, 1997: Hydrography of the Romanche and Chain Fracture Zones. J. Geophys. Res., 102, 10373–10389.

Reid, J. L., 1989: On the total geostrophic circulation of the South Atlantic Ocean: Flow patterns, tracers, and transports. Progr. Oceanogr., 23, 149–244.

Richardson, P. L., and W. J. Schmitz, 1994: Deep cross-equatorial flow in the Atlantic measured with SOFAR floats. J. Geophys. Res., 98, 8371–8387.

Schott, F. A., L. Stramma, and J. Fischer, 1995: The warn water inflow into the western tropical Atlantic boundary regime, Spring 1994. J. Geophys. Res., 100, 24745–24760.

Warren, B. A., and K. G. Speer, 1991: Deep circulation in the eastern South Atlantic Ocean. Deep-Sea Research, 38, Suppl. 1, 281–322.

Weiss, R. F., J. L. Bullister, R. H. Gammon, and M. J. Warner, 1985: Atmospheric chlorofluoromethanes in the deep equatorial Atlantic. Nature, 314, 608–610.

Deployment of RAFOS Floats in the Cape Basin

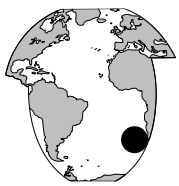

Olaf Boebel, University of Cape Town, Department of Oceanography, South Africa; and Claudia Schmid and Markus Jochum, Institut für Meereskunde, Kiel, Germany.
oboebel@physci.uct.ac.za

Introduction

The global ocean circulation in relation to the world climate (Broecker, 1991; Gordon et al., 1992) has received considerable attention during the last decade. During this period, the oceanographic research community embarked on one of the largest internationally co-ordinated experiments, the World Ocean Circulation Experiment (WOCE) (WCRP, 1988). Both modelling and observational tools were and are being employed to capture the current dynamic state of the oceans. Complemental to conventional hydrographic campaigns, Lagrangian sub-surface drifters have been used in the western South Atlantic (Boebel et al., 1997b) and the Pacific (Davis et al., 1996). So far, these research efforts have focused at intermediate depth, providing direct velocity measurements which can also be used for geostrophic and model calculations. One of the key issues in the understanding of interocean exchange at intermediate depth (1000 m) is the advection of water around southern Africa. Lagrangian measurements in this area are now expected to shed light on the highly variable flow field of this ocean region. In March–April 1997, members of the Institut für Meereskunde, Kiel and the University of Cape Town participated on FS Polarstern cruise ANTXIV/4 to launch the first high resolution Lagrangian experiment in this area. This experiment, being one of three collaborate research efforts (Boebel et al., 1997a), focuses on the intermediate water in the Cape Basin and its major sources, the South Atlantic Current (SAC) (Stramma and Peterson, 1990) and Agulhas rings (Lutjeharms, 1996). The SAC's surface expression forms the southern branch of the subtropical gyre. It crosses the Atlantic from west to east at approximately 40°S, lying predominately at or north of the surface Subtropical Front (STF) (Stramma and Peterson, 1990). The Cape Basin is entered from the south-west after passing the Walvis Ridge.

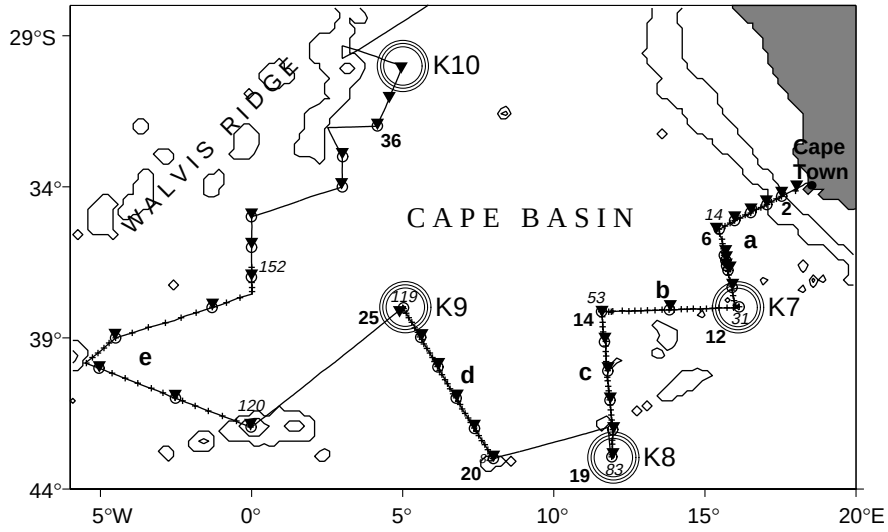

Figure 1. Map of the Cape Basin, showing 1000 m and 3000 m isobaths. The track of Polarstern cruise ANT XIV/4, departing from Cape Town on 21 April 1997, is indicated by the thin solid line. Circles indicate the launch sites of RAFOS floats, triangles CTD casts and plus signs the sites of XBT drops. Triplets of large concentric circles labelled K7 through K10 indicate the mooring positions of sound sources. An additional sound source (M10) was deployed north of the Walvis Ridge in the Angola basin (not shown).

Close to the prime meridian a bifurcation of the SAC is observed (Garzoli and Gordon, 1996), generating an eastward continuation as well as a northward branch. The fraction of mass flux going either way remains unknown. The latter leg, probably carrying the bulk of the inflowing water (Stramma and Peterson, 1990), feeds the recirculation of the anticyclonic subtropical gyre. The eastward flow passes to the south of the Cape of Good Hope around 40°S, continuing into the Indian Ocean. There part of it might become involved in the Agulhas Current retroflection, subsequently feeding the Benguela Current (Gordon, 1996), being probably trapped by migrating Agulhas Rings. Agulhas Rings, shed by occlusions of the Agulhas Current loop at its Retroflection (e.g. Lutjeharms, 1996) are an integral part of the hydrographic elements south-west of the Cape of Good Hope. These energetic rings transport warm and salty water of Indian Ocean origin into the Cape Basin from the south-east. Due to evaporative cooling, they rapidly lose their high temperature contrast with the atmosphere and the embedding watermasses (Duncombe Rae et al., 1996). Therefore they can only be recognised for a limited time by satellite-borne Sea Surface Temperature (SST) observations. However, their dynamic signal reaches down to the Antarctic Intermediate Water (AAIW) level (Duncombe Rae, 1991), making RAFOS floats suitable to track their drift across the Cape Basin and beyond. The general description given above, however, to a large extend refers to surface flow and properties. The degree to which the statements above hold true at intermediate depth is not yet known, and it is the purpose of the experiment outlined below to illuminate this issue.

The South Atlantic Current Experiment

During FS Polarstern cruise ANTXIV/4, 35 RAFOS floats (Rossby et al., 1986) were deployed at intermediate depth (Fig. 1). They were programmed to carry out an underwater mission of 1.5 years in the average. Each float deployment was accompanied by a pre-launch CTD hydrocast (Fig. 1). The hydrography, augmented by expendable Bathythermograph sonde (XBT) drops every 10 nautical miles, was used to identify the various watermasses in order to optimally place the floats. When analysing the subsequent trajectories, it will be used to interpret the floats vertical motion with regard to mixing and advection (Boebel et al., 1995). During the cruise, special attention was given to recognise possible Agulhas Rings, based on the online ship-borne Acoustic Doppler Current Profiler (ADCP) measurements, the ship's drift and the XBT survey. Thermosalinograph measurements provided information on the corresponding near-sea surface temperature and salinity signals. An array of 4 sound-source moorings was launched, covering the Cape Basin with coded signals for tracking purposes (Fig. 1). An additional sound source was moored in the Angola Basin (M10) on behalf of the neighbouring Lagrangian Experiment by a Woods Hole Oceanographic Institution/Lamont-

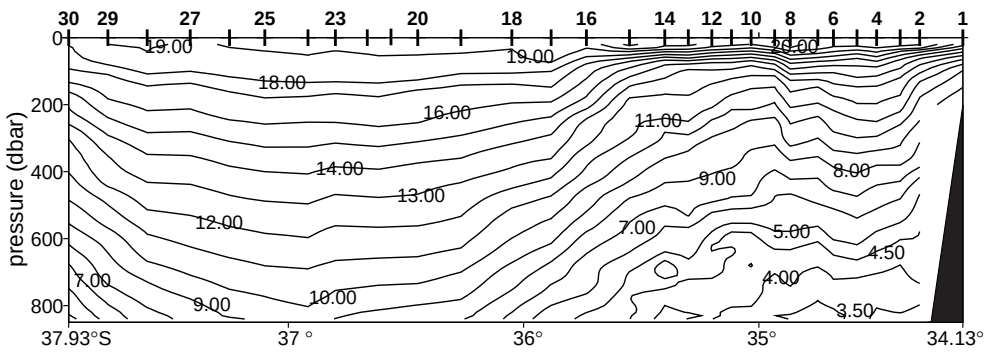

Figure 2. Section 'a' (Fig. 1): Temperature distribution as recorded during Polarstern cruise ANT XIV/4. Selected XBT drops are indicated by numbers on the upper axis. Note the change of course (Fig. 1) at XBT drop No. 14.

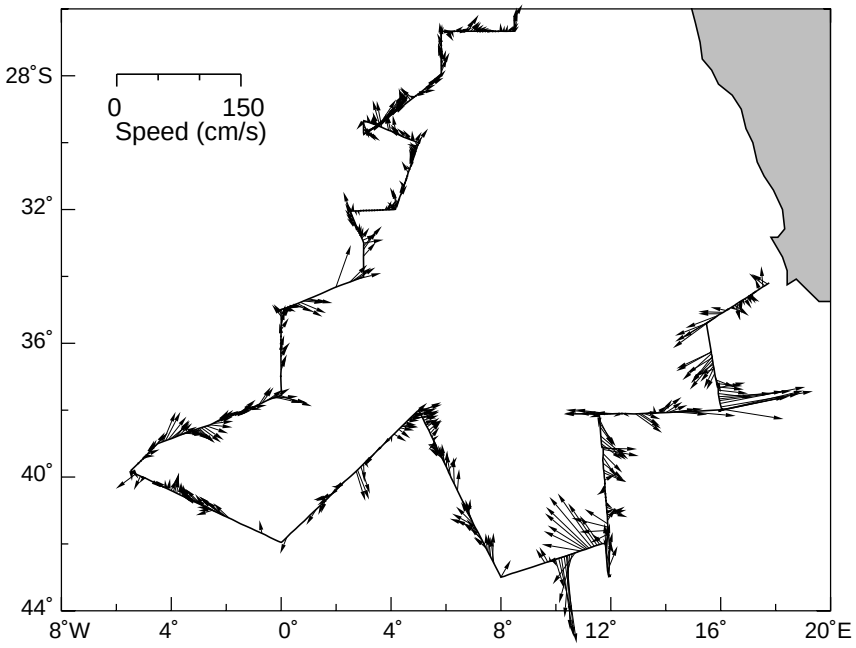

Figure 4. Average flow field between 50 m and 200 m as derived from ship-borne ADCP measurements. The standard deviation of the current's cross-track and along-track velocity component was estimated to be $8\,cm\,s^{-1}$ *and* $6\,cm\,s^{-1}$*, respectively.*

Doherty Earth Observatory collaboration, which will be started later this year (Boebel et al., 1997a). The ANTXIV/4 cruise track intersected the three possible major pathways of intermediate water into this area. The south-westward leg, departing from Cape Town towards mooring K7 (Fig. 1), focuses on the inter oceanic transport of AAIW, e.g. the inflow from the south-east. As mentioned above, Agulhas Rings might be a possible conveyor of such an exchange. A prominent depression of all but the near-surface isotherms is observed in the temperature section 'a' (Fig. 2). The 10°C isotherm drops from 200 dbar to nearly 800 dbar over 100 km distance. The symmetric feature is centred around hydrocast station No. 10 at 36°46'S 15°46'E (Fig. 3, page 21) and spans 300 km in diameter. The corresponding density distribution indicates an anticyclonic deep-reaching feature, suggesting that this feature could be a juvenile Agulhas Ring or the Retroflection loop itself.

Agulhas Ring implanted with RAFOS floats

The dynamic signal encompasses all of the intermediate layer, reaching down as deep as 2000 dbar, the truncation depth of the deeper CTD stations (most of the stations were truncated at 1500 dbar, once the AAIW layer was passed). Around 1100 dbar depth, the proposed importation of Indian Ocean intermediate water is recognised (Fig. 3). There, a weak but deep salinity minimum close to 34.4 replaces the stronger and shallower salinity minimum typical for this regions Atlantic AAIW (salinity lower than 34.3 at approximately 700 dbar). Simultaneous ship-borne ADCP measurements (Fig. 4) indicate a strong current shear along the quasi-meridional section 'a'. Velocity signals averaged over 50 m to 200 m depth depict a westward flow stronger than at the northern end of the segment. After a steady decrease towards station No. 10 (unfortunately a larger data segment is missing due to technical problems at the time) an eastward flow was observed in the southern segment, reaching peak values of more than $110\,cm\,s^{-1}$ at its southern limit. Judging from the flow field's orientation, the rotational centre was located slightly to the east from FS Polarstern's cruise track. While crossing this feature, it was decided to seed 3 floats (cf. Fig. 3) north of the centre at 1050 m (Nos. 183, 200 and 215). Two further floats were seeded south of the centre, (Fig. 3), but at a depth of 850 dbar (No. 184) and 900 dbar (No. 216). The expected trajectories of these instruments will hopefully give final evidence whether this feature is an Agulhas Ring or the Agulhas Retroflection loop. The shallower central floats are aimed to observe the long-term migration of the possible ring and its mixing with the surrounding Atlantic AAIW. The deeper floats shall monitor the trapping depth of the Agulhas Ring with increasing distance from its origin and the fate of the intermediate water of Indian Ocean origin.

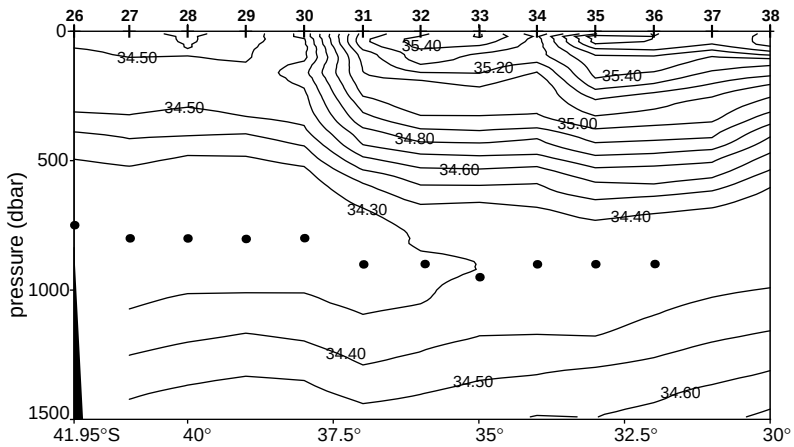

Figure 5. Section 'e' (Fig. 1): Salinity distribution as recorded during Polarstern cruise ANT XIV/4. CTD casts are indicated by numbers on the upper axis. Note the drastic change of course at CTD cast Nos. 28 and 31. Solid dots indicate the launch position and estimated depth of RAFOS floats seeded during the cruise.

Trapping the South Atlantic Current at intermediate depth

During the subsequent sections 'b', 'c' and 'd' (Fig. 1) from K7 to the west it was attempted to capture the direct escape of AAIW into the Indian Ocean as well as the northward branching of AAIW into the Cape Basin. The zonal section 'b' along 38°S captured a smooth thermal structure, as is to be expected north of the zonally oriented STF. When taking a perpendicular southward course from XBT drop No. 53 onward (section 'c'), a steady shoaling of the isotherms and isohalines was detected. This is associated with the STF itself and the corresponding eastward flow through this section and farther east along section 'b'. In the southern portion of section 'c', a thin and weak salinity maximum separates the low salinity of the sea surface from the minimum at intermediate depth. Probably a continuous minimum might have been found farther south, reaching down from the surface to mid-depth. As a result, fresh AAIW might have been introduced to the intermediate layer by direct downwelling, once winter cooling had increased the density. These observations once again open the discussion for a direct import of AAIW along the long trans-oceanic Subantarctic Front (SAF). Continuous thermosalinograph temperature measurements and the XBT sections indicated that the 10°C isotherm, which was used as a proxy for the northern border of subantarctic water (Sverdrup et al., 1942), outcropped around 42°S. During section 'c' the two southernmost floats were seeded south of the 10°C isotherm outcropping, whereas it was only one float during section 'd'. The fate of these floats will hopefully serve to establish a border line between the expected northward branching of the SAC and its direct eastward continuation. After completion of the three quasi-meridional XBT sections 'c', 'd' and 'e' a more intricate and comprehensive definition of the STF could be made. Considering the surface salinity gradient only, using Whitworth and Nowlin's (1987) definition of subtropical water, the STF was found between 39.5°S and 37.5°S with the lower latitudes in the east. This observation possibly indicates the proposed northward branching of the SAC. Finally, leg 'e' transects the STF well into the proposed intermediate subtropical gyre. Both temperature and salinity sections indicate the beforementioned STF near 37.5°S, separating the central waters of the subtropical gyre from less saline water to the south (Fig. 5). Underneath the central waters the low-salinity tongue of AAIW is found, which experiences some vertical constraint due to the overlying high salinity waters. The observed density profile suggests an intermediate westward flow north of 35°S and to the east south of this latitude. The latter, however, is restricted at intermediate depth to the frontal area at 37.5°S. This interpretation, however, is very susceptible to the unknown barotropic component. Nevertheless, the direct velocity measurements (Fig. 4) confirm this general trend, depicting north-eastward to south-eastward flow south of 33°S and a more north-westward to the north. The floats seeded during this leg are hoped to be trapped in the recirculation of the subtropical gyre. A more comprehensive overview of the cruise can be obtained from http://triton.sea.uct.ac.za

Acknowledgement

The continuous support of the crew and officers of FS Polarstern during this last leg of a long cruise has contributed significantly to the success of this project. One of us (O. Boebel) gratefully acknowledges the support of the Alexander von Humboldt Foundation and the University of Cape Town, which enable him to participate in this project. This project is financed by the BMBF, Grant No. 03F0157A (Zenk).

References

Boebel, O., C. Duncombe Rae, S. Garzoli, J. Lutjeharms, P. Richardson, T. Rossby, C. Schmid, and W. Zenk, 1997a: KAPEX: observing the intermediate flow at the tip of Africa. EOS, in preparation.

Boebel, O., C. Schmid, and W. Zenk, 1997b: Flow and recirculation of Antarctic Intermediate Water across the Rio Grande Rise, J. Geophys. Res., accepted.

Boebel, O., K. Schultz Tokos, and W. Zenk, 1995: Calculation of salinity from neutrally buoyant RAFOS floats. J. Atmos. and Oceanic Tech., 12 (4), 923–934.

Broecker, W. S., 1991: The great ocean conveyor. Oceanography, 4 (2), 79–88.

Davis, R. E., P. D. Killworth, and J. R. Blundell, 1996: Comparison of Autonomous Lagrangian Circulation Explorer and fine resolution Antarctic model results in the South Atlantic. J. Geophys. Res., 101 (C1), 855–884.

Duncombe Rae, C. M., 1991: Agulhas retroflection rings in the South Atlantic Ocean; an overview. S. African J. Mar. Sci., 11 (327–344).

Duncombe Rae, C. M., S. L. Garzoli, and A. L. Gordon, 1996: The eddy field of the south-east Atlantic Ocean: A statistical census from the Benguela Sources and Transports Project. J. Geophys. Res., 101 (C5), 11949–11964.

Garzoli, S. L., and A. L. Gordon, 1996: Origins and variability of the Benguela Current. J. Geophys. Res., 101 (C1), 897–906.

Gordon, A. L., 1996: Comment on the South Atlantic's role in the Global Circulation. In: The South Atlantic: Present and Past Circulation, edited by G. Wefer, W. H. Berger, G. Siedler, and D. J. Webb, pp. 121–124. Springer-Verlag, Berlin-Heidelberg.

Gordon, A. L., R. F. Weiss, W. M. Smethie, and M. J. Warner, 1992: Thermocline and intermediate water communication between the South Atlantic and Indian Ocean, J. Geophys. Res., 97 (C5), 7223–7240.

Lutjeharms, J. R. E., 1996: The exchange of water between the South Indian and South Atlantic Oceans. In: The South Atlantic: present and past circulation, edited by G. Wefer, W. H. Berger, G. Siedler, and D. Webb, pp. 122–162. Springer-Verlag, Berlin-Heidelberg.

Rossby, T., D. Dorson, and J. Fontaine, 1986: The RAFOS System. J. Atmos. and Oceanic Tech., 3, 672–679.

Stramma, L., and R. Peterson, 1990: The South Atlantic Current. J. Phys. Oceanogr., 20 (6), 846–859.

Sverdrup, H. U., M. W. Johnson, and R. H. Fleming, 1942: The Oceans: their physics, chemistry and general biology, 1087 pp. Prentice-Hall, New York.

WCRP, 1988: WOCE Implementation Plan, World Climate Research Programme 11, WMO/TD No. 242, pp. 74.

Whitworth, T. I., and W. D. Nowlin, 1987: Water masses and currents of the Southern Ocean at the Greenwich meridian. J. Geophys. Res., 92, 6462–6476.

Water Mass Formation from Thermodynamics: A Framework for Examining Compatibility with Dynamics

Amit Tandon, University of California, Santa Cruz, USA, and Chris Garrett, University of Victoria, BC, Canada. tandon@cascade.ucsc.edu

There are two main approaches to the evaluation of the rate of water mass formation in a particular density range. One method is to evaluate the wind-driven Ekman flux, part of which results in a diapycnal volume flux. The divergence (convergence) of this flux between two isopycnals gives the upwelling (downwelling) between these two isopycnals. Another method, suggested by Walin (1982), is to evaluate the water mass transformation rate due to air-sea fluxes; a buoyancy loss at the surface leads to a volume flux of water from lower density to higher density. Again the convergence of this quantity yields a water mass formation rate. We call these the dynamic method and the thermodynamic method, respectively.

Rhines (1993) pointed out that these two methods should result in identical water mass formation rates, but evaluations based on climatological data show that there can even be a sign discrepancy between the results from the two approaches, as shown in Fig. 4 of Speer and Tziperman (1992).

The purpose of this note is to point out that both methods are incomplete and to suggest improvements. We first define a surface C as the base of the deepest winter mixed layer, and define the water mass formed during the year as the integrated volume flux between two isopycnals intersecting C.

Recent advances in the literature show that:

- For the dynamic method, additional contributions can arise from the bolus flux of mesoscale eddies and from non-Ekman mean flow.
- The thermodynamic method needs to be corrected for mixing processes above the base of the winter mixed layer. These are horizontal stirring in the mixed layer and entrainment at the base of the instantaneous mixed layer during episodes of mixed layer deepening or of upwelling.

We first recapitulate the Walin (1982) thermodynamic approach and then discuss the corrections to the two methods, giving preliminary estimates of their importance.

The Walin framework

A potentially useful way to examine large scale volume and buoyancy budgets is in terms of advective and diffusive fluxes across 'mean' isopycnals. Once the integral time and space scales are chosen to define this mean, the processes occurring at smaller time and space scales determine the separation into advective and diffusive parts.

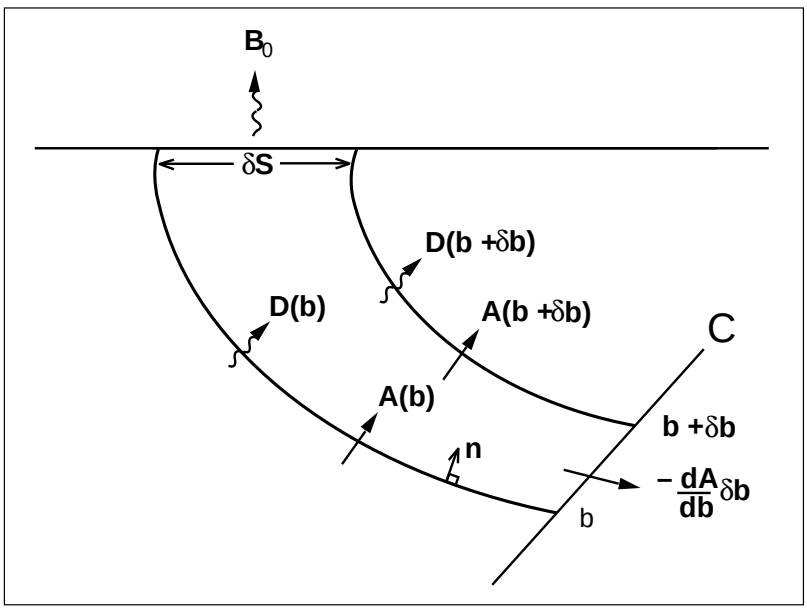

Figure 1. A schematic illustrating the buoyancy budget of a control volume between neighbouring isopycnals with buoyancy b and b + δb which outcrop at the surface. The sea surface area between them is δS which undergoes a spatially-averaged rate of buoyancy loss given by B_0. The control surface C is typically chosen to be the base of the winter mixed layer for water mass formation algorithms. From Garrett et al. (1995).

Near the surface, an innovative application of volume and buoyancy budgets quantifies the rate of water mass transformation from one density to another in terms of air-sea fluxes (Walin, 1982; Tziperman, 1986). The idea, as reviewed by Garrett et al. (1995), is most easily understood for a steady situation (Fig. 1). The rate of water mass formation in the buoyancy range b to b+δb is given by -δb dA/db where the diapycnal volume flux

$$A(b) = F(b) - dD/db \qquad (1)$$

is given in terms of the air-sea transformation rate $F(b) = -B_0\, dS/db$, which can be calculated from the air-sea surface buoyancy loss B_0 and the surface outcrop area S between b and b+δb, and the diapycnal diffusive flux D.

Garrett et al. (1995) showed that the vertical diffusive flux contribution within the surface mixed layer is very small. Thus, if horizontal mixing and the entrainment flux across the base of the mixed layer are

neglected, water mass formation rates can be found from the air-sea transformation rate F(b). This has been calculated for the North Atlantic from the COADS by Speer and Tziperman (1992) and more recently from the revised COADS by Speer, Isemer and Biastoch (1995), following monthly-mean isopycnals over an annual cycle. The latter authors found typical values of O(20 Sv), e.g., $F(\sigma_t = 26.0) = 18\,\mathrm{Sv}$ in the North Atlantic.

The bolus flux correction to the dynamic method

The dynamical approach to water mass formation needs to include the convergence of the wind-driven Ekman component, the volume flux at C due to mesoscale eddies (Tandon and Garrett, 1996; Marshall, 1997), and the contribution due to convergence in the mean flow.

Since the evaluations here depend entirely on dynamics, the control volume above the intersection of isopycnals with C need not be defined by the instantaneous or monthly isopycnal positions that are chosen for the thermodynamic evaluation. We suggest here that the appropriate control volume is that bounded below by C and laterally by the vertical surfaces from the lines where the isopycnals intersect C from below (Fig. 2). The control surfaces for the dynamical approach thus vary seasonally much less than those for the thermodynamic approach. We denote the Ekman volume flux across such a lateral boundary as $A_{\mathrm{Ekman}}(b)$; it is not necessarily the cross-isopycnal volume flux across the surface outcrop of isopycnal b. However, its convergence $-\delta b\, dA_{\mathrm{Ekman}}(b)/db$ is the Ekman contribution to water mass formation between isopycnals b and δb+b.

The total dynamic contribution is given by

$$A(b) = A_{\mathrm{Ekman}}(b) + A_{\mathrm{Bolus}}(b) + A_{\mathrm{Other}}(b), \qquad (2)$$

where $A_{\mathrm{Bolus}}(b)$ is the volume flux due to mesoscale eddies across the vertical surface above the line where the isopycnal with buoyancy b intersects C from below, and $A_{\mathrm{Other}}(b)$ is the contribution due to the mean flow. The dynamical water mass formation rate for buoyancy b is -δb dA(b)/db.

The Gent and McWilliams (1990) parameterisation gives $A_{\mathrm{Bolus}}(b) = \kappa s L$, where κ is the thickness mixing coefficient, s is the isopycnal slope at the base of the winter mixed layer, and L the outcrop length for the isopycnal b (Tandon and Garrett, 1996). For an open ocean value of $s \approx 2\times10^{-4}$, and L=7000 km, with $\kappa = 10^3\,\mathrm{m^2\,s^{-1}}$, this value is 1.4 Sv, small compared to typical values of F. An estimate of $A_{\mathrm{Other}}(b)$ requires further work, but simple dynamical arguments suggest that the ratio of $A_{\mathrm{Other}}(b)$ to $A_{\mathrm{Ekman}}(b)$ scales as the ratio of the mixed layer depth to the thermocline depth and is thus likely to be small.

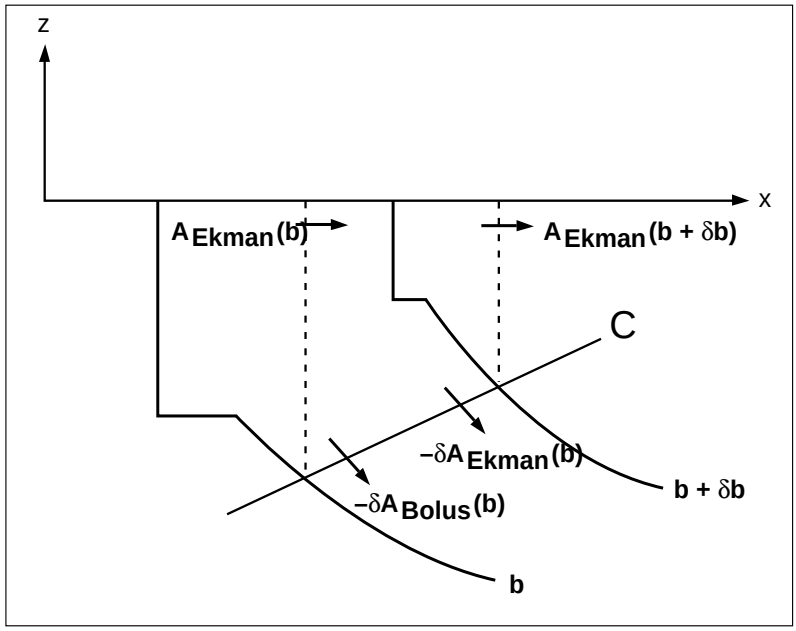

Figure 2. An illustration showing the volume fluxes due to Ekman transport and the contribution due to eddies. The lower control surface C is the base of the winter mixed layer. Dashed vertical lines show the lateral control surfaces for the dynamic method; the instantaneous isopycnal positions shown as solid lines form the lateral control surfaces for the thermodynamic method.

Correction to the thermodynamic method: the role of mixed layer time-dependence and entrainment fluxes

Garrett and Tandon (1997) and Nurser et al. (1997) have made progress in incorporating diapycnal advection due to mixed layer deepening and entrainment. The idea behind Garrett and Tandon's (1997) approach is that vertical mixing (homogenisation) of a water column conserves buoyancy in the vertical, but leads to net advection across isopycnals.

A hierarchy of models shows that the diapycnal advection due to mixed layer deepening and entrainment depends on horizontal and vertical changes in the horizontal buoyancy gradient, on the buoyancy jump b at the base of the mixed layer, and on the mixed layer deepening rate dh/dt. Accounting also for mean upwelling w at the base of the mixed layer leads to this correction as

$$F_{\mathrm{ML}} = \left[\left(\frac{1}{b_{\mathrm{xi}}} - \frac{1}{b_{\mathrm{xs}}}\right)\Delta b - \frac{1}{2} b_{\mathrm{xx}} b_{\mathrm{x}}^{-3} (\Delta b)^2\right]\left(w + \frac{dh}{dt}\right) \qquad (3)$$

which needs to be evaluated whenever w+dh/dt>0. Here b_{xi} is the buoyancy gradient at the base of the mixed layer (interface) and b_{xs} is the buoyancy gradient at the surface, with x the horizontal coordinate normal to the isopycnal. The diagnostic evaluations of Nurser et al. (1997) can be shown to result in an equivalent expression for F_{ML}.

For typical climatological gradients, and allowing for diurnal as well as seasonal cycling, preliminary estimates show this contribution to be O(2 Sv) (Garrett and Tandon,

1997). This is small compared to the air-sea transformation rate, which is of O(20 Sv), but the magnitude is sensitive to large scale gradients and the local mixed layer integrals.

If horizontal mixing due to mesoscale stirring gives rise to a diffusive diapycnal flux $D_H = -K_H b_x$, then an additional thermodynamic contribution to the water mass transformation rate arises from $-dD_H/db$. If b_x changes from $10^{-8}\,s^{-2}$ to an order of magnitude smaller value from $\sigma_t = 23.0$ to $\sigma_t = 26.0$, and using a mixed layer depth of 150 m and outcrop length of 7000 km, dD_H/db is O(0.3 Sv).This is small compared to F, as estimated by Garrett and Tandon (1997), consistent with Marshall (1997).

The overall framework

The net diapycnal flux is given by

$$A(b) = A_{Ekman}(b) + A_{Bolus}(b) + A_{Other}(b) \quad \text{from the dynamics,} \tag{4}$$

$$= F(b) + F_{ML}(b) - dD_H/db \quad \text{from the thermodynamics,} \tag{5}$$

We repeat that the reference surface for the thermodynamic approach is the instantaneous (or, rather, monthly mean) isopycnal with buoyancy b, whereas for the dynamic approach it is the vertical surface from the curved line where this isopycnal intersects the base of the winter mixed layer from below. Given this difference, the instantaneous or monthly mean values for A(b) from the two approaches need not agree precisely. However, the annual mean of dA/db from the two formulae should agree, and it would be useful to check this for various oceanic basins. Considering the North Atlantic, for instance, Speer and Tziperman (1992) evaluated $A_{Ekman}(b)$ based on Isemer and Hasse's (1987) dataset, finding a net δA_{Ekman} of about -4 Sv (downwelling) between $\sigma_t = 23.0$ and $\sigma_t = 26.0$ (Speer, pers. comm.). On the other hand, Speer et al. (1995) estimated from their revised COADS dataset that F is about +10 Sv. (It is even larger, about +30 Sv, with the Isemer and Hasse dataset or from the unrevised COADS dataset used by Speer et al. (1995)).

The water mass formation rates $-\delta A_{Ekman}$ and -δF thus differ in sign in this density range, with a difference $\delta(F - A_{Ekman})$ of at least 14 Sv. This needs to be balanced by all other contributions if we assume that the discrepancy is real and not a consequence of errors in the surface fluxes. However, as discussed above, $A_{Bolus}(b)$, $-dD_H/db$ and F_{ML} are O(1 Sv) or smaller.

Further work is needed to investigate this apparent imbalance between dynamic and thermodynamic requirements. The main possibilities seem to be that F is erroneous, that mixing processes or bolus fluxes make large contributions in the Western Boundary Current, that the divergence in the mean flow is significant, or that storage terms associated with long term changes are important. If buoyancy forcing is the most uncertain part of this balance, perhaps eqns. (4) and (5) can be used as a constraint on B_0 and the air-sea transformation F. There is also a need to reconcile the above approaches with the method of Nurser and Marshall (1991) and Marshall and Nurser (1992) who combine both wind and buoyancy forcing following water parcels but not following isopycnals.

A recent review of oceanic numerical modelling by McWilliams (1996) concludes "the biggest surprises are likely to come in weaning the ocean model from its specified, or at least strongly constrained, surface boundary conditions ...". In this spirit, as the ocean models move towards being forced by both realistic wind stress and surface buoyancy fluxes, we point out that it is important to consider their compatibility for water mass formation. It would be disconcerting if climatological momentum and air-sea buoyancy fluxes are incompatible for water mass formation; this not only leaves considerable uncertainty in formation rates, but would also impose a considerable strain on numerical models run with both dynamic and thermodynamic forcing!

Acknowledgements

We thank John Marshall, Kevin Speer, George Nurser, Jürgen Willebrand and Bill Dewar for discussions. This work is supported by NSF of USA and NSERC of Canada.

References

Garrett, C., K. Speer, and E. Tragou, 1995: The relationship between water mass formation and circulation, with application to Phillips' Red Sea model. J. Phys. Oceanogr., 25, 1696–1705.

Garrett, C. and A. Tandon, 1997: The effects on water mass formation of surface mixed layer time-dependence and entrainment fluxes. Deep-Sea Res., in press.

Gent, P. R. and J. C. McWilliams, 1990: Isopycnal mixing in ocean circulation models. J. Phys. Oceanogr., 20, 150–155.

Isemer, H. J. and L. Hasse, 1987: The Bunker Climate Atlas of the North Atlantic Ocean, Vol. 2: Air-Sea Interactions. Springer-Verlag.

Marshall, D., 1997: Subduction of water masses in an eddying ocean. J. Mar. Res., 55, 201–222.

Marshall, J. C., and A. J. G. Nurser, 1992: Fluid dynamics of the oceanic thermocline ventilation. J. Phys. Oceanogr., 22, 583–595.

McWilliams, J. C., 1996: Modeling the oceanic general circulation. Ann. Rev. Fluid Mech., 28, 215–248.

Nurser, A. J. G., R. Marsh, and R. G. Williams, 1997: Diagnosing water mass formation from air-sea fluxes and surface mixing. J. Phys. Oceanogr., submitted.

Nurser, A. J. G., and J. C. Marshall, 1991: On the relationship between Subduction rates and diabatic forcing of the mixed layer. J. Phys. Oceanogr., 21, 1793–1802.

Rhines, P., 1993: Oceanic general circulation: Wave and advection dynamics. In Rhines, P., editor, Atmosphere-Ocean Dynamics and Interannual Climate Variability. Friday Harbor Laboratories Report.

Speer, K., and E. Tziperman, 1992: Rates of water mass formation in the North Atlantic Ocean. J. Phys. Oceanogr., 22, 94–104.

Speer, K. G., H.-J. Isemer, and A. Biastoch, 1995: Water mass formation from revised COADS data. J. Phys. Oceanogr., 25, 2444–2457.

Tandon, A. and C. Garrett, 1996: On a recent parameterization of mesoscale eddies. J. Phys. Oceanogr., 26, 406–411.

Tziperman, E., 1986: On the role of interior mixing and air-sea fluxes in determining the stratification and circulation of the oceans. J. Phys. Oceanogr., 16, 680–693.

Walin, G., 1982: On the relation between sea-surface heat flow and thermal circulation in the ocean. Tellus, 34, 187–195.

Which is it: Warm or Cold Route, or Maybe Both?

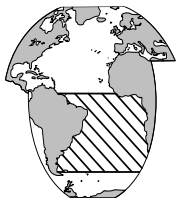

Arnold L. Gordon, Lamont-Doherty Earth Observatory of Columbia University, Palisades, USA. agordon@ldeo.columbia.edu

The title question is related to another more commonly asked question: Why is the North Atlantic thermocline so salty (Fig. 1, page 22)? It is a climate relevant question, as cooling at the poleward edge of the saline upper layer within the North Atlantic enables production of North Atlantic Deep Water (NADW), which drives an ocean overturning circulation cell of global proportions. The exact nature and global configuration of the NADW driven overturning cell is a key target of oceanographic research (Schmitz, 1995 reviews the present status of this research; MacDonald and Wunsch, 1996).

The conventional wisdom response to the Atlantic salinity question may be that excess evaporation from the North Atlantic (including the Mediterranean Sea) with subsequent export of atmospheric moisture to the Pacific drainage basin provides the answer (about 0.3 Sv of water vapour is exported from the North Atlantic, Zaucker et al., 1994). However, I consider that the very production of NADW induces this phenomena, as northward spreading of thermocline water (the upper limb of the overturning cell) spurs warmer than expected sea surface temperatures (SST) with associated enhancement of evaporation. Thus the excess evaporation is not the fundamental reason for the saline thermocline, but rather an important positive feedback response to the production of NADW. What then is the more fundamental reason for a salty Atlantic?

Reid (1961) blames it on the South Atlantic where the far southern latitude of Cape Horn blocks freshwater influx into the Atlantic Ocean. Gordon and Piola (1983) agreed; more specifically they propose that the surface water within the Antarctic Circumpolar Current (ACC) freshens as it passes across the South Atlantic sector due to excess precipitation drawn from the South Atlantic subtropical climate zone. The ACC removes freshwater from the South Atlantic passing it into the Indian and Pacific Oceans. Additionally, the maximum westerlies thermocline well south of Africa, transfer warm, saline Indian Ocean water around the southern rim of Africa into the South Atlantic, adding heat and salt to the Atlantic (Gordon, 1986). Gordon et al., 1992, modified the simple picture presented in 1986 by noting that the cold water route does not pass directly into the south-western subtropical South Atlantic, but rather passes across the South Atlantic to merge with the warm water route in the Agulhas Retroflection region. Some cold route water passes well into the south-west Indian Ocean, before returning to the South Atlantic within the Agulhas Current. This process adds Indian Ocean subtropical salt to the Drake Passage derived water, boosting the salinity of the Atlantic upper layer.

Saline South Atlantic thermocline waters, produced either by the ACC process or the interocean thermocline transfer (more likely both) eventually migrates into the North Atlantic as part of the NADW meridional overturning cell. The North Atlantic thermocline may be salty because it has both evaporative subtropical regions of the Atlantic Ocean to draw upon. In fact, if the Agulhas leakage idea is right it has access to a third, the Indian Ocean evaporative subtropical regime.

My controversial 1986 paper concerning the source of the upper limb water within the North Atlantic driven meridional overturning cell has spawned a plethora of model and observational based studies that address this topic. Some say I'm wrong, others say I'm right, with the publications nearly equally split between favouring the warm (Indian Ocean thermocline, Agulhas) route over the cold (Pacific Ocean subantarctic, Drake Passage) route. Of course, one route does not exclude the existence of the other, nor is the ratio of warm to cold transport fixed in time, though often the arguments are presented in that way.

From the observational side, Rintoul's 1991 inverse solution using a South Atlantic data set spanning some 24 years finds that the main source of the upper layer inflow to the South Atlantic is from the Drake Passage, the cold water route. Schlitzer (1996) essentially finds similar results from a inverse solution using a gridded Atlantic data set. Neither of these deals explicitly with the possibility of "re-working" of cold route water within the south-west Indian Ocean, as proposed by Gordon et al., 1992. Saunders and King, 1995 using the January 1993 WOCE A11 WHP section finds significant amounts of warm, saline Indian Ocean thermocline water must enter the South Atlantic, supporting the warm water route. As expected the ratio of warm to cold water is closely coupled to the magnitude of the heat and freshwater fluxes across 30°S.

From the modelling side, again some models show no Agulhas leakage (Drijfhout et al., 1996) while others show significant coupling of Indian and South Atlantic within the thermocline and Antarctic Intermediate Water (AAIW) layers (Thompson et al., 1997; Shrivers and Hurlburt, 1997). Apparently much of the discrepancy is related to model resolution, the coarse scale models do not allow for Agulhas leakage, the finer scale models do. The link of the source of the upper layer water to South Atlantic meridional fluxes is also noted. Cai and Greatbatch (1995) using the Bryan-Cox global ocean GCM find Agulhas leakage with a circulation pattern much as presented by Gordon et al., 1992. However, while suppression of the Indian Ocean loop does lead to a cooler and fresher Atlantic, in the model it does not lead to a reduction in NADW production rate.

The pathway followed by Indian Ocean water infiltrating the South Atlantic is not entirely clear. Evidence suggests that the primary interocean transport is accomplished by shedding of large rings or eddies of Indian Ocean water at the Agulhas Retroflection. These eddies drift

westward across the South Atlantic near 30°S, moving "uphill" into the axis of the subtropical gyre and may have an influence on the Brazil Current (Byrne et al., 1995). However, the Benguela Current thermocline water between the eddies, is laced with Indian Ocean water (Gordon et al., 1992), which may be introduced by filaments of Agulhas Current or breakdown of Agulhas eddies. The Benguela Current extends seaward towards the north-west as the South Equatorial Current to bifurcate at the South American coast near 10°S in the surface layer, closer to 25°S at AAIW depths. The part that turns to the south forms the source of the Brazil Current. The northward flowing current forms the upper limb water that crosses into the northern hemisphere, accomplished with a few swish-backs within the zonal flowing equatorial currents and coupled with upwelling of intermediate water (and its conversion into thermocline water) within the tropical Atlantic.

Variability in the source waters and transport of the Benguela Current (Garzoli et al. 1996) as well as changes in its seaward trajectory across the South Atlantic within the South Equatorial Current, act to induce SST anomalies within the South Atlantic and perhaps variability in the transfer of southern hemisphere properties into the North Atlantic, from seasonal to decadal (and presumably longer) time scales. The complex circulation and mixing within the Cape Basin needs to be sorted out to better assess the details of the warm water route as well as its blending with the cold water route pathway.

The complex passage of South Atlantic water across the Equator is revealed by the detailed WOCE study reported by Schott et al., 1995 and Stramma and Schott, 1996. The decisive action occurs south of 8°S where the South Equatorial Current bifurcates on reaching South America. The transport of South Atlantic water flowing northward off Recife (8°S) is 16 Sv (10 Sv in the main thermocline; and 6 Sv in the lower thermocline and AAIW levels). The equatorial manoeuvring of NADW components exiting the North Atlantic is equally as complex (F. Schott report at the June 1997 WOCE South Atlantic meeting). Schlitzer (1996) model study suggests that there is significant conversion of AAIW into thermocline water better 30°S and 30°N, amounting to a reversal of the ratio between thermocline and AAIW meridional transport.

The communication of the South and North Atlantic across the equatorial belt and the associated mixing and water mass modification, as well as its coupling with the atmosphere (climate system) is a key area for WOCE AIMS research and future research focus. WOCE AIMS should attempt to arrive at an estimate with "error bars" for the heat and freshwater fluxes across the South Atlantic WOCE zonal and meridional WHP lines. Thermohaline fluxes and divergence are the key oceanic element in the climate system, which once determined will answer the warm vs. cold route question, though time variability still may not be fully appreciated, that's a CLIVAR issue.

My guess as to the best answer to the title question: both routes are active, exist simultaneously and are integrally linked, though their transport ratio changes across a wide range of time scales reflecting larger scale climate variability (Gordon, 1996).

References

Byrne, D., A. Gordon, and W. Haxby, 1995: Agulhas Eddies: A Synoptic View Using Geosat ERM Data. J. Phys. Oceanogr., 25: 902–917.

Cai, W., and R. Greatbatch, 1995: Compensation for the NADW outflow in a Global Ocean General Circulation Model. J. Phys. Oceanogr., 25: 226–241.

Drijfhout, S., E. Maier-Reimer, and U. Mikolajewicz, 1996: Tracing the conveyor belt in the Hamburg large-scale geostrophic ocean general circulation model. J. Geophys. Res., 101(C10): 22,563–22,575.

Garzoli, S. L., A. L. Gordon, V. Kamenkovich, D. Pillsbury, and C. Duncombe-Rae, 1996: Variability and sources of the southeastern Atlantic circulation. J. Mar. Res., 54(6): 1039–1071

Gordon, A., 1986: Inter-Ocean Exchange of Thermocline Water. J. Geophys. Res., 91(C4): 5037–5046.

Gordon, A., and A. R. Piola, 1983: Atlantic Ocean Upper Layer Salinity Budget. J. Phys. Oceanogr., 13(7): 1293–1300.

Gordon, A., Weiss, R. F., W. M. Smethie, Jr., and M. J. Warner, 1992: Thermocline and intermediate water communication between the South Atlantic and Indian Oceans. J. Geophys. Res. 97(C5): 7223-7240.

Gordon, A. L., 1996: Comment on the South Atlantic's Role in the Global Circulation. In: The Southern Atlantic: Present and Past Circulation. Wefer, G., Berger, W., G. Siedler, and Webb D.J. (eds). pp.121–124 Springer-Verlag.

Levitus, S., R. Burgett, and T. Boyer, 1994: World Ocean Atlas 1994, Vol. 3: Salinity. NOAA Atlas NESDIS 3, 99pp.

MacDonald, A. M., and C. Wunsch, 1996: An estimate of global ocean circulation and heat fluxes. Nature, 382: 436–439.

Reid, J. L., Jr., 1961: On the temperature, salinity, and density differences between the Atlantic and Pacific oceans in the upper kilometer. Deep-Sea Res., 7: 265–275.

Saunders, P.M., and B. A. King, 1995: Ocean Fluxes on the WOCE A11 Section. J. Phys. Oceanogr., 25 (9), 329–397, 1942–1958.

Schlitzer, R., 1996: Mass and Heat Transport in the South Atlantic Derived from Historical Hydrographic Data. The South Atlantic: Present and Past Circulation. G. Wefer, W. H. Berger, G. Siedler and D. J. Webb. New York, Springer Verlag: 305–323.

Schmitz, W., 1995: On the interbasin-scale thermohaline circulation. Reviews of Geophysics 33(2): 151–173.

Schott, F. A., L. Stramma, and J. Fischer, 1995: The warm water inflow into the western tropical Atlantic boundary regime, spring 1994. J. Geophys. Res., 100(C12): 24,745–24,760.

Shriver, J. F., and H. E. Hurlburt, 1997: The contribution of the global thermohaline circulation to the Pacific to Indian Ocean throughflow via Indonesia. J. Geophys. Res. 102(C3): 5491–5511.

Stramma, L., and F. Schott, 1996: Western equatorial circulation and inter-hemispheric exchange. The Warm water sphere of the North Atlantic Ocean. W. Krauss, Gebrder Borntraeger: 195–227.

Thompson, S. R., D. P. Stevens, and K. Döös, 1997: The importance of interocean exchange south of Africa in a numerical model. J. Geophys. Res., 102(C2): 3303–3316.

Zaucker, F., T. F. Stocker, et al., 1994: Atmospheric freshwater fluxes and their effect on the global thermohaline circulation. J. Geophys. Res., 99(C6): 12,443–12,458.

WOCE Indian Ocean Workshop to be held in New Orleans (USA) 21–25 September 1998

The World Ocean Circulation Experiment announces a workshop on the large-scale circulation and dynamics of the Indian Ocean, to be held in New Orleans (USA), week of 21–25 September 1998.

The aims of the workshop are to summarise scientific results obtained so far, to identify significant outstanding problems where progress has to be made to reach the goals of WOCE, to encourage and facilitate collaboration among the scientists involved and to prepare data synthesis and publications.

The venue is Hotel Hampton Inn, 226 Carondelet Street (on the edge of the French Quarter; 2 blocks from Canal and Bourbon Streets). A group rate of $109 per night has been negotiated. This is not your typical Hampton Inn, but is a remodelled 1903 "skyscraper" of 14 storeys.

Meeting rooms are available both within the hotel and at the University of New Orleans Conference Center, situated in the same building.

The scientific programme and working group topics are still under discussion, a notice regarding the meeting will be posted shortly on the US WOCE web page **(http://www-ocean.tamu.edu/WOCE/uswoce.html)** and be announced via WOCE Notes, the International WOCE Newsletter and EOS.

Registration will be handled electronically via the US WOCE Office.

Scientific Committee:

Bruce Warren	(WHOI),
Fritz Schott	(U. Kiel, Germany),
John Church	(CSIRO, Australia),
Don Olson	(U. Miami),
Rana Fine	(U. Miami),
Greg Johnson	(PMEL),
Jochem Marotzke	(MIT),
Mark Luther	(U. South Florida)

International CLIVAR Project Office Director

The World Climate Research Programme (WCRP) has launched a Climate Variability and Predictability Study (CLIVAR) aimed at understanding and predicting global climate variations on seasonal, interannual, and multi-decadal time scales. The international coordination and implementation of this study is overseen by the International CLIVAR Project Office at the Max Planck Institute for Meteorology in Hamburg, Germany. A director for this office is now being sought.

Candidates should hold a PhD or equivalent in atmospheric, oceanographic or other climate-related physical sciences, have considerable experience in the organisation of multi-disciplinary international scientific projects, be fluent in English, and be available for not less than four years starting as soon as possible after 1 May 1998.

The exact nature of the appointment will be determined in consultation with the successful candidate and the level of remuneration will be negotiated according to qualifications.

A post of Senior Scientist is also likely to be established at the ICPO in the near future. Please indicate in your letter of application if you wish to be considered for this position as well.

Letters of application with CV are to be sent no later than 1 December 1997 to the Chair of the Search Committee:

Dr R. A. Clarke
Bedford Institute of Oceanography
PO Box 1006
Dartmouth, Nova Scotia
Canada B2Y 4A2
Fax: +1-902-426-7827

and copies to:

Director, WCRP
c/o WMO
CP 2300
CH-1211 Geneva 2
Switzerland.
Fax: +41-22-734-0357.

Note on Copyright

WOCE is a component of the World Climate Research Programme (WCRP), which was established by WMO and ICSU, and is carried out in association with IOC and SCOR. The scientific planning and development of WOCE is under the guidance of the Scientific Steering Group for WOCE, assisted by the WOCE International Project Office.

The International WOCE Newsletter is edited by Roberta Boscolo (roberta.boscolo@soc.soton.ac.uk) at the WOCE IPO at Southampton Oceanography Centre, Empress Dock, Southampton, SO14 3ZH, UK, Tel: 44-1703-596789, Fax: 44-1703-596204, e-mail: woceipo@soc.soton.ac.uk,

http://www.soc.soton.ac.uk/OTHERS/woceipo/ipo.html

We hope that colleagues will see this Newsletter as a means of reporting work in progress related to the Goals of WOCE as described in the Scientific Plan.

The editor will be pleased to send copies of the Newsletter to institutes and research scientists with an interest in WOCE or related research.

Printed by the Design and Print Centre of the University of Southampton